**acp-2018-12 authors' response to reviewers' comments**

**Global modelling of the total OH reactivity: investigations on the "missing" OH sink and its atmospheric implications**

Reviewers' comments are in black, <span style="color:blue">authors' response in blue and</span> <span style="color:red">changes to the text in red</span>.

**Interactive comment on "Global modelling of the total OH reactivity: investigations on the "missing" OH sink and its atmospheric implications" by Valerio Ferracci et al.** <u>**Anonymous Referee #1**</u> Received and published: 6 February 2018

This paper presents a study of the global impacts of "missing OH reactivity" in models used to determine the atmospheric oxidising capacity, and investigates the extent to which additional sinks are required to reconcile observations of OH reactivity with model simulations. The authors use an interesting approach to determine the emissions field necessary to improve the agreement between observed and modelled OH reactivity. The impacts of the reaction between OH and $CH_3O_2$, and its branching ratio, on budgets for OH, $CH_3O_2$ and the global methane lifetime are also discussed.

In general, the paper is well written and will be of interest to the atmospheric science community. However, the discussion would benefit from some additional detail regarding the regions and environments affected most by missing reactivity, and how the OH and $HO_2$ concentrations are affected in the model.

We would like to thank the referee for their support of our paper and for their constructive comments. Below are the answer to the reviewer's comments, point by point.

We feel that the regions affected by measured missing reactivity are already described at length in the introduction (where observations of missing reactivity are discussed) and in Section 4.1, where the geographical distribution of the modelled missing reactivity from multiple linear regression is described. We have added a sentence in the conclusions discussing the regions and environments where the multiple linear regression predicts the presence of missing reactivity.

"The multiple linear regression indicated that the areas most affected by the missing reactivity would be tropical remote regions, where biogenic emission dominate, as well as urban regions all over the globe, where anthropogenic emissions are significant. This result agrees with the type of environments in which missing reactivity has been observed."

Effects of X + OH on OH are already shown in Fig 7 and Figs S2 and S3 (now Figures S8 and S9 in the revised manuscript) and discussed in detail in the text. An additional figure (Figure S10) has been included in the Supplementary Information showing that relative changes in $HO_2$ from X + OH largely mirror those in OH, albeit with a somewhat reduced relative magnitude. Changes in OH and $HO_2$ abundances from $CH_3O_2$ + OH are already discussed at length in Section 5.2.

The results of this work could also be used to provide some recommendations as to where future measurements of OH reactivity are most needed to give better constraint for modelling of global methane lifetimes and ozone budgets.

The Southern Hemisphere was notably underrepresented in the sample of measurements analysed in this study. Aircraft measurements of the missing reactivity would also be desirable, especially at tropical and mid-latitude, to better quantify the impact on global methane lifetimes as well as the vertical profile of the missing reactivity, especially above the boundary layer. A comment to address these points was added to the Conclusions.

"Lastly, as observations of the missing reactivity so far are largely limited to ground level measurements in the Northern Hemisphere, further observations in the Southern Hemisphere as well as aircraft measurements both in the boundary layer and the free troposphere would provide additional constraints to the modelled oxidising capacity of the atmosphere."

Minor comments are listed below.

Page 2, line 6: O($^1$D) production is observed at wavelengths below 340 nm.

Amended.

Page 3, line 5: Please comment on the location for which 80 % of the total $k_{OH}$ is missing.

Some text was added in the first two paragraphs on page 3 to indicate that the measurements of up to 80% missing reactivity took place in the Amazon, where the impact of large

unidentified biogenic emissions as well as the complex oxidation chemistry of measured and unmeasured BVOCs is largest.

Page 4, line 23: Please update the reference to http://iupac.pole-ether.fr/

Amended.

Page 7-8, Table 2: Does the use of the mean $k_{OH}$ measured over the whole duration of each campaign skew the averages in any way? Do all the field campaigns have similar data coverage throughout the day or throughout the campaign?

There are a number of campaigns with discontinuous temporal coverage that were not included in the analysis presented in the manuscript. These include 4 sets of measurements in Tokyo, Japan, which only reported daytime values of the OH reactivity (Yoshino et al., *Atm. Env.*, 2006; Chatani et al., *Atm. Chem. Phys.*, 2006; Kato et al., *Atm. Env.*, 2011; Yoshino et al., *Atm. Env.*, 2012). Similarly, measurements in Suriname (Sinha et al., *Atm. Chem. Phys.*, 2008) were discarded as they only covered a limited interval of time on a single day.

We believe that, whilst there is always a possibility that the measurement temporal coverage in a field campaign is not uniform or continuous, the choice of campaigns that spanned many weeks (which was the case for the vast majority of the datasets considered for the missing reactivity calculations) does at least minimise that risk.

Page 8, Figure 2: Is there a reference for the 20 % measurement uncertainty in observed $k_{OH}$? I would expect this to depend on the specific technique used to measure $k_{OH}$ and the particular instrument configuration.

The reviewer is correct and the error bars in Figure 2 (and Figure 4) have been amended to reflect the different uncertainties of the instruments used in each campaign.

Page 10, line 1: Please quantify, or avoid, the statement 'reasonably good agreement'.

The line has been changed to better quantify the agreement between model and observations in Figure 3.

"Overall more than half (53 %) of the reactivities calculated from modelled sinks agree with observations within a factor of two, and the vast majority (88 %) within a factor of ten."

Page 17, Figure 6: How many iterations are typically required to obtain the emissions field? Is the $R^2$ in the lower panel of Figure 6b skewed by the few points with high reactivity?

The work described in the manuscript involved 10 iterations of the routine described in figure 6.

Exclusion of the points with highest reactivity ($> 50$ s$^{-1}$) from the fit in the lower panel of Figure 6b still returns an $R^2$ value $> 0.95$ (0.9515 to be precise, *cf.* 0.9588 obtained with the full dataset). It is necessary to remove all points of reactivity higher than 40 s$^{-1}$ to get an $R^2$ value $< 0.95$ (0.9489). It has to be noted that we use 0.95 as an arbitrary threshold for the $R^2$ value. Moreover, progressive removal of points of high reactivity indicates that these high values are not skewing the $R^2$ value significantly: a fit considering only values lower than 30 s$^{-1}$ still returns an $R^2$ of 0.943 (a very modest 1.6% decrease compared to the full data set).

**Interactive comment on "Global modelling of the total OH reactivity: investigations on the "missing" OH sink and its atmospheric implications" by Valerio Ferracci et al.**
<u>Anonymous Referee #2</u> Received and published: 1 February 2018

Review of "Global modelling of the total OH reactivity: investigations on the "missing" OH sink and its atmospheric implications" by Valerio Ferracci and colleagues. This is a very interesting study that makes a significant contribution to the field. Increasingly, field experimental campaigns include OH reactivity measurements, which provide an important constraint to our understanding of VOC emissions and their atmospheric oxidation processes. Ferracci et al. introduced a hypothetical sink in their state-of-the-art global atmospheric chemistry transport model to study "missing" OH reactivity, i.e. the reactivity that could not be modelled in comparison to field data. There is one drawback that I would like to see discussed before recommending publication. For the impacts on OH and $O_3$ in section 4.2 it was assumed that the hypothetical emissions of molecule X, probably representing biogenic VOCs, do not recycle OH through their oxidation products (OVOCs). They are assumed to be a simple OH sink without any further chemistry, which is a rather strong simplification. There is growing evidence that biogenic VOCs are unlikely to be ultimate OH sinks and that OH recycling is ubiquitous. Although mentioned on p. 18 and 20, this aspect needs some discussion in view of the interpretation of atmospheric chemistry impacts, notably in the abstract and conclusion section.

We thank the reviewer for their kind words on the manuscript and for their valuable feedback. We understand that the absence of OH recycling constitutes a limitation of this study. However, as also explained at the beginning of Section 4.2, we feel that there are too few constraints to even attempt modelling of OH recycling following reaction 3. In the most optimistic view, it would involve running different recycling scenarios, with each scenario requiring to re-run the iterative routine to determine the emissions of X as the recycling of OH would ultimately perturb steady state [X] and ultimately $k_3$[X], *i.e.* the modelled missing reactivity. We conclude that the work described in the manuscript provides an upper limit on the effects of the missing reactivity on the oxidising capacity of the atmosphere. We have added a statement to address this in both the abstract and conclusions.

"As no OH recycling was introduced following the initial oxidation of X, these results can be interpreted as an upper limit of the effects of the missing reactivity on the oxidative capacity of the troposphere." and "It has to be noted that, as no OH recycling was introduced following

the initial oxidation of X, these results should be interpreted as an upper limit of the effects of the missing reactivity on the oxidative capacity of the troposphere."

Other than that, I recommend publication in ACP with minor revisions.

Minor comments:

-Please define missing reactivity more clearly. Is it missing in the sense that accompanying VOC measurements do not account for all reactivity, or missing in the model. Please make the distinction.

We have added a clearer definition of missing reactivity after Figure 2 in Section 3.

"The total observed $k_{OH}$ in Figure 2 is made up of contributions from the measured OH sinks, from modelled intermediates (only available for some of the field campaigns presented here) and from reactivity that is unaccounted for by known OH sinks, *i.e.* the missing reactivity. "

-p10 bottom/p.11 top: It would be helpful to compare the model calculated OH with some of the published OH measurements in the Amazon. Often, isoprene chemistry mechanisms severely underestimate OH.

The reviewer makes a very valid point. The OH measurements from Liu et al. (Liu et al., *PNAS* 2016) and from the GABRIEL campaign (Martinez et al., *Atm. Chem. Phys.*, 2010) were compared with the model output. It has to be noted that Liu et al. only measured OH for ~7 hours on a single day, and that the GABRIEL campaign in Suriname consisted of airborne measurements. The model underestimated OH by almost a factor of 4 in both cases, indicating that there is a strong possibility that the high concentrations of modelled VOCs for the ATTO site are caused by underpredicted OH. This is consistent with the inverse relationship between OH reactivity and OH concentrations as shown in Figure R1 below.
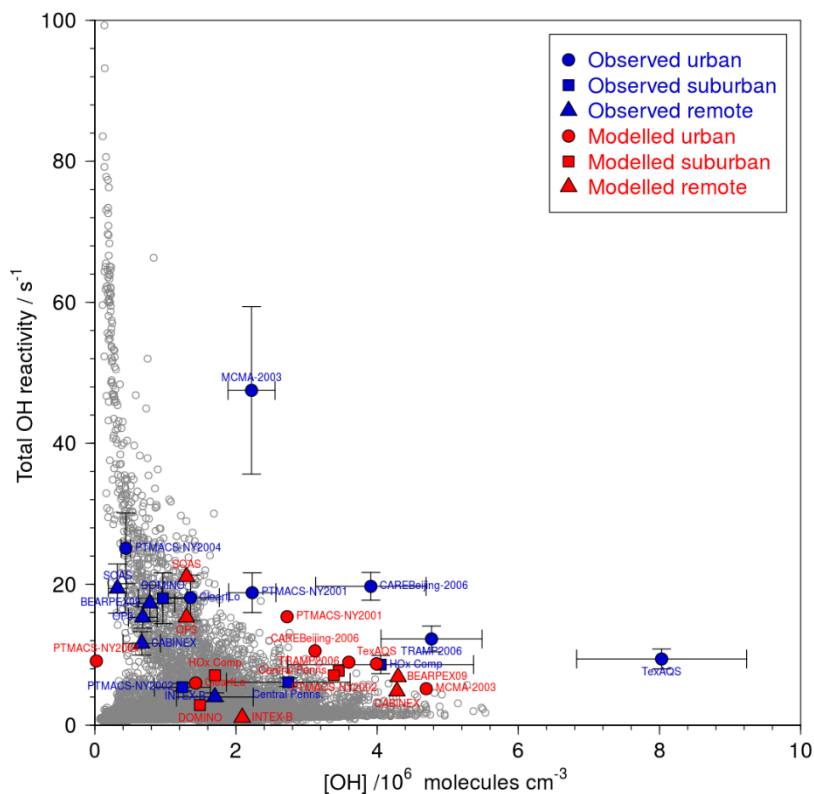
**Figure R1**: Scatter plot of total OH reactivity against OH concentration. Observations from field studies (in blue) and values from the UM-UKCA model for the same locations (in red) are shown. Also shown is the model output for the surface (grey points) to highlight the inverse relationship between $k_{OH}$ and [OH].

The text has been modified to account for this.

"Figure 3 also offers an explanation for the instances in which the model significantly over predicted $k_{OH}$. For example, the abundance of isoprene measured during the wet season of the ATTO campaign in the Amazon (~1 ± 0.1 ppbv, or nmol/mol, in March 2013) was more than an order of magnitude lower than that predicted by the model for the same time of the year (~14.6 ppbv). As discussed above, this might arise from either overestimated isoprene emissions or from underestimated OH abundances in the model. As OH concentrations were not measured during the ATTO campaign, a direct comparison of modelled and observed [OH] is not possible. However [OH] measurements from campaigns carried out in neighbouring parts of the Amazon (Liu et al., 2016) and in the Suriname rainforest (Martinez et al., 2010) might help address this point. Indeed the model underestimates [OH] by almost a factor of four on average in both cases, although it is worth noting that [OH] measurements from Liu et al. (2016) only cover ~7 hours on a single day, while the GABRIEL campaign in Suriname consisted of airborne measurements, and only the OH data for the boundary layer were considered for comparison with the model. It may also be indicative of underrepresented [OH]

in model that the abundance of other short-lived OH sinks in the ATTO campaign is also overestimated by the model; notably, the observed concentration of monoterpenes (reported to be below the detection limit of the PTR-MS used by Nölscher and co-workers, and here approximated to 0.01 ppbv) was much lower than in the model (2.2 ppbv). Underrepresented OH in the model might arise from underestimating the secondary OH originating from the oxidation of large organics (e.g., isoprene and monoterpenes, as described in Archibald et al., 2010). In this specific instance the model also underestimated the concentration of NO (34 pptv, or pmol/mol, vs the observed ~1 ± 0.05 ppbv), which might have limited the production of secondary OH via the reaction of $HO_2$ with NO relative to observations."

**Interactive comment on "Global modelling of the total OH reactivity: investigations on the "missing" OH sink and its atmospheric implications" by Valerio Ferracci et al.**
<u>Anonymous Referee #3</u> Received and published: 1 February 2018

The article entitled "Global modelling of the total OH reactivity: investigations on the "missing" OH sink and its atmospheric implications" concerns first the modelling of the OH reactivity at the global scale with the model UM-UKCA (base case) and the comparison with measured total OH reactivity in various environments (27 field measurement used for the comparison). The model reproduces well the measured OH reactivity (within 20%) for 12 campaigns, underestimate it for 14 cases and overestimate it for one case. An individual analysis of the differences between the modelled and calculated reactivity per species reacting with OH on 11 categories highlights the main source of underestimation by the model: the NMHCs whereas the overestimation case is due to the isoprene concentration overestimation. This work is of high interest because there are only a few studies on the oxidant capacity of the atmosphere with global atmospheric modelling and this study is the first one dedicated to the comparison between measured and modelled OH reactivity.

In a second step, an original approach has been used to represent at the global scale the missing reactivity through the addition of a hypothetical molecule X, reacting with OH (but without OH recycling), at various concentrations depending on the missing reactivity measured in the different campaigns. The emission rate of this species has been determined by a multiple linear regression including 15 categories of emission and an iterative procedure to match the missing reactivity observed. The impact of this addition is analysed through the depletion of OH concentration (up to 90% in the eastern Europe for example), the methane and OH lifetime (respectively 2.3 and −2% at the surface) and the ozone change has been used to quantify the impact of this missing reactivity on the OH lifetime at the global scale as well as the impact on the tropospheric methane lifetime in comparison to the base case. This approach allows to represent the missing reactivity at a global scale but the absence of OH recycling due to this species is a limitation to analyse further the consequence of the missing chemistry highlighted by the missing reactivity measured.

In a third step, the UM-UKCA model has been used to study the impact of the reactions of peroxy radicals with OH on OH reactivity which was found to be weak (maximum of $0.12 \, \text{s}^{-1}$) and can't be the reason for the missing OH reactivity. In the last part of the article, the impact of the products yields of the reaction of $CH_3O_2 + OH$ has been studied with 3 extra model runs

with different branching ratio for the different product channels (producing respectively HO2 or methanol). The branching ratio has been varied for these 2 channels between 1/0 and 0.6/0.4. The conclusion of this work is that, even with the highest branching ratio used for the channel producing methanol (0.4), the additional production of methanol does not explain the under-prediction of methanol by the models. Even if of high interest, this part seems to be decoupled from the other parts of the article dedicated to the OH reactivity. The article is very interesting and the method and the analysis done on the reactivity based on the comparison between measured reactivity and modelled one is well structured. However, I found sometimes difficult to find the information and some improvements in the Figures could help the reader.

We thank the referee for their kind support of the manuscript and for their constructive comments. Below are the answer to the reviewer's comments.

Comments:

(1) P7: would be interesting to add in Table 2 the total modelled $k_{OH}$ per campaign to identify better the cases described p9 and quantify the under or overestimation mentioned P9 L2-3. A graph with the reactivity modelled *vs* reactivity calculated and measured would be useful (in the SI?). For example, for the 14 cases with an OH reactivity underestimated significantly by the model, does it correspond to similar missing reactivity with the calculated reactivity?

An additional column for the total modelled $k_{OH}$ was added to Table 2.

Plots of modelled reactivity *vs* observed and calculated reactivity were added in the Supplementary Material. Generally, the modelled reactivity is in better agreement with the calculated reactivity than the observed reactivity, even though the model still underestimates the calculated reactivity in urban and suburban environments. This can be mainly accounted for in terms of the reactivity arising from NMHCs, as explained in the text.

As Figure 2 was changed to address the following comment, the discussion on the agreement between modelled and observed reactivity was amended to reflect the new information provided by the new version of Figure 2.

(2) P8: similarly, in Figure 2, it would be useful to add the calculated reactivity including the contribution of the species used in Figure 3 for the calculated and the modelled reactivity. Even if the information is redundant with the Figure 3, the different presentation will help to better

identify the different types of environments. The uncertainty varies from one instrument to another one and the same one is used here and in the whole document, please justify this choice.

We changed Figure 2 to show the calculated reactivity from measured species as well as the reactivity from reaction intermediates (when available) and the missing reactivity. We have also included a version of Figure 2 with the speciation of the reactivity (hence incorporating the information in Figure 3) in the Supplementary Material as Figure S5. As the reviewer suggested, this figure offers an effective way to distinguish the different environments: urban sites are dominated by $NO_x$ and NMHCs; remote sites by biogenic VOCs (mainly isoprene and its oxidation products), with suburban environments sitting somewhere in between the previous two. The text between Figures 2 and 3 (as well as the caption of Figure 2) has been amended to reflect this change.

The error bars in Figure 2 (and also in Figure 4) have been amended to reflect the different uncertainties of the instruments used in each campaign.

(3) A short discussion on the different techniques used to measure the OH reactivity and the potential impact on the measurements in the different campaigns should be added.

We have added some additional text on page 2 to describe the main techniques used to measure $k_{OH}$ in the field, however we feel that a too detailed account would detract from the main objectives of the manuscript. The reader is referred to two recent works (Yang et al., 2016 and Fuchs et al., 2017) in which the experimental techniques are extensively reviewed.

(4) P9, Figure 3: the title used for the x axis is not appropriate and confusing, I would change it for "calculated reactivity from measured species"

Amended (the $y$-axis label was also amended).

(5) P10, it is mentioned that "it is difficult to establish whether the differences between observed and modelled OH sinks arise from misrepresenting emissions or abundances of the hydroxyl radical itself without comparing modelled and observed [OH], and measurements of the OH concentrations are only available for a small subset of the campaigns considered here." From these campaigns, at least, wouldn't it be possible to provide a "most probable" reason for the difference?

A correlation plot of modelled *vs* observed [OH] was added in the Supplementary Material for those campaigns that measured OH as well as the total reactivity and the individual OH sinks. In a couple of cases in which the model overestimated [OH] by roughly a factor of six (BEARPEX09 and CABINEX), the modelled isoprene concentrations were approximately a factor of two lower than the observations in both cases. There are no OH measurements available for the campaigns that exhibited the largest disagreement between observations and model (namely, ATTO), but analysis of OH measurements in Amazonia from different campaigns (see response to reviewer 2) indicate that the model might underrepresent OH in these locations, hence resulting in higher isoprene and VOCs than in the observations. This behaviour is illustrated in Figure R1 in the response to reviewer 2. The text on pages 10-12 has been amended accordingly.

"A correlation plot of modelled against observed [OH] is given in the Supplementary Material (Figure S6) for those campaigns that measured OH as well as the total reactivity and the individual OH sinks. In a couple of cases in which the model overestimated [OH] by roughly a factor of six (BEARPEX09 and CABINEX), the modelled isoprene concentrations were approximately a factor of two lower than the observations in both cases."

(6) P11 L8: the difference between modelled and measured NO concentration should be modulated considering the uncertainty and the LOD of the instrument.

The NO instrument used for the ATTO measurements (Ecophysics chemiluminescence analyser, model CLDTR-780) has a LOD = 0.05 ppb and uncertainty < 5% (as reported by Williams et al., *Atm. Env.*, 2016). Even in the light of the measurement uncertainty, the observed [NO] is considerably larger than in the model. We have added the measurement uncertainty to the text for clarity. We have also added the uncertainty in the isoprene measurement (as reported by Yanez-Serrano et al., *Atm. Chem. Phys.*, 2015) at the beginning of the same paragraph.

(7) P11 L22: even if the use of additional species and their intermediates provided different results with most of the time a remaining missing reactivity, it would be interesting to see at the global scale the effect of considering that in complement to the use of X which has the disadvantage of being a unique species, with a unique behavior at the global scale.

This approach, while feasible for box models used to interpret the results of the individual field campaigns, would be extremely burdensome for a global model like UM-UKCA. It is still an interesting area, worth investigating in future studies.

(8) P15: the Figure 5 shows simulated missing reactivity up to 100 $s^{-1}$, which is a lot higher than the highest one observed. Could it be commented (due to the model or to the measurement, also based on the potential underestimation of the OH reactivity in specific environments)?

The vast majority of the missing reactivity values plotted in Figure 5 are below 10 $s^{-1}$ (87% of all non-zero entries), and the near totality are below 50 $s^{-1}$ (99.8%).

Values of the missing reactivity higher than 50 $s^{-1}$ are only found in 12 grid cells over the whole globe in DJF and in 15 grid cells JJA in Figure 5. Upon closer inspection, these correspond to areas of high anthropogenic emissions (principally large urban areas), listed in the table below for the JJA plot in Figure 5. For the majority of these entries the missing reactivity is dominated by large contributions from the highly-correlated organic and black carbon emissions from biofuels (OC and BC biofuel emissions in Table 3 in the manuscript). However in a small number of cases (Caracas, Dubai, Kuwait City) the missing reactivity appears dominated by emissions related to the oil refinery industry (propane, formaldehyde).

| Longitude / °E | Latitude / °N | Location | Missing reactivity from MLR / $s^{-1}$ |
|---|---|---|---|
| 112.5 | -7.5 | Surabaya (East Java), Indonesia | 50.65 |
| 106.875 | -6.25 | Jakarta, Indonesia | 60.61 |
| 292.5 | 10 | Caracas, Venezuela | 58.27 |
| 292.5 | 11.25 | Caracas, Venezuela | 56.21 |
| 106.875 | 21.25 | Hanoi, Vietnam | 56.37 |
| 90 | 23.75 | Dhaka, Bangladesh | 81.36 |
| 56.25 | 25 | Dubai, UEA | 94.30 |
| 90 | 25 | Brahmaputra river, Bangladesh | 67.12 |
| 48.75 | 28.75 | Kuwait City, Kuwait | 66.17 |
| 48.75 | 30 | Kuwait/Iraq/Iran border, North Persian Gulf | 85.46 |
| 69.375 | 41.25 | Tashkent, Uzbekistan | 60.37 |
| 26.25 | 45 | Bucharest, Romania | 62.71 |
| 28.125 | 47.5 | Chisinau, Moldova | 56.93 |
| 37.5 | 56.25 | Moscow, Russia | 99.99 |
| 30 | 60 | St Petersburg, Russia | 91.78 |

We believe these high values are ultimately a result of the MLR approach used in this work. A paragraph describing the distribution and magnitude of the modelled missing reactivity across the globe has been added to Section 4.1 (after Figure 4 and before Table 3).

"Overall, the modelled missing reactivity obtained from the multiple linear regression had values other than zero in 23 % of the surface grid cells in DJF and in 32 % of the grid cells in JJA. Of all the non-zero values plotted in Figure 5, 57 % are below 1 $s^{-1}$, 77 % below 5 $s^{-1}$, 87 % are below 10 $s^{-1}$ and 99.8 % are below 50 $s^{-1}$. Only a very small number of grid cells have modelled missing reactivities in the range 50-100 $s^{-1}$ (12 grid cells in DJF and 15 in JJA). These regions correspond to areas of high anthropogenic emissions that resulted in large contributions of the strongest predictors (OC and BC biofuels) to the calculated missing reactivity."

(9) P16: I do not understand why the OH reactivity calculated at the first step of the iteration is so overestimated. What can be the assumption(s) done on the calculation of the emission rate of X which could explain this disagreement? How does evolve the concentration of X between the first and the last run?

We believe that the large overestimate in OH reactivity due to X after the first step in the iteration is due to the values of [OH] used in Eq. (2). As stated in the text, the [OH] field is taken from the base run (*i.e.*, in the absence of X). As the introduction of an additional OH sink perturbs the OH field itself (leading to lower OH abundances), the OH field from the base run is itself an overestimate of the OH abundances found when X and OH are in steady state. A sentence describing this was added to the manuscript.

Overall the concentration of X decreases between the first and the last run as shown in Figure R2 below (mean and median [X]). The first iteration shows a very large overestimate, for the reasons described above. The second iteration somewhat over-corrects for the first one and the subsequent ones give more or less a steady mean/median values of [X].
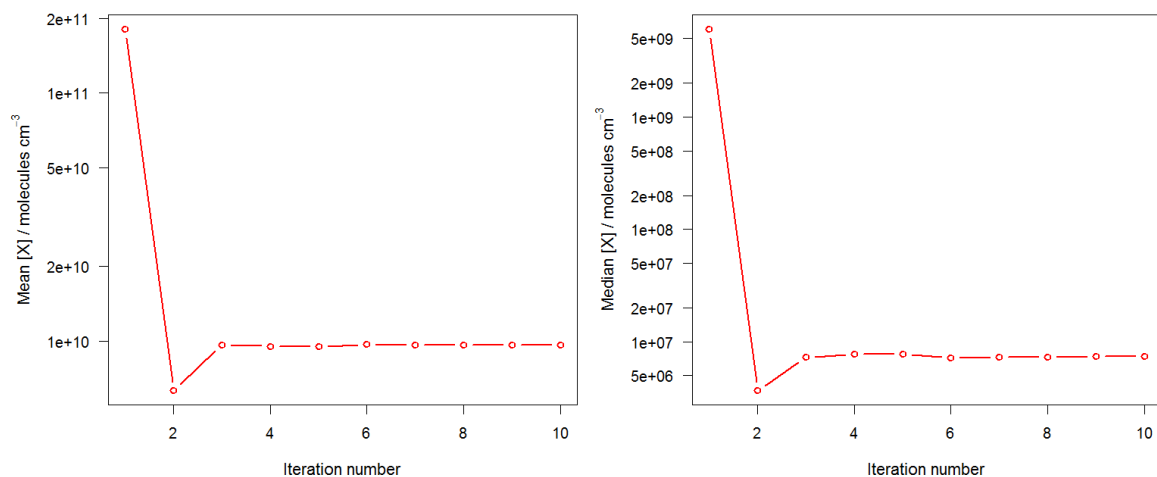
**Figure R2**: Variation of mean (left) and median (right) [X] as a function of iteration number.

(10) P17, L17: wouldn't it be possible to have different runs including different OH recycling to test its influence?

As we mentioned in our reply to Reviewer 2, introducing different OH recycling would involve running the iterative routine to determine the emissions of X in each scenario, as the recycling of OH would ultimately perturb steady state [X] and ultimately $k_3$[X], *i.e.* the modelled missing reactivity. We prefer presenting the work described in the manuscript as an upper limit of the effects of the missing reactivity on the oxidising capacity of the atmosphere. As requested by Reviewer 2, we have re-iterated this in both the abstract and conclusions.

(11) P21: It is not clear in the article what is considered to study the impact of the reaction $RO_2$ + OH on the OH reactivity, first and second generation peroxy radicals produced in the oxidation of isoprene are mentioned but what about the other products and the products of these reactions? Could you clarify this point? It would be useful also to provide (in the SI?) a map of the $RO_2$ and also $HO_2$ concentrations. As the reaction of $HO_2$ + OH is as fast as the $RO_2$+OH, could you specify if this reaction has been added in the reactivity?

A clearer list of the peroxy radicals included in the model was added to the first paragraph of Section 5.1. We have also specified more clearly that the contribution of all $RO_2$ radicals to the total $k_{OH}$ was calculated offline, so that the individual $RO_2$ + OH reactions were not added to the model, as this would require some degree of knowledge of their products. The one exception is of course the reaction of methyl peroxy + OH, which is described in Section 5.2.

Maps of $HO_2$ and total $RO_2$ concentrations were added to the Supplementary Material as Figures S2 and S3 respectively..

The $HO_2$ + OH reaction was included in the main reactivity calculations described in Section 3 of the manuscript. The magnitude of this term is smaller than that calculated for the total $RO_2$, as shown below in Figure R3 (in $s^{-1}$, using the same scale as Figure 10a and 10b).
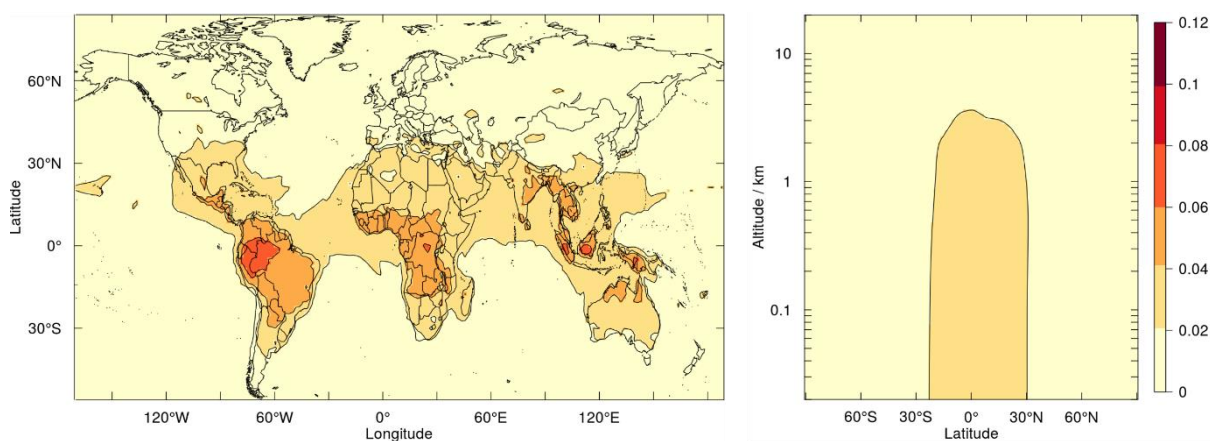


**Figure R3**: Annual mean reactivity from the $HO_2$ + OH reaction in $s^{-1}$.

(12) P23: as mentioned previously, even if of high interest, the last part of the article, on the impact of the branching ratios for the reaction $CH_3O_2$ + OH seems to be decoupled from the other parts of the article dedicated to OH reactivity. Indeed, the aim of this study is to determine the impact of the reaction on the $HO_2$, $CH_3O_2$ and methanol concentrations but without further analysis on the OH reactivity. A part dedicated to the $RO_2$ + OH and the impact of their products on the reactivity, including the different $RO_2$ would fit better in the article than the part only based on the change in the concentration of the products of $CH_3O_2$ + OH.

A paragraph was added at the end of Section 5.2 to better address how the chemistry of $CH_3O_2$ + OH fits within with the wider theme of OH reactivity; figures have also been added in the Supplementary Material to illustrate the changes in $k_{OH}$ brought about by R4 (Figures S13 and S14).

"As the species affected by R4 ($HO_2$, $CH_3O_2$ and $CH_3OH$) are all OH sinks, changes in their concentrations are accompanied by changes in $k_{OH}$. However these are modest ($< 0.25$ $s^{-1}$) in all the scenarios considered in this work, as shown in Figures S13 and S14 in the Supplementary Material. While the reactions of OH with both $HO_2$ and $CH_3O_2$ have large rate constants ($> 1 \times 10^{-10}$ $cm^3$ molecules$^{-1}$ $s^{-1}$), the general low abundance of these species (of the

order of ~$10^8$ molecules cm$^{-3}$, as shown in Figures S2 and S3) results in small changes to the total $k_{OH}$. On the other hand, while some of the changes in methanol concentrations arising from R4 are significant (with increases up to 400 pptv in run 3, corresponding to ~1 ×$10^{10}$ molecules cm$^{-3}$), the very small rate constant of its reaction with OH ($< 1\times 10^{-12}$ cm$^3$ molecules$^{-1}$ s$^{-1}$) leads to a small contributions to $k_{OH}$. These results are consistent with the magnitude of the changes in $k_{OH}$ calculated offline for all RO$_2$ radicals in Section 5.1. It remains to be seen if any of the reaction products of more complex RO$_2$ radicals with OH, or their combination, might have a significant impact on $k_{OH}$."

(13) P25: the change in methanol concentration is only provided in the text whereas it is the main result of this section. It would be useful to provide a figure similar to Figure 11 and 12 but for methanol and for the 3 runs. It would be useful to write in the Legend of Figure 11 and 12 the corresponding run.

Agreed. A figure showing the changes in methanol under the three scenario was added (Figure 13).

The corresponding run for both Figures 11 and 12 was added to the captions.

(14) P25: the conclusion that the branching ratio needed for this channel (0.8) is not possible seems too extreme because the branching ratio for channel 1 (producing HO$_2$) has been determined only at low pressure.

Agreed. As theoretical studies seem to indicate the presence of a termolecular association channel (Müller et al., *Nat. Commun.*, 2016; but also Liu et al., *Chem. Res. Chin. Univ.*, 2017 for ethyl peroxy + OH) leading to the formation of CH$_3$OOOH (which could potentially decompose to CH$_3$OH and O$_2$), we have added a sentence to highlight the need for further characterisation of the branching at ambient pressure.

"However it has to be noted that so far the product branching of R4 has only been measured at low pressure (50 Torr) by Assaf et al. (2017b). Calculations by Müller et al. (2016) suggest the presence of an association channel leading to the formation of a trioxide (CH$_3$OOOH) species, which might potentially decompose to methanol and molecular oxygen. As the stabilisation of association products is generally a pressure-dependent process, it is very important that future studies address the branching of R4 at ambient pressure."

# Global modelling of the total OH reactivity: investigations on the "missing" OH sink and its atmospheric implications

Valerio Ferracci[1,a], Ines Heimann[1], N. Luke Abraham[1,2], John A. Pyle[1,2] and Alexander T. Archibald[1,2]

[1]Centre for Atmospheric Science, Department of Chemistry, University of Cambridge, Lensfield Road, CB2 1EW, UK
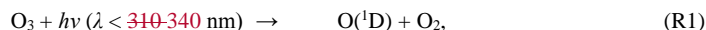[2]National Centre for Atmospheric Science, University of Cambridge, Cambridge, UK
[a]now at: Centre for Environmental and Agricultural Informatics, Cranfield University, College Road, MK43 0AL, UK

*Correspondence to*: Valerio Ferracci (v.ferracci@cranfield.ac.uk~~vf257@cam.ac.uk~~)

**Abstract.** The hydroxyl radical (OH) plays a crucial role in the chemistry of the atmosphere as it initiates the removal of most trace gases. A number of field campaigns have observed the presence of a "missing" OH sink in a variety of regions across the planet. Comparison of direct measurements of the OH loss frequency, also known as total OH reactivity ($k_{OH}$), with the sum of individual known OH sinks (obtained *via* the simultaneous detection of species such as volatile organic compounds and nitrogen oxides) indicates that, in some cases, up to 80 % of $k_{OH}$ is unaccounted for. In this work, the UM-UKCA chemistry-climate model was used to investigate the wider implications of the missing reactivity on the oxidising capacity of the atmosphere. Simulations of the present-day atmosphere were performed and the model was evaluated against an array of field measurements to verify that the known OH sinks were reproduced well, with a resulting good agreement found for most species. Following this, an additional sink was introduced to simulate the missing OH reactivity as an emission of a hypothetical molecule, X, which undergoes rapid reaction with OH. The magnitude and spatial distribution of this sink were underpinned by observations of the missing reactivity. Model runs showed that the missing reactivity accounted for on average 6 % of the total OH loss flux at the surface, and up to 50 % in regions where emissions of the additional sink were high. The lifetime of the hydroxyl radical was reduced by 3 % in the boundary layer, while tropospheric methane lifetime increased by 2 % when the additional OH sink was included. As no OH recycling was introduced following the initial oxidation of X, these results can be interpreted as an upper limit of the effects of the missing reactivity on the oxidative capacity of the troposphere. The UM-UKCA simulations also allowed us to establish the atmospheric implications of the newly characterised reactions of peroxy radicals ($RO_2$) with OH. While the effects of this chemistry on $k_{OH}$ were minor, the reaction of the simplest peroxy radical, $CH_3O_2$, with OH was found to be a major sink for $CH_3O_2$ and source of $HO_2$ over remote regions at the surface and in the free troposphere. Inclusion of this reaction in the model increased tropospheric methane lifetime by up to 3 %, depending on its product branching. Simulations based on the latest kinetic and product information showed that this reaction cannot reconcile models with observations of atmospheric methanol, in contrast to recent suggestions.

1

## 1 Introduction

The removal of the vast majority of trace gases emitted into the atmosphere is initiated by reaction with the hydroxyl radical, OH. OH is primarily formed following the reaction of excited oxygen atoms, $O(^1D)$, originating from the photolysis of ozone at short wavelengths, with water:

5

$$O_3 + h\nu \ (\lambda < \cancel{310}\ 340 \ nm) \ \rightarrow \quad O(^1D) + O_2, \qquad\qquad (R1)$$

$$O(^1D) + H_2O \qquad\qquad \rightarrow \quad 2OH. \qquad\qquad\qquad (R2)$$

OH generated *via* any route other than R1 and R2 is referred to as secondary OH; examples of processes yielding secondary
10   OH include the photolysis of $H_2O_2$ and the reaction of $HO_2$ with NO. Crucially, OH abundance and availability (and consequently the oxidising capacity of the atmosphere) are governed by the balance between OH sources (primary and secondary) and sinks, consisting of the totality of the species that react with OH: these include volatile organic compounds (VOCs), nitrogen oxides ($NO_x$) and many others species, both biogenic and anthropogenic.

In this respect, the total OH loss frequency, also known as the total OH reactivity ($k_{OH}$), is a useful measure of the total amount
15   of OH sinks present in a particular environment. $k_{OH}$ is defined as the pseudo-first order rate constant for OH loss and is equivalent to the inverse of the OH lifetime, $\tau_{OH}$, as shown in Eq. (1):

$$k_{OH} = \sum_{i=1}^{n} k_{OH+X_i}[X_i] = 1/\tau_{OH}, \qquad\qquad (1)$$

20   where $[X_i]$ designates the concentration (usually in molecules $cm^{-3}$) of OH sink $X_i$, and $k_{OH+X_i}$ is the rate constant for the reaction of OH with $X_i$ (usually expressed in $cm^3$ $molecule^{-1}$ $s^{-1}$). It follows from Eq. (1) that, if the atmospheric abundance of all OH sinks is measured, and provided that the rate constants for their reaction with OH are known, $k_{OH}$ can be determined as the sum of the individual sink reactivities.

Over the last two decades, techniques capable of measuring the total OH reactivity *directly*, without the need to quantify
25   individual sinks, have become available: these rely either on direct measurements of the OH decay rate (Di Carlo et al., 2004; Ingham et al., 2009; Kovacs and Brune, 2001) or on the comparative reactivity method (Sinha et al., 2008), in which $k_{OH}$ is determined from the reactivity of a reference species (typically pyrrole). A review (Yang et al., 2016) recently described these techniques in detail, whilst the various instruments developed for direct measurements of $k_{OH}$ have been the subject of an extensive intercomparison (Fuchs et al., 2017). These techniques, when deployed in the field along with instruments for the
30   detection of trace species, have enabled the comparison of direct measurements of the total $k_{OH}$ with the sum of reactivities of the individual OH sinks. In this respect, measurements of the total OH reactivity can be used to test our understanding of tropospheric oxidation: provided that the totality of OH sinks are accounted for and measured, the sum of individual reactivities and the total $k_{OH}$ should agree.

2

Field campaigns across the globe have however highlighted discrepancies between these two approaches, with most measurements reporting values of the total $k_{OH}$ higher than the sum of the individual reactivities (Yang et al., 2016). These results indicate that a fraction of the total OH reactivity cannot be accounted for; this is often referred to as "missing" reactivity and attributed to a "missing" OH sink. The magnitude of the observed missing reactivity in the literature varies depending on

5 the geographic location of the measurement and the season, but could amount to as much as 80% of the total $k_{OH}$ as measured by Nölscher et al. (2016) in the Amazon rainforest. ~~(Nölscher et al., 2016).~~

Many studies have attempted to identify the missing sink: while some authors have attributed the missing reactivity to the presence of primary emissions that escaped detection (Holzinger et al., 2005; Kaiser et al., 2016; Sinha et al., 2010), others have pointed at the reactions of OH with short-lived oxidation intermediates (Hansen et al., 2014; Nakashima et al., 2014),

10 which are notoriously challenging to measure in the field. Other studies still, including that by Nölscher et al. (2016) in the Amazon rainforest, attributed the missing reactivity to both unidentified biogenic emissions and photooxidation products.

An exponential temperature dependence of the missing reactivity was observed during two campaigns carried out in the same North American forest, consistent with either primary biogenic emissions (Di Carlo et al., 2004) or with their oxidation products (Hansen et al., 2014). Some of the campaigns carried out in other forested environments also observed a similar trend

15 (Kaiser et al., 2016; Mao et al., 2012; Zannoni et al., 2017), whereas others found no evidence for this correlation (Ren et al., 2006b; Sinha et al., 2010).

In an attempt to account for the additional OH reactivity potentially arising from unmeasured oxidation intermediates, a number of studies invoked box modelling to determine the abundance of these species and their contribution to $k_{OH}$. These efforts have been met with mixed results: while some managed to reconcile the total $k_{OH}$ with the sum of reactivities once the oxidation

20 intermediates were taken into account (Whalley et al., 2016), others obtained different degrees of improvement on the agreement between the two, leaving different fractions of $k_{OH}$ still unaccounted for (Edwards et al., 2013; Elshorbany et al., 2012; Kaiser et al., 2016; Kovacs et al., 2003; Lee et al., 2009; Lou et al., 2010; Mao et al., 2012; Mogensen et al., 2011; Yang et al., 2017).

Regardless of its identity, the very presence of an additional OH sink would lead to shorter $\tau_{OH}$ in the real atmosphere than in

25 current models; this would, in turn, lead to longer lifetimes for species that are primarily removed by reaction with OH, such as the vast majority of biogenic and anthropogenic VOCs as well as high-impact greenhouse gases such as methane. Given the complex interactions of the OH radical in the photochemistry of the troposphere, global atmospheric modelling provides a powerful tool to investigate potential candidates for the missing sink, as well as to establish its impacts on the oxidising capacity of the lower atmosphere.

30 So far only two studies have attempted global modelling of $k_{OH}$: the focus of these works was either modelling the global OH budget (Lelieveld et al., 2016) or that of the total reactive organic carbon (Safieddine et al., 2017). Detailed comparisons of the modelled $k_{OH}$ with observations or the missing reactivity were not addressed.

This work will make an extensive comparison between modelled $k_{OH}$ and observations, with particular attention to the contribution of individual sinks to the total OH reactivity. Section 3 describes our base integration and discusses a comparison

3

with observations.    Sections 4 and 5 tackle the challenge of modelling the missing reactivity using two approaches. Firstly (section 4), we introduce an additional OH sink, the geographical distribution and abundance of which are underpinned by the observations of missing reactivity available.  Secondly (Section 5), we include in the model the reactions of peroxy radicals ($RO_2$) with OH. As this novel $RO_2$ + OH chemistry has been characterised in the laboratory only in recent years, the role of $RO_2$ as an OH sink may have been overlooked (Fittschen et al., 2014).  The implications of both approaches for the oxidising capacity of the atmosphere are then discussed.


## 2 Method

State-of-the-art chemistry-climate models have become an extremely important tool in the study of atmospheric science, allowing the exploration of a number of global scenarios with an unprecedented level of detail.  However recent studies have shown that the way the chemistry is implemented in the model (*e.g.*, different oxidation schemes for complex emitted species) can have a major impact on crucial properties of the atmosphere such as the formation of tropospheric ozone (Squire et al., 2015). It is therefore important to validate these models against observations of relevant chemical species whenever possible. In this work, a global chemistry-climate model, the Met Office's Unified Model with the United Kingdom Chemistry and Aerosols scheme, UM-UKCA version 8.4, (Abraham et al., 2012) was used to investigate the total OH reactivity, $k_{OH}$. The model was run in the N96-L85 configuration, providing a horizontal resolution of 1.875° in longitude $\times$ 1.25° in latitude on 85 vertical levels from the surface up to a height of 85 km.

UM-UKCA was run with the Chemistry of the Stratosphere and Troposphere (CheST) scheme, combining previous tropospheric (O'Connor et al., 2014) and stratospheric (Morgenstern et al., 2009) chemical schemes as used by Banerjee et al. (2014). The scheme includes 83 advected chemical tracers and 310 photochemical reactions, describing the $O_x$, $HO_x$ and $NO_x$ chemical cycles and the oxidation of CO, methane, ethane, propane and isoprene (Archibald et al., 2010, 2011).

Reaction rate coefficients were based on recommended values from the International Union of Pure and Applied Chemistry (IUPAC) Subcommittee for Gas Kinetic Data Evaluation (http://iupac.pole-ether.fr~~http://www.iupac-kinetic.ch.cam.ac.uk~~), the JPL-NASA Evaluation of Chemical Kinetics and Photochemical Data for Use in Atmospheric Studies (Burkholder et al., 2015) and the Master Chemical Mechanism, MCM v3.2 (Jenkin et al., 2015) , *via* the website: http://mcm.leeds.ac.uk/MCM.

Surface emissions for the years 2000-2005 of nine trace gas species ($NO_x$, methane, CO, formaldehyde, ethane, propane, acetone, acetaldehyde and isoprene) were included based on Banerjee et al. (2014)  as well as multi-level aircraft emissions for $NO_x$.  Isoprene emissions were based on MEGAN (Guenther et al., 2006).  The aerosol scheme also included emissions of organic carbon (OC, from both fossil fuels and biofuels), black carbon (BC, also from both fossil fuels and biofuels), monoterpenes, $SO_2$, dimethyl sulphide and biogenic methanol.

The model runs used in this work are described in Table 1. They comprise a Base run, discussed in detail in Section 3, a run with an imposed sink to account for the missing $k_{OH}$ ('X + OH run'), whose results are described in Section 4, and three additional experiments to explore the possible role of reactions of peroxy radicals. In each run, the model was run for five years, with one year spin-up time.

A number of diagnostics widely used in models to evaluate the oxidising capacity of the troposphere, such as methane lifetime with respect to tropospheric loss *via* reaction with OH ($\tau_{CH_4}$), OH lifetime ($\tau_{OH}$) and tropospheric ozone burden, were calculated for each model scenario. $\tau_{CH_4}$ was calculated in accordance with Lawrence et al. (2001), with the troposphere defined as the domain below 250 hPa. This is also consistent with the convention used in the Atmospheric Chemistry and Climate Model Intercomparison Project (ACCMIP) (Naik et al., 2013; Voulgarakis et al., 2013). The same definition of the troposphere was used here in the calculation of tropospheric reaction fluxes and $\tau_{OH}$. For the calculation of the tropospheric ozone burden, the troposphere was defined as the domain in which the ozone mixing ratio was below 150 ppbv (or nmol/mol), in accordance with previous studies and model intercomparisons (Ehhalt et al., 2001; Stevenson et al., 2006; Young et al., 2013). Species lifetimes were calculated by dividing the species burden by their removal rate.

**Table 1: Summary of the model runs described in this work**

| Run name | Chemistry scheme | Description |
|---|---|---|
| Base run | CheST | This run provides a means to assess how well the model captures known OH sinks, *i.e.* the individual reactivities in the sum term of Eq. (1). It also provides a point of comparison for the runs that follow. The Base run is discussed in Section 3. |
| X + OH run | CheST with R3 | An additional OH sink, species X, is introduced in the model to account for the missing $k_{OH}$. This run is described in Section 4. |
| $CH_3O_2$ + OH run 1 | CheST with R4 | The multi-channel reaction of methyl peroxy radicals ($CH_3O_2$) with OH was included in the chemistry scheme with branching ratios $\alpha = 1$, $\gamma = 0$ [a]. This run is described in Section 5.2. |
| $CH_3O_2$ + OH run 2 | CheST with R4 | Same as $CH_3O_2$ + OH run 1 but with branching ratios $\alpha = 0.8$, $\gamma = 0.2$ [a]. This run is described in Section 5.2. |
| $CH_3O_2$ + OH run 3 | CheST with R4 | Same as $CH_3O_2$ + OH run 1 but with branching ratios $\alpha = 0.6$, $\gamma = 0.4$ [a]. This run is described in Section 5.2. |
| **Notes**: | | |

**3 Comparison of modelled $k_{OH}$ and known OH sinks with observations**

The modelled $k_{OH}$ at the surface, obtained from the Base run using the standard CheST scheme, is shown in Figure 1. The total OH reactivity is lowest over oceans and remote deserts ($< 1$ s$^{-1}$), highest over tropical forests ($> 10$ s$^{-1}$) and somewhat

5 intermediate between these values in urban influenced areas. This global distribution and magnitude of $k_{OH}$ are in reasonably good agreement with those calculated in previous modelling studies (Lelieveld et al., 2016; Safieddine et al., 2017). For reference, the modelled abundances of OH, HO$_2$ and RO$_2$ radicals in the base run are shown in Figures S1-S3 in the Supplementary Material.
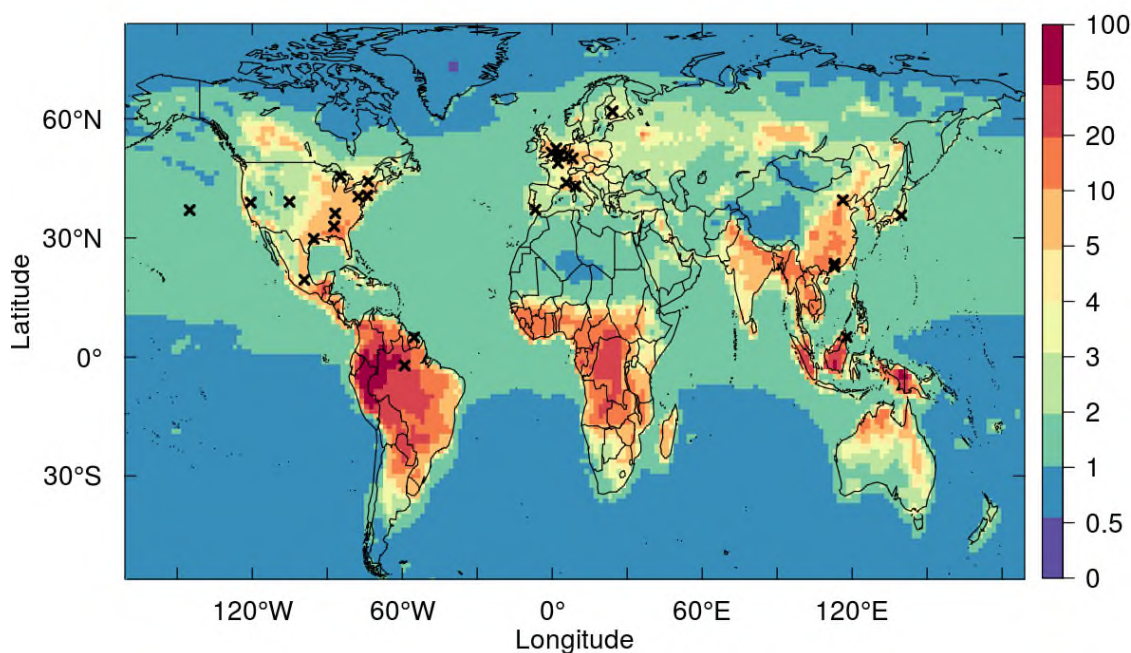


10 **Figure 1: Annual mean of the total OH reactivity (in s$^{-1}$) calculated in the Bbase run at the surface. Crosses indicate sites of field campaigns against which the model is compared.**

As described in Section 1, many measurements of $k_{OH}$ have been performed over the last two decades, with an exhaustive summary presented in a recent review (Yang et al., 2016). Only measurements of $k_{OH}$ and its speciation performed over

15 reasonably long timescales ($\geq$ 1 week) and covering the full diurnal variation of $k_{OH}$ and the OH sinks were considered in this

6

work, in order to minimise biases due to day-to-day variability and to obtain a meaningful comparison with the model. A small number of field campaigns measured only the total $k_{OH}$ and not the abundance of the individual sinks, therefore precluding the quantification of the missing reactivity or any further analysis on the speciation of $k_{OH}$ (Michoud et al., 2015; Ren et al., 2005; Sinha et al., 2008, 2012). For these reasons, 27 field measurements of the total $k_{OH}$ and of the individual OH sinks were used in the analysis described in this work; these are summarised in Table 2, where the values of the total $k_{OH}$ and of the missing reactivity, averaged over the whole duration of each campaign, are reported. These observations were performed in a variety of environments, the vast majority of which were situated in the Northern Hemisphere (as shown in Figure 1). Measurement sites can be grouped into suburban (6 measurements), urban (10 measurements) and remote areas (11 measurements).

**Table 2: Total observed OH reactivity and missing reactivity from field campaigns. These values represent averages over the whole duration of each campaign. Measurement sites are grouped into three categories (suburban, urban, remote environments respectively).**

| | Location (Campaign) | Total observed $k_{OH}$/ $s^{-1}$ * | Missing $k_{OH}$/ $s^{-1}$ ** | Missing $k_{OH}$ after the inclusion of model intermediates / $s^{-1}$ *** | $k_{OH}$ from UKCA base run / $s^{-1}$ | Reference |
|---|---|---|---|---|---|---|
| Suburban | Whiteface Mountain, USA (PMTACS-NY2002) | 5.40 | 0.02 | | 7.1 | (Ren et al., 2006b) |
| | Weybourne, UK (TORCH-2) | 4.6 | 2.0 | 1.3 | 7.4 | (Lee et al., 2009) |
| | Yufa, China (CAREBeijing-2006) | 19.7 | 2.2 | | 10.5 | (Lu et al., 2010) |
| | Backgarden, China (PRIDE-PRD) | 31.4 | 15.7 | 6.3 | 16.2 | (Lou et al., 2010) |
| | Jülich, Germany (HOx Comp) | 8.6 | 3.2 | 2.5 | 7.1 | (Elshorbany et al., 2012) |
| | Heshan, China | 30.6 | 9.8 | 5.3 | 5.4 | (Yang et al., 2017) |
| | Ersa, Corsica (CARBOSOR-ChArMeX) | 5.6 | 2.3 | | 5.2 | (Zannoni et al., 2017) |
| Urban | Nashville, USA (SOS) | 11.0 | 3.8 | | 14.8 | (Kovacs et al., 2003) |
| | New York, USA (PMTACS-NY2001) | 18.8 | 0.7 | | 15.4 | (Ren et al., 2003a, 2003b) |
| | New York, USA (PMTACS-NY2004) | 25.1 | 4.0 | | 9.1 | (Ren et al., 2006a) |
| | Mexico City, Mexico (MCMA-2003) | 47.5 | 14.3 | | 5.2 | (Shirley et al., 2006) |
| | Houston, USA (TexAQS) | 9.4 | 0.4 | | 8.7 | (Mao et al., 2010) |
| | Houston, USA (TRAMP2006) | 12.24 | 0.03 | | 8.9 | (Mao et al., 2010) |
| | Paris, France (MEGAPOLI) | 40.3 | 22.8 | | 4.6 | (Dolgorouky et al., 2012) |

| | | | | | |
|---|---|---|---|---|---|
| Lille, France | 7.4 | 0 | | 4.8 | (Hansen et al., 2015) |
| London, UK (ClearfLo) | 18.1 | 5.9 | 2.7[†] | 6.0 | (Whalley et al., 2016) |
| Michigan, USA (Prophet2000) | 7.8 | 2.6 | | 4.8 | (Di Carlo et al., 2004) |
| Hyytiälä, Finland (BFORM) | 8.6 | 3.9 | | 6.3 | (Sinha et al., 2010) |
| Hyytiälä, Finland (HUMPPA-COPEC2010) | 11.5 | 8.9 | | 6.6 | (Nölscher et al., 2012) |
| Rocky Mountains, USA (BEACHON-SRM08) | 6.7 | 2.1 | | 3.5 | (Nakashima et al., 2014) |
| Michigan, USA (CABINEX) | 11.6 | 6.3 | | 4.8 | (Hansen et al., 2014) |
| Amazon, Brazil (ATTO) dry season | 49.6 | 35.8 | | 35.8 | (Nölscher et al., 2016) |
| Amazon, Brazil (ATTO) wet season | 8.3 | 3.9 | | 43.4 | (Nölscher et al., 2016) |
| Haute Provence, France (CANOPEE) | 17.9 | 1.1 | | 5.6 | (Zannoni et al., 2016) |
| Borneo, Malaysia (OP3) | 15.3 | 10.2 | 5.8 | 15.3 | (Edwards et al., 2013) |
| Alabama, USA (SOAS) | 19.4 | 4.9 | 3.6 | 21.1 | (Kaiser et al., 2016) |
| California, USA (BEARPEX09) | 17.3 | 7.1 | 3.5 | 6.9 | (Mao et al., 2012) |
| North Pacific (INTEX-B) | 4.0 | 2.2 | | 1.1 | (Mao et al., 2009) |

(The first two rows are in a different category; "Remote" labels the rows from Michigan (Prophet2000) through North Pacific (INTEX-B).)

**Notes:**

* these values are the mean of the total $k_{OH}$ measured over the whole duration of each field campaign

** missing reactivity calculated as the difference between the total $k_{OH}$ and the sum of the individual reactivities arising *exclusively* from measured OH sinks

*** missing reactivity calculated as the difference between the total $k_{OH}$ and the sum of the individual reactivities arising from *both* measured OH sinks *and* intermediates modelled in the particular studies referenced

[†]the addition of unidentified compounds observed by GC×GC-FID reduced the missing reactivity further to only ~1.1 s$^{-1}$
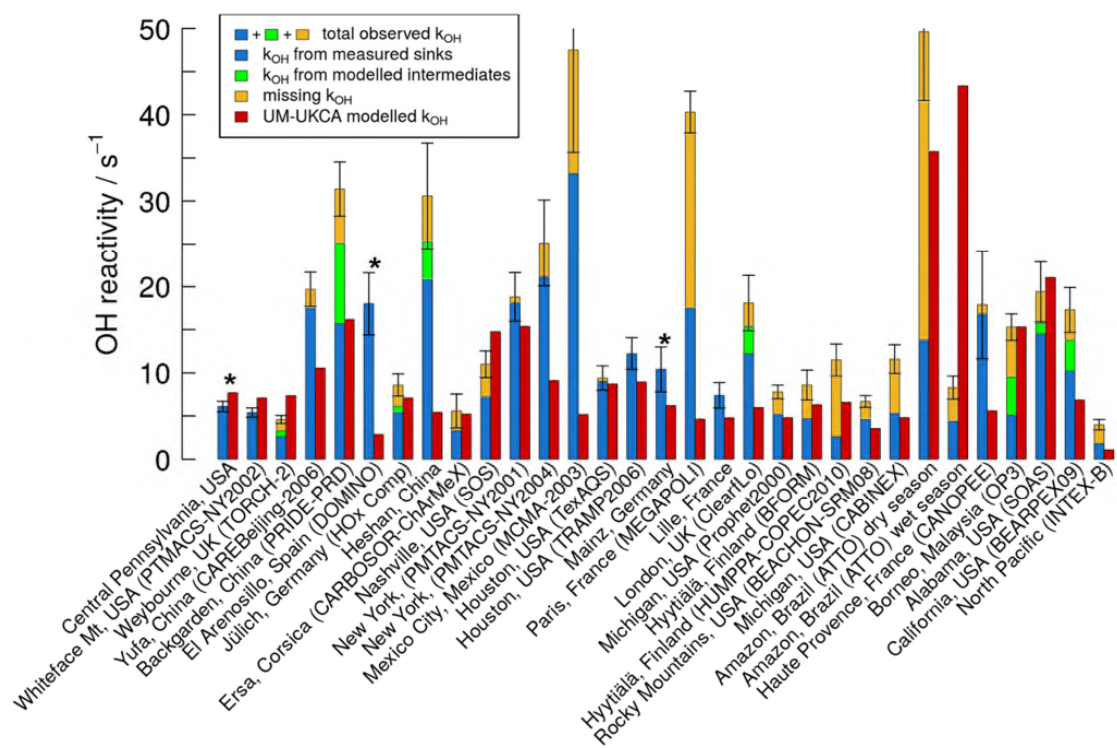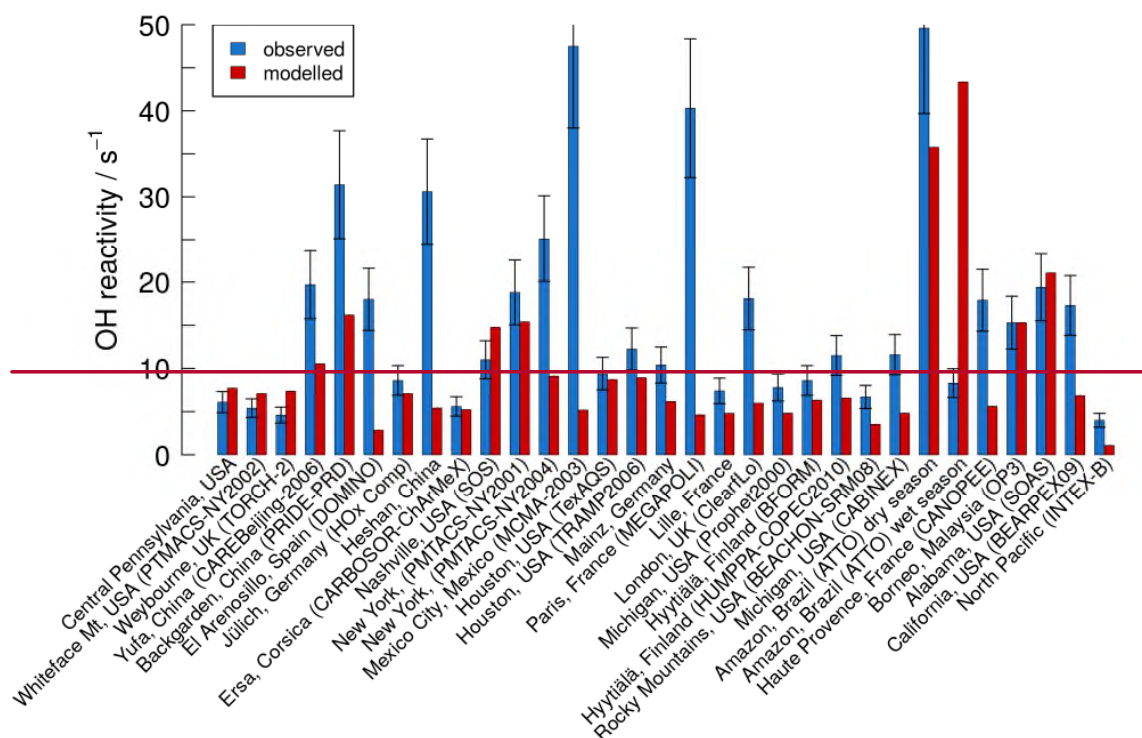
**Figure 2: Comparison of the average observed $k_{OH}$ with modelled $k_{OH}$.** The total $k_{OH}$ measured in each field campaign is represented by the sum of the blue, green and yellow bars. Blue bars represent the OH reactivity accounted for by measured OH sinks, green bars represent the OH reactivity accounted for by modelled reaction intermediates (only available for some of the studies presented here) and yellow bars represent the OH reactivity which is unaccounted for (*i.e.*, the missing reactivity). Red bars represents the total OH reactivity calculated from the modelled data in the UM-UKCA base run. Error bars represent the uncertainties (at the $1\sigma$ level) (20%, relative) are commensurate with the~~in~~ the total $k_{OH}$ measurement. Asterisks indicate campaigns in which only the total $k_{OH}$ was measured, without detection of the individual OH sinks. In these cases the blue bar represents the total observed $k_{OH}$. A version of this plot detailing the speciation of both observed and modelled reactivity is given in the Supplementary Material in Figure S5.~~measurement uncertainty of the observed $k_{OH}$.~~

Observed $k_{OH}$ is compared to that simulated by UM-UKCA for the same longitude, latitude and month in Figure 2.~~-~~ (and in Figure S4 in the Supplementary Material as a scatter plot). The total ~~O~~observed $k_{OH}$ in Figure 2 is made up of~~by~~ contributions from the measured OH sinks, from modelled intermediates (only available for some of the field campaigns presented here) and from reactivity that is unaccounted for by known OH sinks, *i.e.* the missing reactivity. The total modelled reactivity is expected to be in good agreement with that arising from measured sinks, but this was only the case (to within ~20 %) in 12 out of 28 cases. Of the remaining 16 campaigns, the model underestimated the reactivity from measured sinks in 9 cases and overestimated it in 7. ~~and modelled $k_{OH}$ agree within 20 % of one another in 12 out of 27 cases. Of the remaining 15 campaigns, the model underestimates $k_{OH}$ in 14 cases and overestimates it in only one. That the model underestimates the total $k_{OH}$ is not a surprise; if the missing sink was an overlooked primary emission, it would not be accounted for in the model, whereas if the~~

missing reactivity arose from oxidation intermediates, these would also be underestimated by the model, as the oxidation schemes of large VOCs (*e.g.*, isoprene) are somewhat simplified in the CheST scheme compared to a complete mechanism, and also because only a limited number of VOCs are emitted in the model compared to the atmosphere. In the one case in which the model significantly overestimated $k_{OH}$ compared to the measurements (Amazon ATTO, during the wet season), this was mainly the result of high levels of isoprene in the model (see below).

It is therefore Even in the cases in which the model and observations are in good agreement, it is important to ascertain that the modelled OH reactivity is indeed the result of the same sinks observed in the field. F; for this purpose, individual reactivities measured in each campaign provide a large amount of information that can be used to establish how well the model captures the speciation of $k_{OH}$. This is shown in Figure 3, where the modelled reactivities from the known OH sinks are plotted against those measured in the field, and in Figure S5 in the Supplementary Material.

11
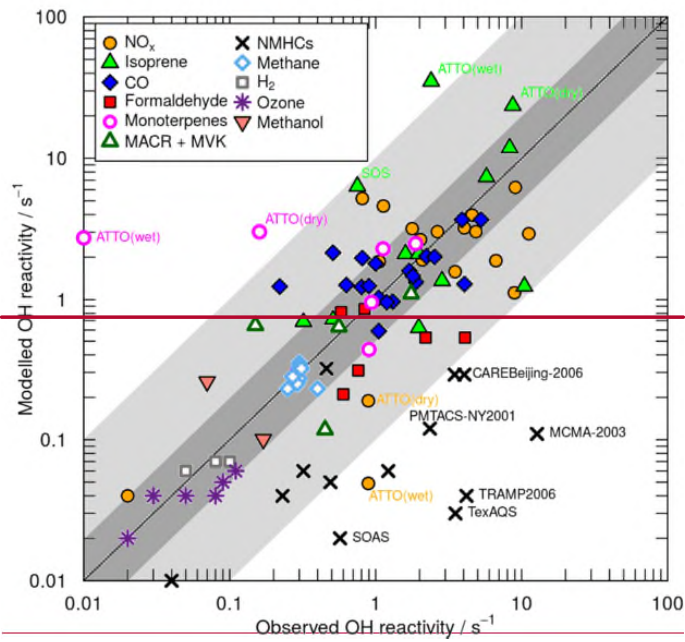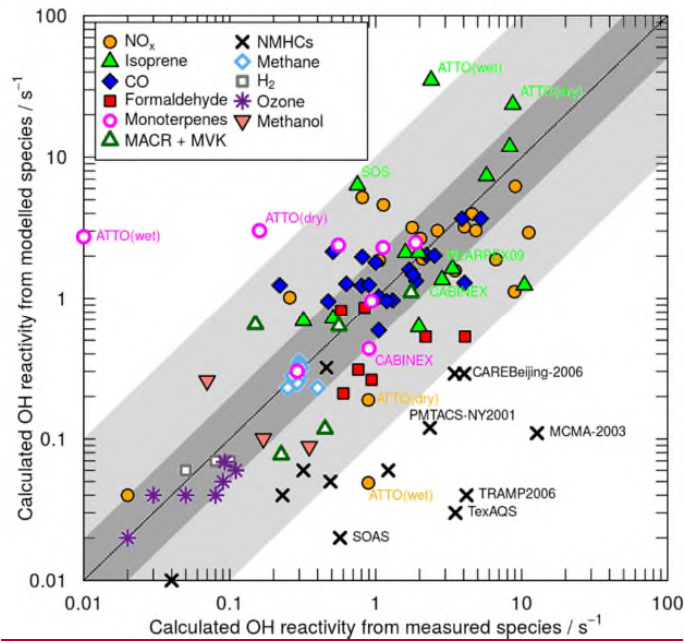
**Figure 3: Scatter plot of modelled OH reactivity arising from known OH sinks against measurements. Also shown is the 1:1 line (solid black line) as well as the factor-of-2 and factor-of-10 deviations from it (dark grey and light grey areas respectively). Specific data points that are discussed in the text are labelled with the name of the field campaign in which those particular measurements were performed.**

5

Figure 3 and Figure S5 provides a useful guide on the magnitude of the contribution of different OH sinks to the total $k_{OH}$. The main contributors to $k_{OH}$, with reactivities ranging between 1 and 10 $s^{-1}$, are isoprene in forested environments and $NO_x$, CO, formaldehyde and non-methane hydrocarbons (NMHCs, indicating primarily alkanes and alkenes) in urban environments. At the other end of the spectrum, species such as methane, ozone and hydrogen only give rise to small contributions ($< 1 \ s^{-1}$) to

10 the total $k_{OH}$.

Overall more than half (53 %) of the reactivities calculated from modelled sinks agree with observations within a factor of two, and the vast majority (88 %) within a factor of ten. We see overall a reasonably good agreement between modelled and observed sinks, albeit with some scatter within an order of magnitude. The main source of discrepancy between modelled and

15 observed individual reactivities are differences in the number densities of the OH sinks ($[X_i]$ in Eq.(1)) and not the temperature-dependent rate constants, as temperature differences between the model and the measurements only have a minor effect on the rate constants used to calculate the reactivities. The abundance of each individual OH sink species is determined by the balance between its sources (*e.g.*, emissions) and sinks (largely, reaction with OH). It is however difficult to establish whether the differences between observed and modelled OH sinks arise from misrepresenting emissions or abundances of the hydroxyl

20 radical itself without comparing modelled and observed [OH], and measurements of the OH concentrations are only available for a small subset of the campaigns considered here. A correlation plot of modelled against observed [OH] is given in the Supplementary Material (Figure S6) for those campaigns that measured OH as well as the total reactivity and the individual OH sinks. In a couple of cases in which the model overestimated [OH] by roughly a factor of six (BEARPEX09 and CABINEX), the modelled isoprene concentrations were approximately a factor of two lower than the observations in both

25 cases.

Figure 3 provides a useful guide on the magnitude of the contribution of different OH sinks to the total $k_{OH}$. The main contributors to $k_{OH}$, with reactivities ranging between 1 and 10 $s^{-1}$, are isoprene in forested environments and $NO_x$, CO, formaldehyde and non-methane hydrocarbons (NMHCs, indicating primarily alkanes and alkenes) in urban environments. At

30 the other end of the spectrum, species such as methane, ozone and hydrogen only give rise to small contributions ($< 1 \ s^{-1}$) to the total $k_{OH}$.

The speciation of the total OH reactivity shown in Figure 3 allows us to investigate the reasons for the discrepancy between some of the modelled $k_{OH}$ and observations highlighted in Figure 2. For instance, the disagreement between modelled and

35 observed $k_{OH}$ in some urban environments (notably Mexico City, wintertime New York, Houston and Beijing/Yufa) is almost

13

entirely attributable to the underrepresentation of NMHCs in the model. This can be accounted for in terms of species lumping. As with many state-of-the-art models, instead of adding numerous hydrocarbons to the emission and chemistry schemes, the heavier alkanes and alkenes were lumped into the emission fields of ethane and propane, weighted by carbon number. We can see that lumping serves as a reasonable approximation for the representation of the abundance of some carbon-containing species (such as CO and formaldehyde, the ultimate products of hydrocarbon oxidation, which are in reasonable agreement with observations as shown in Figure 3 and also in Figure S~~1~~7 in the Supplementary Material for CO). However lumping introduces an additional complication when the OH reactivity of NMHCs is calculated. As the reactivity is defined as the product of the rate constant for the reaction of the NMHCs with OH and the number density of the NMHCs, and as the rate constants for the reaction of OH with ethane and propane are 1-2 orders of magnitude smaller than those of OH with higher alkanes (C $\geq$ 4) and alkenes (C $\geq$ 2), lumping leads to an underestimate of the same magnitude in the reactivity of the NMHCs.

Figure 3 also offers an explanation for the ~~only~~ instances in which the model significantly over predicted $k_{OH}$. For example, ~~T~~the abundance of isoprene measured during the wet season of the ATTO campaign in the Amazon (~1 $\pm$ 0.1 ppbv, or nmol/mol, in March 2013) was more than an order of magnitude lower than that predicted by the model for the same time of the year (~14.6 ppbv).  As discussed above, this might arise from either overestimated isoprene emissions or from underestimated OH abundances in the model.  As OH concentrations were not measured during the ATTO campaign, a direct comparison of modelled and observed [OH] is not possible. However [OH] measurements from campaigns carried out in neighbouring parts of the Amazon (Liu et al., 2016) and in the Suriname rainforest (Martinez et al., 2010) might help address this point. Indeed the model underestimates [OH] by almost a factor of four on average in both cases, although it is worth noting that [OH] measurements from Liu et al. (2016) only cover ~7 hours on a single day, while the GABRIEL campaign in Suriname consisted of airborne measurements, and only the OH data for the boundary layer were considered for comparison with the model. It may also be indicative of underrepresented [OH] in model that ~~However~~ the abundance of other short-lived OH sinks in the ATTO campaign is also overestimated by the model; notably, the observed concentration of monoterpenes (reported to be below the detection limit of the PTR-MS used by Nölscher and co-workers, and here approximated to 0.01 ppbv) was much lower than in the model (2.2 ppbv). Underrepresented OH in the model might arise from ~~This might be the result of the model~~ underestimating the secondary OH originating from the oxidation of large organics (*e.g.*, isoprene and monoterpenes, as described in Archibald et al., 2010). In this specific instance the model also underestimated the concentration of NO (34 pptv, or pmol/mol, *vs* the observed ~1 $\pm$ 0.05 ppbv), which might have limited the production of secondary OH via the reaction of $HO_2$ with NO relative to observations.

The methane lifetime with respect to tropospheric loss *via* reaction with OH, $\tau_{CH_4}$, for the base run was 8.75 years, which is within 1$\sigma$ of the ACCMIP multimodel mean for the year 2000 (9.7 $\pm$ 1.5 years). $\tau_{CH_4}$ from the base run is also in good agreement with the value of 8.5 years reported by Lelieveld et al. (2016).  Notably the model used by these authors exhibited some differences from the one used in the current work: Lelieveld et al. (2016) used emissions for the year 2010, defined the

14

tropopause *via* their own diagnostic and employed an extensive chemistry scheme consisting of 1630 reactions. Notwithstanding these differences, the values for $\tau_{CH_4}$ from the two studies are in very good agreement. In the Base run, the average lifetime of the OH radical, $\tau_{OH}$, was 1.18 s for the whole troposphere, 0.57 s within the boundary layer and 0.45 s at the surface, as summarised in Table 4.

5    **4 Modelling the missing reactivity: addition of sink X**

Figure 3 highlights that whilst the model represents many of the individual components of OH reactivity within at least an order of magnitude (and often within a factor of two) of observations, the model underrepresents total $k_{OH}$ in the majority of the cases (Figure 2). There are a number of ways to account for this missing reactivity in the model. For example, additional species (such as more reactive NMHCs or more reactive reaction intermediates) and their chemistry could be included in the

10    model. However observations indicate that this approach would still leave outstanding missing reactivity (Edwards et al., 2013; Elshorbany et al., 2012; Kaiser et al., 2016; Kovacs et al., 2003; Lee et al., 2009; Lou et al., 2010; Mao et al., 2012; Mogensen et al., 2011; Yang et al., 2017). In this work, we have taken a different, simpler approach. A new species representing a direct sink of OH was added into the model and its atmospheric implications were assessed. Emissions of the unspecified OH sink, species X, were introduced in the model simulations along with the reaction:

15

X + OH                    →          products,                    (R3)
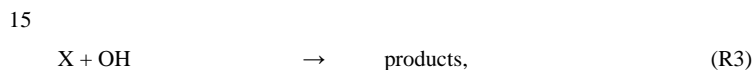
with a temperature independent bimolecular rate constant, $k_3 = 1 \times 10^{-10}$ cm$^3$ molecules$^{-1}$ s$^{-1}$, set to represent reactions with a very reactive compound (*i.e.*, OH + reactive VOCs). Crucially, the global and seasonal abundance of X was underpinned by

20    field observations of missing $k_{OH}$. This section discusses the implementation of this scheme in the model and its effects.

**4.1 Generating a global field of missing reactivity**

To generate a surface field for the missing reactivity, multiple linear regression was applied. This method consisted of fitting the missing reactivity from observations to the corresponding model grid box emissions of VOCs, NO$_x$ and aerosol precursors at the individual observation sites where the OH reactivity was measured (described in Section 2). This resulted in a time-

25    varying spatial field for the missing reactivity based on the predictors (emission fields) listed in Table 3. Correlation of the missing $k_{OH}$ with some of the emitted species would be expected both if the missing sink was an oxidation intermediate (in which case it would correlate with its precursors) and if it was a primary emission (in which case it could be expected to correlate to other primary emitted VOCs such as anthropogenic or biogenic VOCs). This is also supported by observations. For instance, measurements taken during the INTEX-B campaign (Mao et al., 2009) found that the missing reactivity correlated

30    with formaldehyde concentrations; the authors concluded that this indicated that the missing reactivity potentially arose from VOCs that formed formaldehyde upon oxidation. Similarly, measurements performed in a forest in Michigan during the

15

CABINEX campaign showed good correlation between the missing reactivity and both isoprene and its oxidation products (methyl vinyl ketone, MVK, and methacrolein, MACR) when the missing reactivity was highest (Hansen et al., 2014).

The results of the multiple linear regression using all 15 predictors in Table 3 are shown in Figure 4; the $R^2$ value for the fit

5   was 0.75. The strongest predictors for the missing reactivity were the emissions of organic carbon from biofuels (OC biofuel), black carbon from biofuels (BC biofuel), acetone and CO. Whilst these might indicate both an anthropogenic and a biogenic component of the missing reactivity, none of the predictors had a $p$-value $\leq 0.05$ (with OC biofuel coming close with $p = 0.067$), perhaps as a result of the small sample size available. The coefficients from the multiple linear regression are shown in Table 3. The fact that the strongest predictors were the emissions for aerosol tracers not included in the model gaseous

10   chemistry might also indicate potential contributions to the total $k_{OH}$ from condensed-phase particles. However the role of particulate matter in OH loss is very poorly characterised, as highlighted in the recent review by Yang et al. (2016).

To establish the robustness of the outcome of the multiple linear regression routine, the analysis was repeated using different subsets of predictors. Unsurprisingly, the iterations using larger numbers of predictors returned better error statistics ($R^2$ values,

15   normalised mean biases, *etc.*). The inclusion of the bottom three predictors in Table 3 (biogenic methanol, ethane and propane emissions) led to only marginal improvements in the quality of the fit (*e.g.*, increases in $R^2 < 0.1\%$) in all cases. On the other hand the top four entries in Table 3 were the strongest predictors in all iterations that included them and their exclusion from the fitting routine affected the quality of the fit significantly (*e.g.*, decreases in $R^2 > 10\%$). For the purpose of this work, the
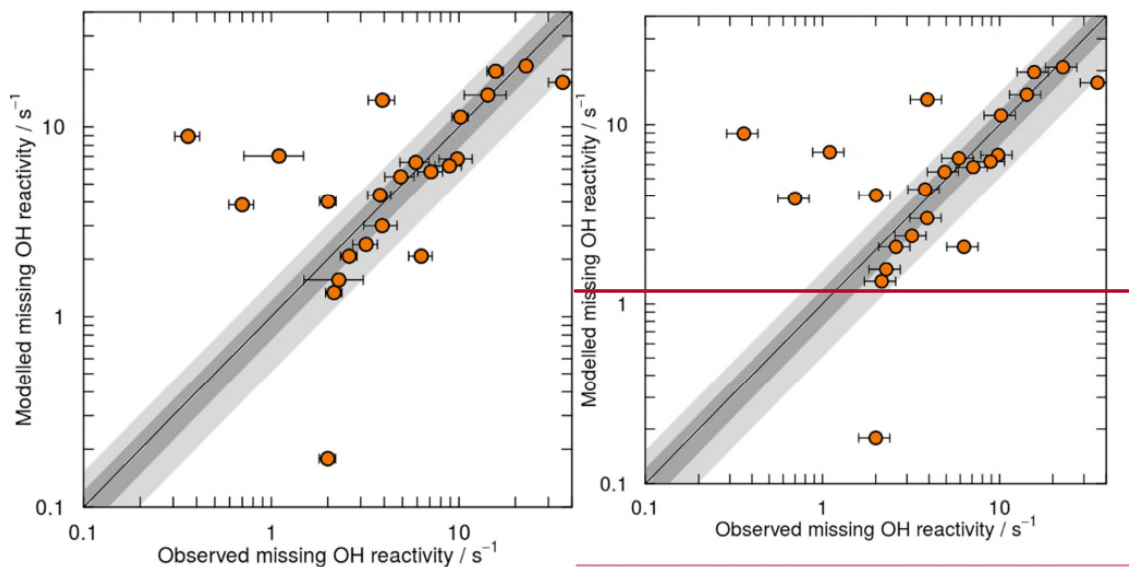
**Figure 4: Scatter plot of missing OH reactivity modelled by multiple linear regression against observed missing OH reactivity (as reported in Table 2). Each point represents one observation site. The error bars mirror the uncertainties (at the 1σ level) from each individual measurement of the total $k_{OH}$~~The error bars (20%, relative) are commensurate to the uncertainty in the $k_{OH}$ measurements in the field (Yang et al., 2016)~~. Also shown are the 1:1 line (solid line), as well as 20% and 50% deviations from it (dark grey and light grey areas respectively). The $R^2$ value from the multiple linear regression was 0.75.**

outcome of the multiple linear regression using all 15 predictors was used.

The multiple linear regression resulted in an expression of missing reactivity at the surface varying with longitude, latitude and time. Figure 5 shows global seasonal averages of the modelled missing reactivity at the surface in the boreal winter (DJF) and summer (JJA).  The multiple linear regression captured some of the seasonality of the missing reactivity over forested regions at mid-latitudes: this behaviour is consistent with the temperature dependence of the missing reactivity observed in a number of field campaigns in forested areas (as described in Section 1).  In addition, a number of urban areas are also distinguishable as regions of high missing reactivity.

Overall, the modelled missing reactivity obtained from the multiple linear regression had values other than zero in 23 % of the surface grid cells in DJF and in 32 % of the grid cells in JJA. Of all the non-zero values plotted in Figure 5, 57 % are below 1 $s^{-1}$, 77 % below 5 $s^{-1}$, 87 % are below 10 $s^{-1}$ and 99.8 % are below 50 $s^{-1}$. Only a very small number of grid cells have modelled missing reactivities in the range 50-100 $s^{-1}$ (12 grid cells in DJF and 15 in JJA). These regions correspond to areas of high anthropogenic emissions that resulted in large contributions of the strongest predictors (OC and BC biofuels) to the calculated missing reactivity.

**Table 3: Outcome of the multiple linear regression (MLR); the predictors are sorted by increasing $p$-value.**

| Predictor | Coefficient/$10^{12}$ kg$^{-1}$ m$^2$ |
|---|---|
| OC biofuel emissions | 4.41 |
| BC biofuel emissions | -12.97 |
| Acetone emissions | 0.78 |
| CO emissions | -0.02 |
| OC fossil fuel emissions | -0.67 |
| BC fossil fuel emissions | 1.25 |
| Monoterpene emissions | 0.04 |

17

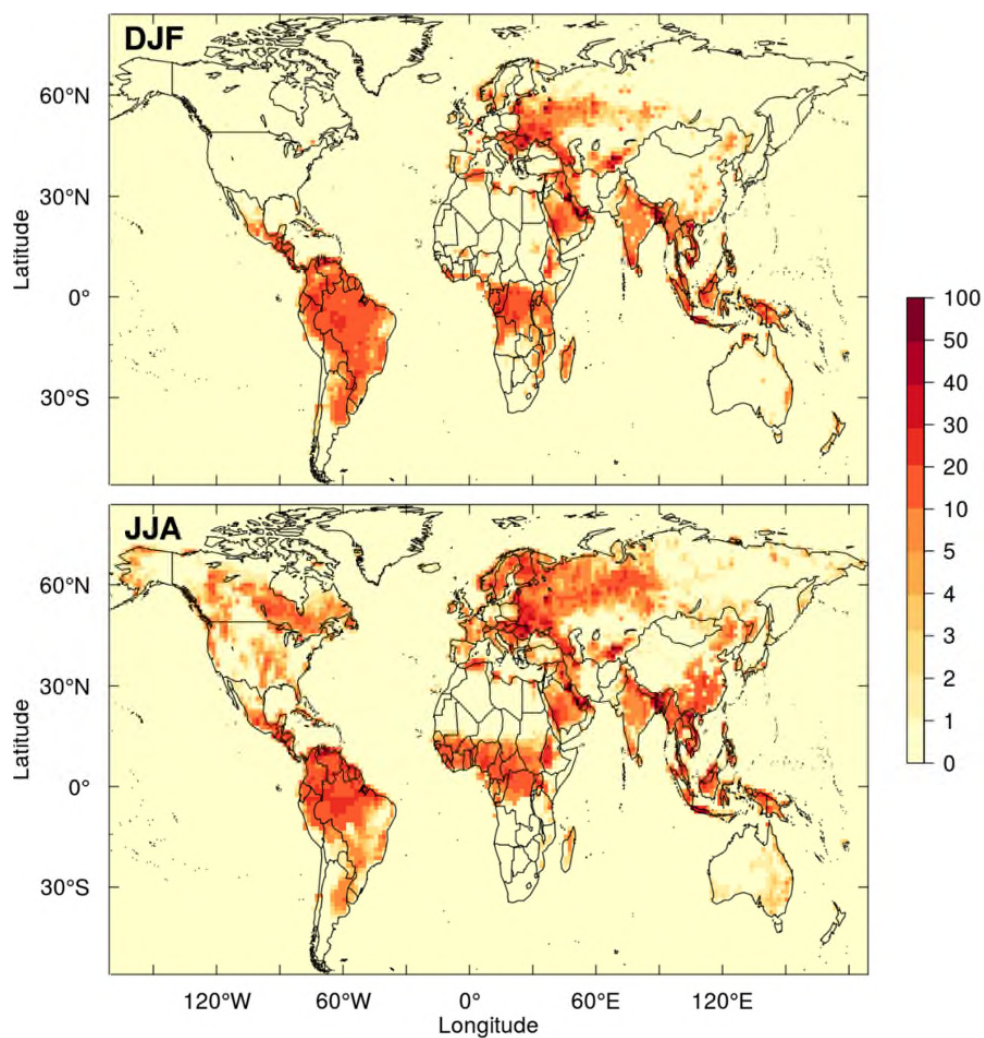| | |
|---|---|
| NO$_x$ emissions | -0.02 |
| Isoprene emissions | -0.02 |
| Methane emissions | 0.01 |
| Acetaldehyde emissions | -1.18 |
| Formaldehyde emissions | 1.20 |
| Biogenic methanol emissions | -0.02 |
| Ethane emissions | -0.22 |
| Propane emissions | 0.76 |

**Figure 5: Global distribution of the simulated missing OH reactivity (in s$^{-1}$) in the boreal winter (DJF, top panel) and boreal summer (JJA, bottom panel).**

5    In order to establish the effects of the additional sink on tropospheric oxidation chemistry it is necessary to emit species X in the model and let it interact with OH *via* R3. However the conversion of the global missing reactivity derived from the multiple linear regression into an emission field is not straightforward. Initially, the emission rate of X is calculated as equal to the rate of removal of X within the turbulent boundary layer for each surface grid cell, according to Eq. (2):

$$emission\ rate\ of\ X\ /\ \mathrm{kg\ m^{-2}s^{-1}} = k_3[\mathrm{X}][\mathrm{OH}] \times \frac{h\,M_r}{N_A} \times 10^3 \qquad (2)$$

where $k_3$ is the rate constant for R3 (in $\mathrm{cm^3\ molecules^{-1}\ s^{-1}}$), [X] and [OH] are the number densities of X and OH respectively (in units of molecules $\mathrm{cm^{-3}}$), $h$ is the height of the turbulent boundary layer (in m), $M_r$ is the molar mass of species X (arbitrarily assigned a value of 30 g $\mathrm{mol^{-1}}$) and $N_A$ is Avogadro's number (in molecules $\mathrm{mol^{-1}}$). The term $k_3[\mathrm{X}]$ corresponds to the missing reactivity from the multiple linear regression, while the values of [OH] are taken from the base run. The model was run for one year with these emissions of X. Then the OH reactivity arising from the newly emitted species X was calculated for the model run (as $k_3[\mathrm{X}]$) and compared with the missing reactivity obtained from the multiple linear regression. It was found that the OH reactivity arising from species X in this initial model run was significantly higher than the missing reactivity determined *via* multiple linear regression (as shown in Figure 6b). This overestimate was attributed to the fact that the OH field from the base run used in Eq. (2) is itself an overestimate of the OH field from a scenario where an additional sink (species X) is introduced. A routine was therefore developed, in which the initial emission field of species X was iteratively optimised in a series of model runs until the OH reactivity from species X in the model matched the missing reactivity determined *via* multiple linear regression within the tolerances specified in Figure 6a. The procedure used is summarised in Figure 6. As the missing reactivity from the multiple linear regression was underpinned by observations, this routine ensured that the additional sink emitted in the model would still account for the observed missing reactivity.
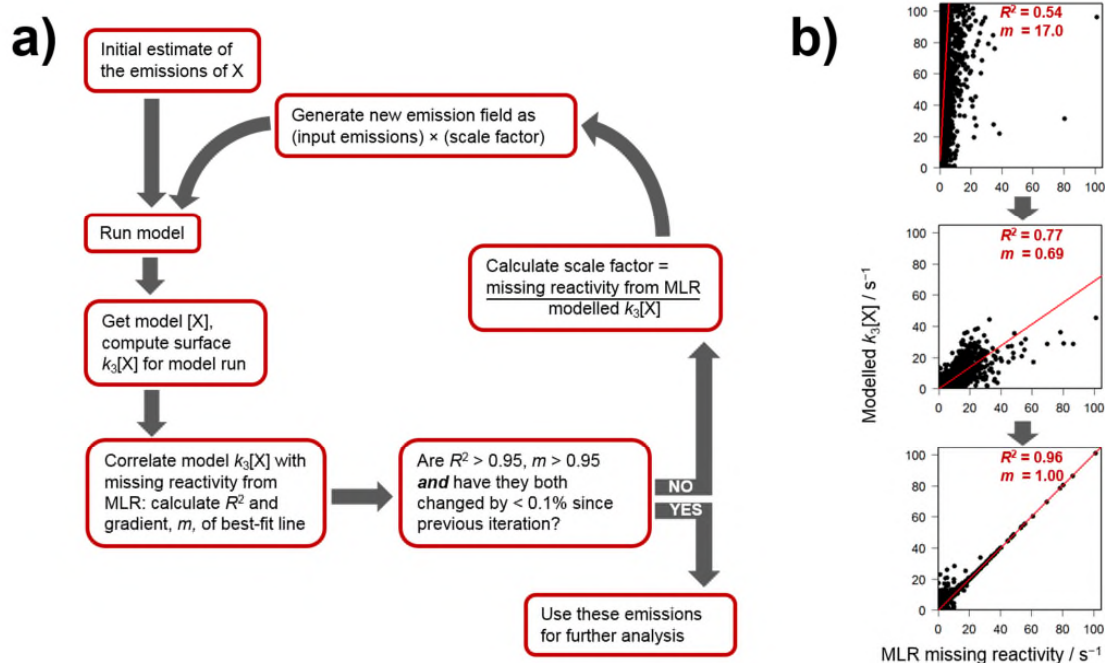
**Figure 6: Implementation of the routine used to convert the global missing reactivity field obtained from multiple linear regression (MLR) into emissions of species X. Panel a) illustrates the procedure as a flow chart, while panel b) shows the correlation plots between modelled $k_3[X]$ and the MLR missing reactivity from non-consecutive iterations: as the $R^2$ values and the gradients of the correlation plots converge to 1, the emissions of X in the model lead to X-reactivities identical to the missing reactivity derived by MLR.**

## 4.2 Effects of introducing sink X

The chemistry used for sink X does not allow any secondary OH formation following the initial oxidation of X in R3. This is unrealistic, as the oxidation of the vast majority of trace species leads to some degree of secondary OH production; however, with so little information available on the identity of species X, the system was too poorly constrained to even attempt an educated guess on the OH recycling probability of the products of R3. Therefore the effects of introducing sink X in the model, discussed at length in this Section, can be seen as a 'worst case' scenario, one in which no OH is regenerated following R3 and in which OH is removed from regions of high emissions of X. This may be the case for reactions of OH on aerosol surfaces.

OH abundances are reduced following inclusion of R3 in the chemistry scheme, as a result of both direct removal of OH *via* R3 and less efficient production of secondary OH (as highlighted in the fluxes reported in the Supplementary Material). As shown in Figure 7, the most OH-depleted areas at the surface include Scandinavia, Eastern Europe and the coastlines of the

Persian Gulf, Venezuela and Java. Peak OH reductions in these regions are of the order of 5-6 $\times$ 10$^6$ molecules cm$^{-3}$. In these regions as much as 90% of the mean annual [OH] is removed, but it must be stressed that secondary OH production from the products of R3 would mitigate these effects. Interestingly some of the regions affected by the highest emissions of X (*i.e.*, the Amazon region and Central Africa) only exhibit relatively small decreases in OH concentrations, down by ~20 %; as these

5  areas are rich in OH sinks, the introduction of an additional sink does not affect the OH budget significantly. OH depletion is most pronounced at the surface and in the boundary layer in the Northern Hemisphere (also in Figure 7), which is consistent with the vertical distribution of the additional OH reactivity brought about by species X shown in Figure 8. Mean tropospheric OH decreased by 1.6 %, while mean OH abundances in the boundary layer and at the surface were reduced by 5.6 and 8.1 % respectively. Seasonal changes in OH abundances, both in absolute and relative terms, are shown in Figures S8̶2 and S3̶9 in

10  the Supplementary Material. These show significant relative reductions in the mean boreal winter OH in the Northern
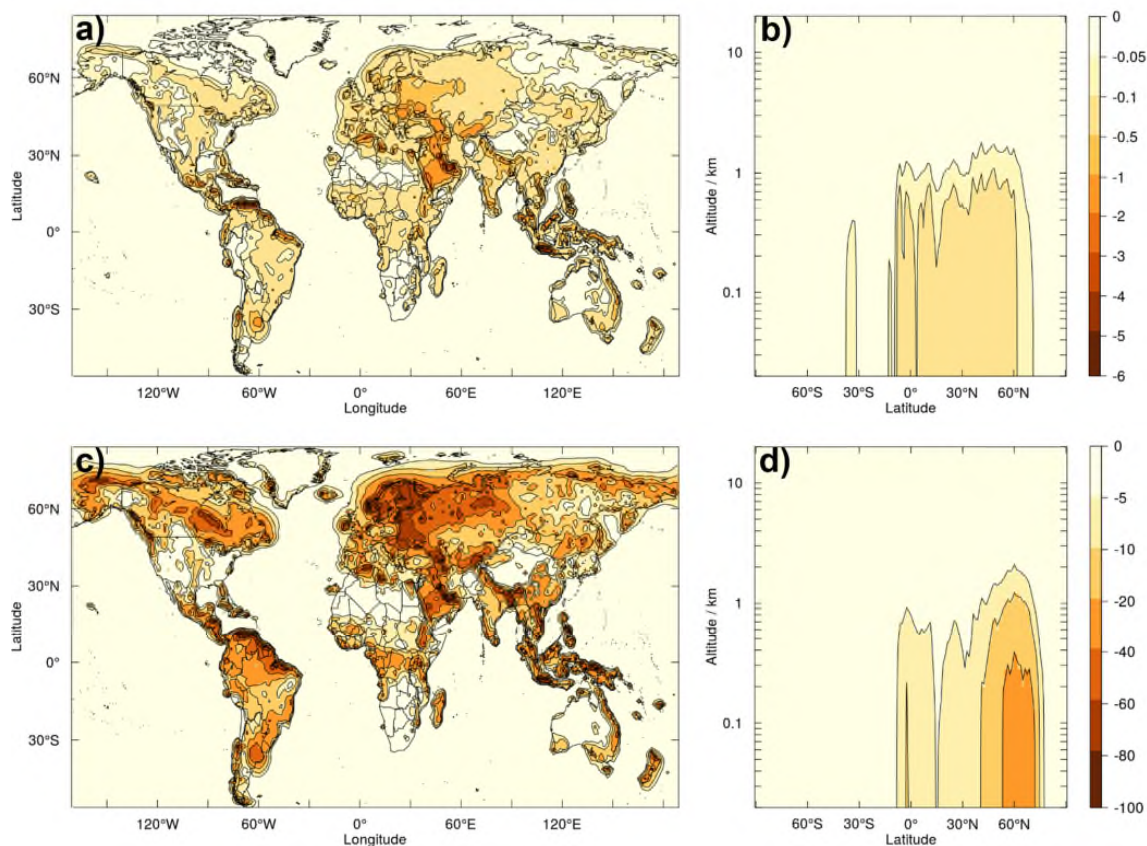


**Figure 7: Annual mean change in OH concentration following inclusion of R3: absolute change in 10$^6$ molecules cm$^{-3}$ a) at the surface and b) as a zonal mean, and relative percentage change c) at the surface and d) as a zonal mean.**
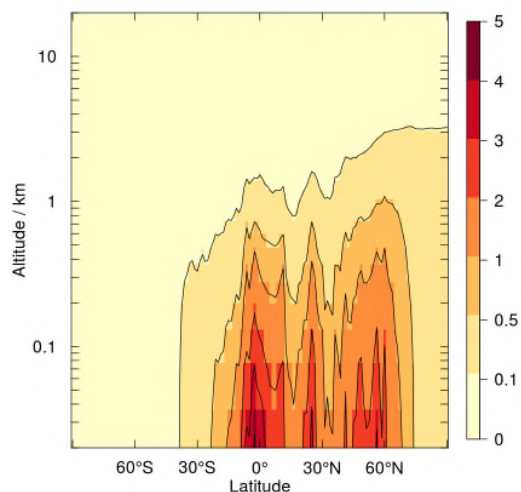
**Figure 8: Annual zonal mean of the OH reactivity (in s⁻¹) arising from sink X.**

Hemisphere (> 60 %), which are however very small in absolute terms (< $5 \times 10^4$ molecules cm⁻³). <u>Changes in $HO_2$ mainly mirror those in OH, albeit with a somewhat smaller relative magnitude (see Figure S10 in the Supplementary Material).</u>

$\tau_{CH_4}$ for the model run including R3 was 8.95 years (~2.3 % higher than the base run). $\tau_{OH}$ was reduced by approximately 2 % at the surface, by 3% in the boundary layer and by 1.5 % in the whole troposphere (Table 4). Another metric of interest when discussing tropospheric oxidation chemistry is the OH recycling probability, $r$, which describes the sensitivity of the OH chemistry to perturbations (Lelieveld et al., 2002). $r$ was calculated in accordance with Lelieveld et al. (2002, 2016), using Eq. (3):

$$r = 1 - P/G \qquad (3)$$

where $P$ is the rate of formation of primary OH (*i.e.*, *via* R1 and R2) and $G$ is the gross OH formation rate, consisting of the sum of $P$ and the formation rate of secondary OH, $S$ (*i.e.*, *via* any route other than R1 and R2). Using the OH formation fluxes tabulated in the Supplementary Material, it was found that $r$ remained larger than 60 % in both runs, indicating that tropospheric oxidation was effectively 'buffered'.
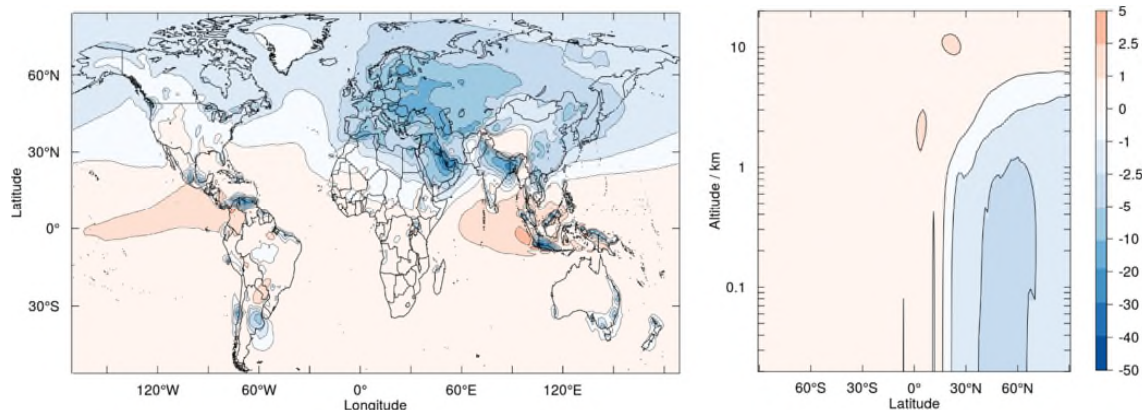
23

**Figure 9: Annual mean percentage change in O₃ concentration at the surface (left) and as a zonal mean (right).**

The ozone burden at the surface decreased slightly by 0.9%, but the overall tropospheric ozone burden increased by 0.3 %. This somewhat contradictory behaviour in ozone, also shown in Figure 9, can be accounted for in terms of the changes brought about by decreases in OH in regions with different $NO_x$ abundances. In general, OH decreases are accompanied by lower concentrations of $HO_2$ and peroxy radicals ($RO_2$); in OH-depleted, $NO_x$-rich regions (*e.g.*, Europe in Figure 9) less $HO_2$ and $RO_2$ are available to react with NO, leading to a reduction in ozone produced from $NO_2$ photolysis. On the other hand, in remote regions with low $NO_x$ the lower abundance of $HO_2$ and $RO_2$ following sequestration of OH by X leads to less efficient ozone removal *via* the reaction of $O_3$ with $HO_2$ (and, to a lesser extent, *via* the reaction of $HO_2$ with $RO_2$, producing soluble alkyl hydroperoxides), which appears as a slight positive change in Figure 9. Decreases in surface ozone in the Northern Hemisphere are also exacerbated by the absence of further chemistry following R3. This rules out the production of X-peroxy radicals from the initial oxidation of X, which in turn would react with NO to produce $NO_2$, the photolysis of which would then lead to $O_3$ formation. However to what degree the ozone changes shown in Figure 9 would be mitigated by subsequent chemistry would be highly dependent on the actual nature of the missing sink. Comparison of ozone seasonal observations from a number of remote sites with the model output (illustrated in Figure S11 in the Supplementary Material) shows that, while generally the model and the observation are in good agreement in a number of the locations shown, the inclusion of the additional OH sink X has a minimal impact on the modelled ozone at these locations.

On average, R3 accounts for approximately 6 % of the total OH loss flux at the surface (see Supplementary Material); in some particular regions, such as the Amazon rainforest, this contribution increases to up to 20 %, whilst in areas of Eastern Europe it went up to 50 % (see Figure S12 in the Supplementary Material). As a result, reactions of OH with other sinks (*e.g.*, methane) become less efficient and the lifetime of such species increases: the lifetime of isoprene, a major tropospheric OH sink, increases by 17% from 2.36 hours to 2.76 hours. This is reflected in the reduced flux through its reaction with OH in the

regions of high X reactivity (Tables S1-S3). As a result of its longer lifetime, isoprene is transported to higher altitudes than in the base run, as the flux through its reaction with OH increases above the boundary layer.

**Table 4: Values of the OH and methane lifetimes in the model runs described in this work. Numbers in brackets indicate the percentage change with respect to the base run.**

|  | Base run | X + OH run | $CH_3O_2$ + OH run 1 | $CH_3O_2$ + OH run 2 | $CH_3O_2$ + OH run 3 |
|---|---|---|---|---|---|
| $\tau_{OH}$ surface / s | 0.455 | 0.447 (−1.8%) | 0.442 (−2.7%) | 0.442 (−2.7%) | 0.442 (−2.7%) |
| $\tau_{OH}$ boundary layer / s | 0.574 | 0.557 (−3.2%) | 0.558 (−2.8%) | 0.558 (−2.8%) | 0.558 (−2.8%) |
| $\tau_{OH}$ troposphere / s | 1.18 | 1.16 (−1.5%) | 1.15 (−2.5%) | 1.15 (−2.5%) | 1.15 (−2.5%) |
| $\tau_{CH_4}$ / years | 8.75 | 8.95 (+2.3%) | 8.92 (+2.0%) | 8.97 (+2.5%) | 9.01 (+3.0%) |

While the work described in this Section can be considered a worst-case scenario due to the absence of OH recycling following R3, it is important to observe that the impacts on the wider atmosphere are relatively minor. Reconciling the observations of missing OH reactivity in our model in a worst-case scenario (for OH) has little impact on the global oxidising capacity. We report a small increase in methane lifetime, and an overall minor decrease in surface ozone; however the actual extent of these changes in the real atmosphere is likely to be mitigated to some degree by OH recycling following the initial oxidation of the missing sink.

## 5 Effects of $RO_2$ + OH chemistry

The previous Section focused on simulating the observed missing reactivity by introducing an additional sink in the form of species X. Based on structural-reactivity arguments, Archibald et al., (2009) postulated that there could be a reaction between peroxy radicals ($RO_2$) and OH, which could act as a sink for OH and, depending on the mechanism, a potential source of oxygenated VOC. A lack of any experimental data hampered estimations of the rate constant for the reaction. However recent laboratory studies have confirmed that peroxy radicals do indeed react with OH and, subsequently, the kinetics of the simplest $RO_2$ + OH reactions have been characterised (Fittschen et al., 2014). The potential impact of $RO_2$ species as OH sinks and their contribution to the total OH reactivity have not been investigated to date.

### 5.1 Overall contribution of modelled $RO_2$ to $k_{OH}$

The UM-UKCA base model described in Section 2 includes the formation and reactions of a number of peroxy radicals. ~~This~~ These include~~s~~ not only those originating from the oxidation of the simplest ~~hydrocarbons (~~alkanes (methane, ethane and propane) and carbonyl ~~co~~compounds (acetaldehyde, propanal, aceton~~entaining species up to three carbon atoms~~), but also those formed from isoprene and its oxidation products (methacrolein and methyl vinyl ketone) ~~first and second generation~~

25

~~peroxy radicals produced in the oxidation of isoprene~~. This allowed the offline calculation of an additional term for $k_{OH}$ arising from the contributions of all $RO_2$ radicals in the model, $k'_{OH}$, as shown in Eq. (4):

$$k'_{OH} = \sum_{i=1}^{n} k_{OH+RO_{2,i}} \left[ RO_{2,i} \right], \qquad\qquad (4)$$

where $[RO_{2,i}]$ is the concentration of peroxy radical $i$ and $k_{OH+RO_{2,i}}$ is the rate constant of its reaction with OH. The total concentration of all $RO_2$ species in the base run is shown in Figure S3 in the Supplementary Material. Assumptions had to be made on the individual values of $k_{OH+RO_{2,i}}$, as only the rate constants of the reactions of OH with methyl (Assaf et al., 2016, 2017b; Bossolasco et al., 2014; Yan et al., 2016), ethyl (Assaf et al., 2017a; Faragó et al., 2015), propyl (Assaf et al., 2017a) and $i$- and $n$-butyl (Assaf et al., 2017a) peroxy radicals have been measured in the laboratory to date. Reported experimental values for the rate constant of the reaction of the simplest peroxy radical, $CH_3O_2$, with OH disagree by more than a factor of 3. The highest value to date, reported by Bossolasco et al. (2014) ($2.8 \times 10^{-10}$ cm$^3$ molecule$^{-1}$ s$^{-1}$ at $T = 294$ K), has since been revised to a lower value ($1.6 \times 10^{-10}$ cm$^3$ molecule$^{-1}$ s$^{-1}$ at $T = 295$ K) by the same group (Assaf et al., 2016): the difference is thought to arise from complicating secondary chemistry due to the presence of electronically excited iodine atoms following the photolysis of the gaseous mixture used by Bossolasco et al. (2014). However an even lower value has been reported by Yan and co-workers ($8.4 \times 10^{-11}$ cm$^3$ molecule$^{-1}$ s$^{-1}$ at $T = 298$ K), and the reason for the discrepancy between this study and that by Assaf et al. is still unclear.

In general, the rate constant of these reactions exhibit no significant dependence on the size of the alkyl group on the $RO_2$ radical. For the purpose of this study all $k_{OH+RO_{2,i}}$ were assumed to be equal to the rate constant of the reaction of the methyl peroxy radical with OH at $T = 295$ K as measured by Assaf et al. (2016), and independent of temperature. Eq. (4) therefore can be re-written as:

$$k'_{OH} = k_{OH+RO_2} \sum_{i=1}^{n} \left[ RO_{2,i} \right], \qquad\qquad (5)$$

where $k_{OH+RO_2} = 1.6 \times 10^{-10}$ cm$^3$ molecule$^{-1}$ s$^{-1}$.

The additional annual mean OH reactivity at the surface resulting from $RO_2$ chemistry is shown in Figure 10: while the largest contributions in absolute terms to the total $k_{OH}$ are found in forested tropical regions (Figure 10a, where $RO_2$ radicals from isoprene dominate), these are indeed very small when compared to the total reactivity present in the same regions. In relative terms, $RO_2$ radicals are most significant as OH sinks over remote tropical oceans (Figure 10c), where the majority (> 90%) of the $RO_2$ contribution to $k_{OH}$ arises from the methyl peroxy radical. This contribution extends beyond the boundary layer and into the free troposphere over tropical latitudes, as shown in Figure 10b and Figure 10d.
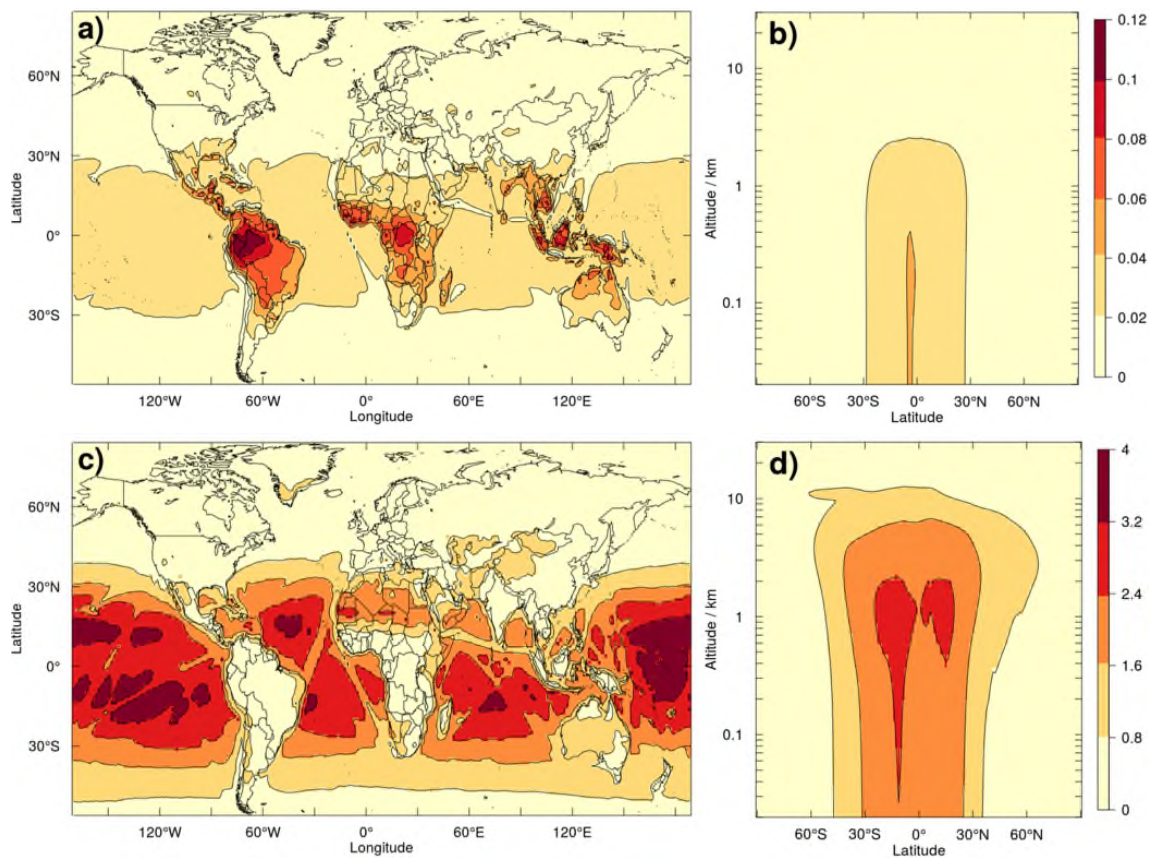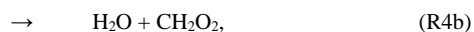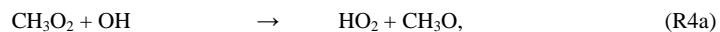
26

**Figure 10: changes in total $k_{OH}$ from the inclusion of RO$_2$ + OH reactions: a) global surface change in s$^{-1}$ and b) zonal mean in s$^{-1}$; c) percentage change at the surface and d) percentage change zonal mean.**

5

**5.2 The CH$_3$O$_2$ + OH reaction and product branching simulations**

Recent studies on the products of the reaction of the simplest peroxy radical, CH$_3$O$_2$, with OH may help establish the wider atmospheric implications of this novel peroxy radical chemistry, both on the total $k_{OH}$ as well as on the concentrations of species of interest. Three product channels can be envisaged for this reaction (Archibald et al., 2009):

10

$$CH_3O_2 + OH \quad\rightarrow\quad HO_2 + CH_3O, \qquad (R4a)$$
$$\rightarrow\quad H_2O + CH_2O_2, \qquad (R4b)$$

27

$$\rightarrow \quad O_2 + CH_3OH, \qquad\qquad (R4c)$$

with branching ratios defined as:

$$\alpha = k_{4a}/(k_{4a} + k_{4b} + k_{4c}), \qquad\qquad (5a)$$
$$\beta = k_{4b}/(k_{4a} + k_{4b} + k_{4c}), \qquad\qquad (5b)$$
$$\gamma = k_{4c}/(k_{4a} + k_{4b} + k_{4c}). \qquad\qquad (5c)$$

Recent laboratory studies identified R4a as the major product channel, with $\alpha = 0.80 \pm 0.20$ (Assaf et al., 2017b). Channel R4b, producing the Criegee intermediate $CH_2O_2$, was found to be a minor contributor to the overall reaction ($\beta < 0.05$). As the set-up used in the study was not suitable for the detection of methanol ($CH_3OH$), the magnitude of $\gamma$ could not be established. A theoretical study identified R4c as a potentially significant source of methanol in the remote boundary layer and modelled its impacts (Müller et al., 2016). However this study predated the first (and, so far, only) experimental determination of the products of R4, and also used the very high value of $k_4$ reported by Bossolasco et al. (2014), which has since been revised to a value almost a factor of 2 lower than the original (as discussed in Section 5.1).

In the current work, three simulations were run with different sets of values for $\alpha$ and $\gamma$ (run 1: $\alpha = 1$, $\gamma = 0$; run 2: $\alpha = 0.8$, $\gamma = 0.2$; run 3: $\alpha = 0.6$, $\gamma = 0.4$) in order to establish the atmospheric implications of different product branching for R4 over the uncertainty range of $\alpha$ reported by Assaf et al (2017b).

As shown in Table 4, introduction of R4 in the model led to shorter $\tau_{OH}$ (by approximately 3 %), regardless of the product branching. Tropospheric methane lifetime increased by as much as 3 % in run 3. $HO_2$ abundances increased in all runs and in particular in run 1, which exhibited $HO_2$ concentrations higher than the base run by as much as 12 % over remote oceans, as shown in Figure 11. Mean tropospheric $HO_2$ abundances increased by 3.9 % in run 1, 2.8 % in run 2 and 1.7 % in run 3.
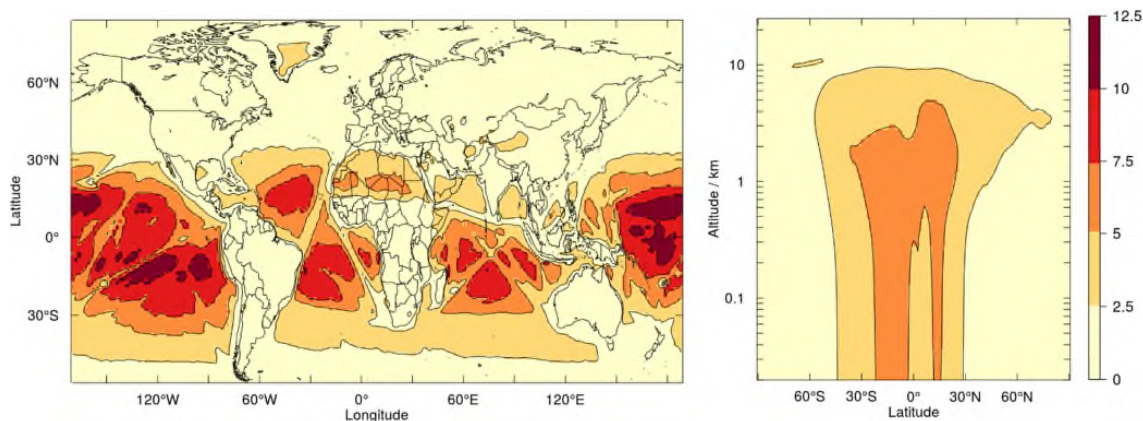
**Figure 11: Annual mean percentage change in HO₂ concentrations from run 1 (relative to the base run) at the surface (left) and as a zonal mean (right).**
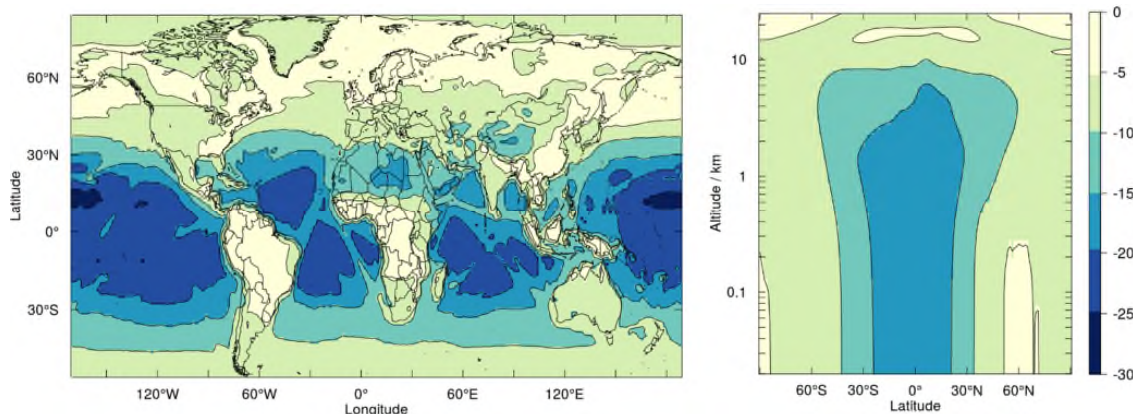


**Figure 12: Annual mean percentage change in CH₃O₂c concentrations from run 1 (relative to the base run) at the surface (left) and as a zonal mean (right).**

Regardless of the product branching of R4, the concentration of methyl peroxy radicals at the surface decreased significantly (by as much as 30%) over remote oceans and more moderately (by 5-10%) over land at mid-latitudes (Figure 12). Mean tropospheric CH₃O₂ abundances decreased by 14 % in all runs, whilst mean tropospheric OH was reduced by 1.5 % in run 1, 2.1 % in run 2 and 2.7 % in run 3.

The inclusion of R4 in the model led to a small reduction (~ −1 %) in the tropospheric ozone burden. This is mainly driven by the increase in HO₂ abundances, leading to enhanced ozone removal *via* O₃ + HO₂ over remote oceans. Ozone abundances over NOₓ-rich areas were largely unchanged, as the reaction of CH₃O₂ with NO dominates over R4 and therefore HO₂ concentrations did not deviate significantly from the base run.

The largest difference in the impact of different branching ratios for R4 was observed for methanol concentrations, as shown in Figure 13. In the scenario in which $\alpha = 1$ (and $\gamma = 0$), methanol concentrations decrease by as much as 40-50 % over remote oceans as R4a efficiently inhibits methanol production *via* the CH₃O₂ self-reaction. However increasing $\gamma$ increases methanol mixing ratios. When $\gamma = 0.4$ methanol abundances are enhanced by up to 200-300 % (relative to the base case) over remote regions. Mean tropospheric methanol decreased by 8.4 % in run 1 and increased by 35.9 and 80.2 % in runs 2 and 3 respectively. There remains uncertainty in the tropospheric methanol budget (Khan et al., 2014; Millet et al., 2008), with models currently underestimating atmospheric methanol concentrations significantly. Müller and co-workers suggested that a scenario with high methanol yield from R4 could reconcile models with observation, based on a model run with effectively $\gamma = 0.4$ which produced an additional 117 Tg year⁻¹ of methanol (Müller et al., 2016). However these simulations used the high

value of $k_4$ reported by Bossolasco et al. (2014). If the preferred lower value reported more recently by Assaf et al. (2016) is used with $\gamma = 0.4$, we calculate methanol production *via* R4c to be 60 Tg year$^{-1}$ and we estimate that a value of $\gamma$ greater than 0.8 is needed to produce the amount of methanol necessary to reconcile models with observations. This is well beyond the uncertainty in the laboratory measurements of the branching of R4 and highlights that missing sources of methanol must come from direct emissions (or re-emissions) or as yet-undiscovered photochemical sources, rather than from the reaction between OH and $CH_3O_2$. However it has to be noted that so far the product branching of R4 has only been measured at low pressure (50 Torr) by Assaf et al. (2017b). Calculations by Müller et al. (2016) suggest the presence of an association channel leading to the formation of a trioxide ($CH_3OOOH$) species, which might potentially decompose to methanol and molecular oxygen. As the stabilisation of association products is generally a pressure-dependent process, it is very important that future studies address the branching of R4 at ambient pressure.
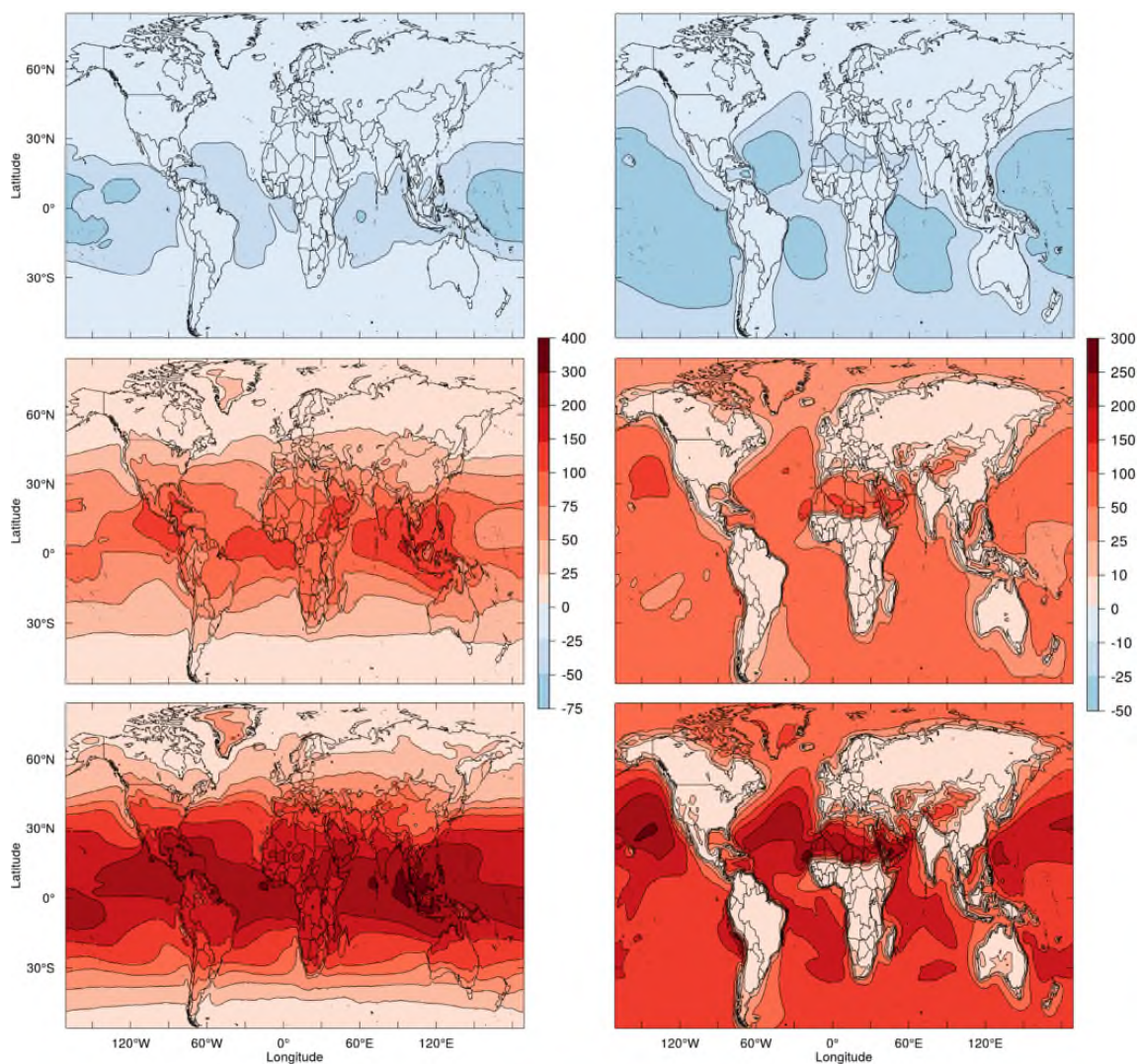
**Figure 13: Annual mean changes in methanol abundances from run 1 ($\gamma = 0$, top row), run 2 ($\gamma = 0.2$, middle row), and run 3 ($\gamma = 0.4$, bottom row), relative to the base run. Changes are shown in absolute (in pptv, left column) and relative terms (percentage change, right column).**

As the species affected by R4 ($HO_2$, $CH_3O_2$ and $CH_3OH$) are all OH sinks, changes in their concentrations are accompanied by changes in $k_{OH}$. However these are modest ($< 0.25$ s$^{-1}$) in all the scenarios considered in this work, as shown in Figures S13 and S14 in the Supplementary Material. While the reactions of OH with both $HO_2$ and $CH_3O_2$ have large rate constants ($>$

$1\times10^{-10}$ cm$^3$ molecules$^{-1}$ s$^{-1}$), the general low abundance of these species (of the order of ~$10^8$ molecules cm$^{-3}$, as shown in Figures S2 and S3) results in small changes to the total $k_{OH}$. On the other hand, while some of the changes in methanol concentrations arising from R4 are significant (with increases up to 400 pptv in run 3, corresponding to ~$1 \times10^{10}$ molecules cm$^{-3}$), the very small rate constant of its reaction with OH ($< 1\times 10^{-12}$ cm$^3$ molecules$^{-1}$ s$^{-1}$) leads to a small contributions to $k_{OH}$. These results are consistent with the magnitude of the changes in $k_{OH}$ calculated offline for all RO$_2$ radicals in Section 5.1. It remains to be seen if any of the reaction products of more complex RO$_2$ radicals with OH, or their combination, might have a significant impact on $k_{OH}$.

Results from this work agree with the box model calculations performed by Assaf et al. (2017b), indicating that the largest impacts of R4 are on HO$_2$ and CH$_3$O$_2$ abundances. In addition, we show that these effects are not limited to the surface or the boundary layer but also extend well into the free troposphere.

## 6 Conclusions

The hydroxyl radical plays a pivotal role in the chemistry of the atmosphere. Its abundance determines the lifetime of most emitted compounds so that OH is often known as the "atmospheric detergent". However, our understanding of the chemistry and distribution of OH is far from complete. This study has examined the total tropospheric OH reactivity, $k_{OH}$, using the UM-UKCA chemistry-climate model. In the first instance, the model was evaluated against available measurements of known OH sinks. This comparison indicated that, while the model captured the abundances of a number of known OH sinks reasonably well in a variety of regions across the planet, the total modelled OH reactivity was generally much lower than observed, and there are significant biases in the model's ability to accurately simulate reactivity from NMHCs. Partly, this error was linked to the limited NMHC chemistry included in Chemistry-Climate models like UM-UKCA.

Existing observations of the missing OH reactivity were used to develop a method to account for the missing OH sink in the model by introducing an additional reaction and OH sink species, X, in the model chemistry scheme. Observations of missing reactivity were correlated with underlying inputs into the model (emissions of VOCs, NO$_x$ and aerosol precursors) through multiple linear regression analysis. The multiple linear regression fit highlighted correlation with both biogenic and anthropogenic emissions, consistent with observations of missing reactivity in remote and urban environments. The fitting routine also indicated strong correlation of the missing reactivity with the emissions of particulate matter, perhaps pointing at OH loss processes involving condensed-phase particles that have been overlooked to date. The multiple linear regression indicated that the areas most affected by the missing reactivity would be tropical remote regions, where biogenic emission dominate, as well as urban regions all over the globe, where anthropogenic emissions are significant. This result agrees with the type of environments in which missing reactivity has been observed. Our simulations showed that the largest impacts of the global missing OH reactivity were at the surface and in the boundary layer, where sink X accounted on average for 6 % of

32

the total OH loss flux. Inclusion of X in the model led to decreases in mean OH abundances of 8.1% at the surface, 5.6 % in the boundary layer and 1.6 % in the whole troposphere. Inclusion of missing reactivity, in the form of X, reduces and increases the lifetimes of OH and methane, respectively, by approximately 2 %. The inclusion of X modifies the global ozone burden only slightly (< 1 %) but has larger impacts on simulated surface ozone, particularly in the Northern Hemisphere. It has to be noted that, as no OH recycling was introduced following the initial oxidation of X, these results should be interpreted as an upper limit of the effects of the missing reactivity on the oxidative capacity of the troposphere.

Finally, we performed a series of model simulations including novel reactions of peroxy radicals with OH. These reactions have been recently confirmed (Bossolasco et al., 2014, Assaf et al., 2017) after being postulated to be potentially important in the marine boundary layer (Archibald et al., 2009). Using the UM-UKCA model, we have calculated that while these processes cannot account for the missing OH reactivity, they have important implications for the troposphere. Model runs including the reaction of the simplest peroxy radical, $CH_3O_2$, with OH indicated that this process is a major sink of peroxy radicals (with $[CH_3O_2]$ reduced by a third) and an important source of $HO_2$ radicals, the abundance of which increased by up to 12 % over remote oceans. These runs also show that, with the current understanding of the kinetics and product branching of this process, reaction of $CH_3O_2$ with OH cannot be a major source of atmospheric methanol. As information on the kinetics and products of these reactions become available from laboratory studies, and given the impact they have on tropospheric radical species, we recommend their inclusion in atmospheric models.

There remain a number of challenges in understanding the chemistry of hydroxyl radicals in the atmosphere. We have shown using the UM-UKCA model that accounting for potential new sinks of OH and including a representation of the observed missing OH reactivity in the model has relatively negligible impact on important long-lived atmospheric trace gases. However, we conclude that further studies are needed to identify the source and nature of the observed missing OH reactivity in particular to understand if it acts as a net OH sink (as we have included) or of it couples with other radical propagation cycles and so feeds back on OH itself. Lastly, as observations of the missing reactivity so far are largely limited to ground level measurements in the Northern Hemisphere, further observations in the Southern Hemisphere as well as aircraft measurements both in the boundary layer and the free troposphere would provide additional constraints to the modelled oxidising capacity of the atmosphere.

33

**References**

Abraham, N. L., Archibald, A. T., Bellouin, N., Boucher, O., Braesicke, P., Bushell, A., Carslaw, K., Collins, B., Dalvi, M., Emmerson, K., Folberth, G., Haywood, J., Johnson, C., Kipling, Z., Macintyre, H., Mann, G., Telford, P., Merikanto, J., Morgenstern, O., Connor, F. O., Ord, C., Osprey, S., Pringle, K., Pyle, J., Rae, J., Reddington, C., Savage, N., Spracklen, D., Stier, P. and West, R.: Unified Model Documentation Paper No. 84: United Kingdom Chemistry and Aerosol (UKCA) Technical Description MetUM Version 8.4, , (84), 74, 2012.

Archibald, A. T., Petit, A. S., Percival, C. J., Harvey, J. N. and Shallcross, D. E.: On the importance of the reaction between OH and $RO_2$ radicals, Atmos. Sci. Lett., 10(2), 102–108, doi:10.1002/asl.216, 2009.

Archibald, A. T., Cooke, M. C., Utembe, S. R., Shallcross, D. E., Derwent, R. G. and Jenkin, M. E.: Impacts of mechanistic changes on $HO_x$ formation and recycling in the oxidation of isoprene, Atmos. Chem. Phys., 10(17), 8097–8118, doi:10.5194/acp-10-8097-2010, 2010.

Archibald, A. T., Levine, J. G., Abraham, N. L., Cooke, M. C., Edwards, P. M., Heard, D. E., Jenkin, M. E., Karunaharan, A., Pike, R. C., Monks, P. S., Shallcross, D. E., Telford, P. J., Whalley, L. K. and Pyle, J. A.: Impacts of $HO_x$ regeneration and recycling in the oxidation of isoprene: Consequences for the composition of past, present and future atmospheres, Geophys. Res. Lett., 38(5), 1–6, doi:10.1029/2010GL046520, 2011.

Assaf, E., Song, B., Tomas, A., Schoemaecker, C. and Fittschen, C.: Rate Constant of the Reaction between $CH_3O_2$ Radicals and OH Radicals Revisited, J. Phys. Chem. A, acs.jpca.6b07704, doi:10.1021/acs.jpca.6b07704, 2016.

Assaf, E., Tanaka, S., Kajii, Y., Schoemaecker, C. and Fittschen, C.: Rate constants of the reaction of $C_2 – C_4$ peroxy radicals with OH radicals, Chem. Phys. Lett., 684, 245–249, doi:10.1016/j.cplett.2017.06.062, 2017a.

Assaf, E., Sheps, L., Whalley, L. K., Heard, D. E., Tomas, A., Schoemaecker, C. and Fittschen, C.: The Reaction between $CH_3O_2$ and OH Radicals: Product Yields and Atmospheric Implications, Environ. Sci. Technol., acs.est.6b06265, doi:10.1021/acs.est.6b06265, 2017b.

Bossolasco, A., Faragó, E. P., Schoemaecker, C. and Fittschen, C.: Rate constant of the reaction between $CH_3O_2$ and OH radicals, Chem. Phys. Lett., 593, 7–13, doi:10.1016/j.cplett.2013.12.052, 2014.

Burkholder, J. B., Sander, S. P., Abbatt, J. P. D., Barker, J. R., Huie, R. E., Kolb, C. E., Kurylo, M. J., Orkin, V. L., Wilmouth, D. M. and Wine, P. H.: Chemical Kinetics and Photochemical Data for Use in Atmospheric Studies - Evaluation No. 18, 2015.

Di Carlo, P., Brune, W. H., Martinez, M., Harder, H., Lesher, R., Ren, X., Thornberry, T., Carroll, M. A., Young, V., Shepson, P. B., Riemer, D., Apel, E. and Campbell, C.: Missing OH Reactivity in a Forest: Evidence for Unknown Reactive Biogenic VOCs, Science (80-. )., 304(5671), 2004.

Dolgorouky, C., Gros, V., Sarda-Esteve, R., Sinha, V., Williams, J., Marchand, N., Sauvage, S., Poulain, L., Sciare, J. and

Bonsang, B.: Total OH reactivity measurements in Paris during the 2010 MEGAPOLI winter campaign, Atmos. Chem. Phys., 12(20), 9593–9612, doi:10.5194/acp-12-9593-2012, 2012.

Edwards, P. M., Evans, M. J., Furneaux, K. L., Hopkins, J., Ingham, T., Jones, C., Lee, J. D., Lewis, A. C., Moller, S. J., Stone, D., Whalley, L. K. and Heard, D. E.: OH reactivity in a South East Asian tropical rainforest during the oxidant and particle
5  photochemical processes (OP3) project, Atmos. Chem. Phys., 13(18), 9497–9514, doi:10.5194/acp-13-9497-2013, 2013.

Ehhalt, D., Prather, M., Dentener, F., Derwent, R., Dlugokencky, E., Holland, E., Isaksen, I., Katima, J., Kirchhoff, V., Matson, P., Midgley, P. and Wang, M.: Atmospheric Chemistry and Greenhouse Gases, in Climate Change 2001: The Scientific Basis. Contribution of Working Group I to the Third Assessment Report of the Intergovernmental Panel on Climate Change, pp. 239–287., 2001.

10  Elshorbany, Y. F., Kleffmann, J., Hofzumahaus, A., Kurtenbach, R., Wiesen, P., Brauers, T., Bohn, B., Dorn, H. P., Fuchs, H., Holland, F., Rohrer, F., Tillmann, R., Wegener, R., Wahner, A., Kanaya, Y., Yoshino, A., Nishida, S., Kajii, Y., Martinez, M., Kubistin, D., Harder, H., Lelieveld, J., Elste, T., Plass-Dlmer, C., Stange, G., Berresheim, H. and Schurath, U.: $HO_x$ budgets during HOxComp: A case study of $HO_x$ chemistry under $NO_x$-limited conditions, J. Geophys. Res. Atmos., 117(3), 1–16, doi:10.1029/2011JD017008, 2012.

15  Faragó, E. P., Schoemaecker, C., Viskolcz, B. and Fittschen, C.: Experimental determination of the rate constant of the reaction between $C_2H_5O_2$ and OH radicals, Chem. Phys. Lett., 619, 196–200, doi:10.1016/j.cplett.2014.11.069, 2015.

Fittschen, C., Whalley, L. K. and Heard, D. E.: The reaction of $CH_3O_2$ radicals with OH radicals: A neglected sink for $CH_3O_2$ in the remote atmosphere, Environ. Sci. Technol., 48(14), 7700–7701, doi:10.1021/es502481q, 2014.

Fuchs, H., Novelli, A., Rolletter, M., Hofzumahaus, A., Pfannerstill, E. Y., Kessel, S., Edtbauer, A., Williams, J., Michoud,
20  V., Dusanter, S., Locoge, N., Zannoni, N., Gros, V., Truong, F., Sarda-Esteve, R., Cryer, D. R., Brumby, C. A., Whalley, L. K., Stone, D., Seakins, P. W., Heard, D. E., Schoemaecker, C., Blocquet, M., Coudert, S., Batut, S., Fittschen, C., Thames, A. B., Brune, W. H., Ernest, C., Harder, H., Muller, J. B. A., Elste, T., Kubistin, D., Andres, S., Bohn, B., Hohaus, T., Holland, F., Li, X., Rohrer, F., Kiendler-Scharr, A., Tillmann, R., Wegener, R., Yu, Z., Zou, Q. and Wahner, A.: Comparison of OH reactivity measurements in the atmospheric simulation chamber SAPHIR, Atmos. Meas. Tech., 10(10), 4023–4053,
25  doi:10.5194/amt-10-4023-2017, 2017.

Guenther, A., Karl, T., Harley, P., Wiedinmyer, C., Palmer, P. I. and Geron, C.: Estimates of global terrestrial isoprene emissions using MEGAN (Model of Emissions of Gases and Aerosols from Nature), Atmos. Chem. Phys., 6(11), 3181–3210, doi:10.5194/acpd-6-3181-2006, 2006.

Hansen, R. F., Griffith, S. M., Dusanter, S., Rickly, P. S., Stevens, P. S., Bertman, S. B., Carroll, M. a., Erickson, M. H., Flynn,
30  J. H., Grossberg, N., Jobson, B. T., Lefer, B. L. and Wallace, H. W.: Measurements of total hydroxyl radical reactivity during CABINEX 2009 - Part 1: field measurements, Atmos. Chem. Phys., 14(6), 2923–2937, doi:10.5194/acp-14-2923-2014, 2014.

Hansen, R. F., Blocquet, M., Schoemaecker, C., Léonardis, T., Locoge, N., Fittschen, C., Hanoune, B., Stevens, P. S., Sinha, V. and Dusanter, S.: Intercomparison of the comparative reactivity method (CRM) and pump-probe technique for measuring total OH reactivity in an urban environment, Atmos. Meas. Tech., 8(10), 4243–4264, doi:10.5194/amt-8-4243-2015, 2015.

Holzinger, R., Lee, A., Paw U, K. T. and Goldstein, a. H.: Observations of oxidation products above a forest imply biogenic emissions of very reactive compounds, Atmos. Chem. Phys., 5(1), 67–75, doi:10.5194/acp-5-67-2005, 2005.

Ingham, T., Goddard, A., Whalley, L. K., Furneaux, K. L., Edwards, P. M., Seal, C. P., Self, D. E., Johnson, G. P., Read, K. A., Lee, J. D. and Heard, D. E.: A flow-tube based laser-induced fluorescence instrument to measure OH reactivity in the troposphere, Atmos. Meas. Tech., 2(2), 465–477, doi:10.5194/amt-2-465-2009, 2009.

Jenkin, M. E., Young, J. C. and Rickard, A. R.: The MCM v3.3.1 degradation scheme for isoprene, Atmos. Chem. Phys., 15(20), 11433–11459, doi:10.5194/acp-15-11433-2015, 2015.

Kaiser, J., Skog, K. M., Baumann, K., Bertman, S. B., Brown, S. B., Brune, W. H., Crounse, J. D., De Gouw, J. A., Edgerton, E. S., Feiner, P. A., Goldstein, A. H., Koss, A., Misztal, P. K., Nguyen, T. B., Olson, K. F., St Clair, J. M., Teng, A. P., Toma, S., Wennberg, P. O., Wild, R. J., Zhang, L. and Keutsch, F. N.: Speciation of OH reactivity above the canopy of an isoprene-dominated forest, Atmos. Chem. Phys., 16(14), 9349–9359, doi:10.5194/acp-16-9349-2016, 2016.

Khan, M. A. H., Cooke, M. C., Utembe, S. R., Xiao, P., Derwent, R. G., Jenkin, M. E., Archibald, A. T., Maxwell, P., Morris, W. C., South, N., Percival, C. J. and Shallcross, D. E.: Reassessing the photochemical production of methanol from peroxy radical self and cross reactions using the STOCHEM-CRI global chemistry and transport model, Atmos. Environ., 99, 77–84, doi:10.1016/j.atmosenv.2014.09.056, 2014.

Kovacs, T. A. and Brune, W. H.: Total OH loss rate measurement, J. Atmos. Chem., 39(2), 105–122, doi:10.1023/A:1010614113786, 2001.

Kovacs, T. A., Brune, W. H., Harder, H., Martinez, M., Simpas, J. B., Frost, G. J., Williams, E., Jobson, T., Stroud, C., Young, V., Fried, A. and Wert, B.: Direct measurements of urban OH reactivity during Nashville SOS in summer 1999, J. Environ. Monit., 5(1), 68–74, doi:10.1039/b204339d, 2003.

Lawrence, M. G., Jöckel, P. and von Kuhlmann, R.: What does the global mean OH concentration tell us?, Atmos. Chem. Phys., 1(1), 37–49, doi:10.5194/acp-1-37-2001, 2001.

Lee, J. D., Young, J. C., Read, K. A., Hamilton, J. F., Hopkins, J. R., Lewis, A. C., Bandy, B. J., Davey, J., Edwards, P., Ingham, T., Self, D. E., Smith, S. C., Pilling, M. J. and Heard, D. E.: Measurement and calculation of OH reactivity at a United Kingdom coastal site, J. Atmos. Chem., 64(1), 53–76, doi:10.1007/s10874-010-9171-0, 2009.

Lelieveld, J., Peters, W., Dentener, F. J. and Krol, M. C.: Stability of tropospheric hydroxyl chemistry, J. Geophys. Res. Atmos., 107(D23), ACH 17-1-ACH 17-11, doi:10.1029/2002JD002272, 2002.

Lelieveld, J., Gromov, S., Pozzer, A. and Taraborrelli, D.: Global tropospheric hydroxyl distribution, budget and reactivity, Atmos. Chem. Phys., 16(19), 12477–12493, doi:10.5194/acp-16-12477-2016, 2016.

Liu, Y., Brito, J., Dorris, M. R., Rivera-Rios, J. C., Seco, R., Bates, K. H., Artaxo, P., Duvoisin, S., Keutsch, F. N., Kim, S., Goldstein, A. H., Guenther, A. B., Manzi, A. O., Souza, R. A. F., Springston, S. R., Watson, T. B., McKinney, K. A. and Martin, S. T.: Isoprene photochemistry over the Amazon rainforest, Proc. Natl. Acad. Sci., 113(22), 6125–6130, doi:10.1073/pnas.1524136113, 2016.

Lou, S., Holland, F., Rohrer, F., Lu, K., Bohn, B., Brauers, T., Chang, C. C., Fuchs, H., Häseler, R., Kita, K., Kondo, Y., Li,

X., Shao, M., Zeng, L., Wahner, A., Zhang, Y., Wang, W. and Hofzumahaus, A.: Atmospheric OH reactivities in the Pearl River Delta - China in summer 2006: Measurement and model results, Atmos. Chem. Phys., 10(22), 11243–11260, doi:10.5194/acp-10-11243-2010, 2010.

Lu, K., Zhang, Y., Su, H., Brauers, T., Chou, C. C., Hofzumahaus, A., Liu, S. C., Kita, K., Kondo, Y., Shao, M., Wahner, A., Wang, J., Wang, X. and Zhu, T.: Oxidant ($O_3$ + $NO_2$) production processes and formation regimes in Beijing, J. Geophys. Res., 115(D7), D07303, doi:10.1029/2009JD012714, 2010.

Mao, J., Ren, X., Brune, W. H., Olson, J. R., Crawford, J. H., Fried, A., Huey, L. G., Cohen, R. C., Heikes, B., Singh, H. B., Blake, D. R., Sachse, G. W., Diskin, G. S., Hall, S. R. and Shetter, R. E.: Airborne measurement of OH reactivity during INTEX-B, Atmos. Chem. Phys., 9(1), 163–173, doi:10.5194/acp-9-163-2009, 2009.

Mao, J., Ren, X., Chen, S., Brune, W. H., Chen, Z., Martinez, M., Harder, H., Lefer, B., Rappenglück, B., Flynn, J. and Leuchner, M.: Atmospheric oxidation capacity in the summer of Houston 2006: Comparison with summer measurements in other metropolitan studies, Atmos. Environ., 44(33), 4107–4115, doi:10.1016/j.atmosenv.2009.01.013, 2010.

Mao, J., Ren, X., Zhang, L., Van Duin, D. M., Cohen, R. C., Park, J. H., Goldstein, A. H., Paulot, F., Beaver, M. R., Crounse, J. D., Wennberg, P. O., Digangi, J. P., Henry, S. B., Keutsch, F. N., Park, C., Schade, G. W., Wolfe, G. M., Thornton, J. A. and Brune, W. H.: Insights into hydroxyl measurements and atmospheric oxidation in a California forest, Atmos. Chem. Phys., 12(17), 8009–8020, doi:10.5194/acp-12-8009-2012, 2012.

Martinez, M., Harder, H., Kubistin, D., Rudolf, M., Bozem, H. and Eerdekens, G.: Hydroxyl radicals in the tropical troposphere over the Suriname rainforest : airborne measurements, October, 15491–15536, 2010.

Michoud, V., Hansen, R. F., Locoge, N., Stevens, P. S. and Dusanter, S.: Detailed characterizations of the new Mines Douai comparative reactivity method instrument via laboratory experiments and modeling, Atmos. Meas. Tech., 8(8), 3537–3553, doi:10.5194/amt-8-3537-2015, 2015.

Millet, D. B., Jacob, D. J., Custer, T. G., de Gouw, J. A., Goldstein, A. H., Karl, T., Singh, H. B., Sive, B. C., Talbot, R. W., Warneke, C. and Williams, J.: New constraints on terrestrial and oceanic sources of atmospheric methanol, Atmos. Chem. Phys., 8(23), 6887–6905, doi:10.5194/acp-8-6887-2008, 2008.

Mogensen, D., Smolander, S., Sogachev, A., Zhou, L., Sinha, V., Guenther, A., Williams, J., Nieminen, T., Kajos, M. K., Rinne, J., Kulmala, M. and Boy, M.: Modelling atmospheric OH-reactivity in a boreal forest ecosystem, Atmos. Chem. Phys., 11(18), 9709–9719, doi:10.5194/acp-11-9709-2011, 2011.

Morgenstern, O., Braesicke, P., O'Connor, F. M., Bushell, A. C., Johnson, C. E., Osprey, S. M. and Pyle, J. A.: Evaluation of the new UKCA climate-composition model – Part 1: The stratosphere, Geosci. Model Dev., 2(1), 43–57, doi:10.5194/gmd-2-43-2009, 2009.

Müller, J.-F., Liu, Z., Nguyen, V. S., Stavrakou, T., Harvey, J. N. and Peeters, J.: The reaction of methyl peroxy and hydroxyl radicals as a major source of atmospheric methanol, Nat. Commun., 7(May), 13213, doi:10.1038/ncomms13213, 2016.

Naik, V., Voulgarakis, A., Fiore, A. M., Horowitz, L. W., Lamarque, J. F., Lin, M., Prather, M. J., Young, P. J., Bergmann, D., Cameron-Smith, P. J., Cionni, I., Collins, W. J., Dalsøren, S. B., Doherty, R., Eyring, V., Faluvegi, G., Folberth, G. A.,

Josse, B., Lee, Y. H., MacKenzie, I. A., Nagashima, T., Van Noije, T. P. C., Plummer, D. A., Righi, M., Rumbold, S. T., Skeie, R., Shindell, D. T., Stevenson, D. S., Strode, S., Sudo, K., Szopa, S. and Zeng, G.: Preindustrial to present-day changes in tropospheric hydroxyl radical and methane lifetime from the Atmospheric Chemistry and Climate Model Intercomparison Project (ACCMIP), Atmos. Chem. Phys., 13(10), 5277–5298, doi:10.5194/acp-13-5277-2013, 2013.

5  Nakashima, Y., Kato, S., Greenberg, J., Harley, P., Karl, T., Turnipseed, A., Apel, E., Guenther, A., Smith, J. and Kajii, Y.: Total OH reactivity measurements in ambient air in a southern Rocky mountain ponderosa pine forest during BEACHON-SRM08 summer campaign, Atmos. Environ., 85, 1–8, doi:10.1016/j.atmosenv.2013.11.042, 2014.

Nölscher, A. C., Williams, J., Sinha, V., Custer, T., Song, W., Johnson, A. M., Axinte, R., Bozem, H., Fischer, H., Pouvesle, N., Phillips, G., Crowley, J. N., Rantala, P., Rinne, J., Kulmala, M., Gonzales, D., Valverde-Canossa, J., Vogel, A., Hoffmann,

10  T., Ouwersloot, H. G., Vilà-Guerau De Arellano, J. and Lelieveld, J.: Summertime total OH reactivity measurements from boreal forest during HUMPPA-COPEC 2010, Atmos. Chem. Phys., 12(17), 8257–8270, doi:10.5194/acp-12-8257-2012, 2012.

Nölscher, A. C., Yañez-Serrano, A. M., Wolff, S., de Araujo, A. C., Lavrič, J. V, Kesselmeier, J., Williams, Jlscher, A. C., Yañez-Serrano, A. M., Wolff, S., de Araujo, A. C., Lavrič, J. V, Kesselmeier, J. and Williams, J.: Unexpected seasonality in quantity and composition of Amazon rainforest air reactivity., Nat. Commun., 7, 10383, doi:10.1038/ncomms10383, 2016.

15  O'Connor, F. M., Johnson, C. E., Morgenstern, O., Abraham, N. L., Braesicke, P., Dalvi, M., Folberth, G. A., Sanderson, M. G., Telford, P. J., Voulgarakis, A., Young, P. J., Zeng, G., Collins, W. J. and Pyle, J. A.: Evaluation of the new UKCA climate-composition model – Part 2: The Troposphere, Geosci. Model Dev., 7(1), 41–91, doi:10.5194/gmd-7-41-2014, 2014.

Ren, X., Harder, H., Martinez, M., Lesher, R. L., Oliger, A., Shirley, T., Adams, J., Simpas, J. B. and Brune, W. H.: $HO_x$ concentrations and OH reactivity observations in New York City during PMTACS-NY2001, Atmos. Environ., 37(26), 3627–

20  3637, doi:10.1016/S1352-2310(03)00460-6, 2003a.

Ren, X., Harder, H., Martinez, M., Lesher, R. L., Oliger, A., Simpas, J. B., Brune, W. H., Schwab, J. J., Demerjian, K. L., He, Y., Zhou, X. and Gao, H.: OH and $HO_2$ chemistry in the urban atmosphere of New York City, Atmos. Environ., 37(26), 3639–3651, doi:10.1016/S1352-2310(03)00459-X, 2003b.

Ren, X., Brune, W. H., Cantrell, C. A., Edwards, G. D., Shirley, T., Metcalf, A. R. and Lesher, R. L.: Hydroxyl and peroxy

25  radical chemistry in a rural area of central Pennsylvania: Observations and model comparisons, J. Atmos. Chem., 52(3), 231–257, doi:10.1007/s10874-005-3651-7, 2005.

Ren, X., Brune, W. H., Mao, J., Mitchell, M. J., Lesher, R. L., Simpas, J. B., Metcalf, A. R., Schwab, J. J., Cai, C., Li, Y., Demerjian, K. L., Felton, H. D., Boynton, G., Adams, A., Perry, J., He, Y., Zhou, X. and Hou, J.: Behavior of OH and $HO_2$ in the winter atmosphere in New York City, Atmos. Environ., 40(SUPPL. 2), 252–263, doi:10.1016/j.atmosenv.2005.11.073,

30  2006a.

Ren, X., Brune, W. H., Oliger, A., Metcalf, A. R., Simpas, J. B., Shirley, T., Schwab, J. J., Bai, C., Roychowdhury, U., Li, Y., Cai, C., Demerjian, K. L., He, Y., Zhou, X., Gao, H. and Hou, J.: OH, $HO_2$, and OH reactivity during the PMTACS-NY Whiteface Mountain 2002 campaign: Obervations and model comparison, J. Geophys. Res. Atmos., 111(10), 1–12, doi:10.1029/2005JD006126, 2006b.

38

Safieddine, S. A., Heald, C. L. and Henderson, B. H.: The global nonmethane reactive organic carbon budget: A modeling perspective, Geophys. Res. Lett., 44(8), 3897–3906, doi:10.1002/2017GL072602, 2017.

Shirley, T. R., Brune, W. H., Ren, X., Mao, J., Lesher, R., Cardenas, B., Volkamer, R., Molina, L. T., Molina, M. J., Lamb, B., Velasco, E., Jobson, T. and Alexander, M.: Atmospheric oxidation in the Mexico City Metropolitan Area (MCMA) during

5    April 2003, Atmos. Chem. Phys., 6, 2753–2765, doi:10.5194/acpd-5-6041-2005, 2006.

Sinha, V., Williams, J., Crowley, J. N. and Lelieveld, J.: The Comparative Reactivity Method - a new tool to measure total OH reactivity in ambient air, Atmos. Chem. Phys., 8(8), 2213–2227, doi:doi:10.5194/acp-8-2213-2008, 2008.

Sinha, V., Williams, J., Lelieveld, J., Ruuskanen, T. M., Kajos, M. K., Patokoski, J., Hellen, H., Hakola, H., Mogensen, D., Boy, M., Rinne, J. and Kulmala, M.: OH reactivity measurements within a boreal forest: Evidence for unknown reactive

10    emissions, Environ. Sci. Technol., 44(17), 6614–6620, doi:10.1021/es101780b, 2010.

Sinha, V., Williams, J., Diesch, J. M., Drewnick, F., Martinez, M., Harder, H., Regelin, E., Kubistin, D., Bozem, H., Hosaynali-Beygi, Z., Fischer, H., Andrés-Hernández, M. D., Kartal, D., Adame, J. A. and Lelieveld, J.: Constraints on instantaneous ozone production rates and regimes during DOMINO derived using in-situ OH reactivity measurements, Atmos. Chem. Phys., 12(15), 7269–7283, doi:10.5194/acp-12-7269-2012, 2012.

15    Squire, O. J., Archibald, A. T., Griffiths, P. T., Jenkin, M. E., Smith, D. and Pyle, J. A.: Influence of isoprene chemical mechanism on modelled changes in tropospheric ozone due to climate and land use over the 21st century, Atmos. Chem. Phys., 15(9), 5123–5143, doi:10.5194/acp-15-5123-2015, 2015.

Stevenson, D. S., Dentener, F. J., Schultz, M. G., Ellingsen, K., van Noije, T. P. C., Wild, O., Zeng, G., Amann, M., Atherton, C. S., Bell, N., Bergmann, D. J., Bey, I., Butler, T., Cofala, J., Collins, W. J., Derwent, R. G., Doherty, R. M., Drevet, J., Eskes,

20    H. J., Fiore, A. M., Gauss, M., Hauglustaine, D. A., Horowitz, L. W., Isaksen, I. S. A., Krol, M. C., Lamarque, J. F., Lawrence, M. G., Montanaro, V., Müller, J. F., Pitari, G., Prather, M. J., Pyle, J. A., Rast, S., Rodriquez, J. M., Sanderson, M. G., Savage, N. H., Shindell, D. T., Strahan, S. E., Sudo, K. and Szopa, S.: Multimodel ensemble simulations of present-day and near-future tropospheric ozone, J. Geophys. Res. Atmos., 111(8), doi:10.1029/2005JD006338, 2006.

Voulgarakis, A., Naik, V., Lamarque, J. F., Shindell, D. T., Young, P. J., Prather, M. J., Wild, O., Field, R. D., Bergmann, D.,

25    Cameron-Smith, P., Cionni, I., Collins, W. J., Dalsøren, S. B., Doherty, R. M., Eyring, V., Faluvegi, G., Folberth, G. A., Horowitz, L. W., Josse, B., MacKenzie, I. A., Nagashima, T., Plummer, D. A., Righi, M., Rumbold, S. T., Stevenson, D. S., Strode, S. A., Sudo, K., Szopa, S. and Zeng, G.: Analysis of present day and future OH and methane lifetime in the ACCMIP simulations, Atmos. Chem. Phys., 13(5), 2563–2587, doi:10.5194/acp-13-2563-2013, 2013.

Whalley, L. K., Stone, D., Bandy, B., Dunmore, R., Hamilton, J. F., Hopkins, J., Lee, J. D., Lewis, A. C. and Heard, D. E.:

30    Atmospheric OH reactivity in central London: Observations, model predictions and estimates of in situ ozone production, Atmos. Chem. Phys., 16(4), 2109–2122, doi:10.5194/acp-16-2109-2016, 2016.

Yan, C., Kocevska, S. and Krasnoperov, L. N.: Kinetics of the Reaction of $CH_3O_2$ Radicals with OH Studied over the 292-526 K Temperature Range, J. Phys. Chem. A, 120(31), 6111–6121, doi:10.1021/acs.jpca.6b04213, 2016.

Yang, Y., Shao, M., Wang, X., Nölscher, A. C., Kessel, S., Guenther, A. and Williams, J.: Towards a quantitative

understanding of total OH reactivity: A review, Atmos. Environ., 134, 147–161, doi:10.1016/j.atmosenv.2016.03.010, 2016.

Yang, Y., Shao, M., Keßel, S., Li, Y., Lu, K., Lu, S., Williams, J., Zhang, Y., Zeng, L., Nölscher, A. C., Wu, Y., Wang, X. and Zheng, J.: How the OH reactivity affects the ozone production efficiency: Case studies in Beijing and Heshan, China, Atmos. Chem. Phys., 17(11), 7127–7142, doi:10.5194/acp-17-7127-2017, 2017.

Young, P. J., Archibald, A. T., Bowman, K. W., Lamarque, J.-F., Naik, V., Stevenson, D. S., Tilmes, S., Voulgarakis, A., Wild, O., Bergmann, D., Cameron-Smith, P., Cionni, I., Collins, W. J., Dalsøren, S. B., Doherty, R. M., Eyring, V., Faluvegi, G., Horowitz, L. W., Josse, B., Lee, Y. H., MacKenzie, I. A., Nagashima, T., Plummer, D. A., Righi, M., Rumbold, S. T., Skeie, R. B., Shindell, D. T., Strode, S. A., Sudo, K., Szopa, S. and Zeng, G.: Pre-industrial to end 21st century projections of tropospheric ozone from the Atmospheric Chemistry and Climate Model Intercomparison Project (ACCMIP), Atmos. Chem. Phys., 13(4), 2063–2090, doi:10.5194/acp-13-2063-2013, 2013.

Zannoni, N., Gros, V., Lanza, M., Sarda, R., Bonsang, B., Kalogridis, C., Preunkert, S., Legrand, M., Jambert, C., Boissard, C. and Lathiere, J.: OH reactivity and concentrations of biogenic volatile organic compounds in a Mediterranean forest of downy oak trees, Atmos. Chem. Phys., 16(3), 1619–1636, doi:10.5194/acp-16-1619-2016, 2016.

Zannoni, N., Gros, V., Sarda Esteve, R., Kalogridis, C., Michoud, V., Dusanter, S., Sauvage, S., Locoge, N., Colomb, A. and Bonsang, B.: Summertime OH reactivity from a receptor coastal site in the Mediterranean Basin, Atmos. Chem. Phys., 17(20), 12645–12658, doi:10.5194/acp-17-12645-2017, 2017.

5

10

15

20

25

**Supplementary material**

Tables S1, S2 and S3 below report the values of OH production and loss fluxes in the whole troposphere, boundary layer and at the surface respectively, obtained in the UM-UKCA runs described in the current work.  The values for the base run are in reasonably good agreement with those reported by Lelieveld and co-workers (Lelieveld et al., 2016).

5

10

15

20

25

30

| OH production | Lelieveld et al., 2016 | Base run | X + OH run | $CH_3O_2$ + OH run 1 | $CH_3O_2$ + OH run 2 | $CH_3O_2$ + OH run 3 |
|---|---|---|---|---|---|---|
| $O(^1D) + H_2O$ | 84.0 (33%) | 79.1 (39.5%) | 79.4 (39.7%) | 78.0 (38.6%) | 78.1 (38.9%) | 78.2 (39.1%) |
| $NO + HO_2$ | 76.6 (30%) | 55.0 (27.5%) | 55.0 (27.5%) | 56.7 (28.1%) | 56.5 (28.1%) | 56.2 (28.1%) |
| $O_3 + HO_2$ | 34.4 (14%) | 23.5 (11.8%) | 23.5 (11.7%) | 24.1 (11.9%) | 23.9 (11.9%) | 23.7 (11.8%) |
| $H_2O_2 + h\nu$ | 24.8 (10%) | 20.9 (10.5%) | 20.9 (10.5%) | 22.9 (11.4%) | 22.4 (11.2%) | 22.0 (11.0%) |
| OVOCs, ROOH + $h\nu$ | 31.4 (13%) | 21.5 (10.8%) | 21.1 (10.6%) | 20.2 (10%) | 20.0 (10.0%) | 19.9 (10.0%) |
| **Total OH production** | **251.2** | **200.1** | **199.9** | **201.9** | **200.9** | **199.9** |
| **OH loss** | | | | | | |
| $OH + HO_y$ [a] | 46.2 (18%) | 32.5 (16.3%) | 31.9 (16.0%) | 33.0 (16.4%) | 32.6 (16.2%) | 32.1 (16.1%) |
| $OH + NO_x$ | 4.1 (1.5%) | 2.2 (1.1%) | 2.1 (1.0%) | 2.2 (1.1%) | 2.2 (1.1%) | 2.2 (1.1%) |
| $OH + NO_z$ [b] | | 1.4 (0.7%) | 1.4 (0.7%) | 1.4 (0.7%) | 1.4 (0.7%) | 1.4 (0.7%) |
| $OH + CH_4$ | 29.8 (12%) | 26.7 (13.3%) | 26.1 (13.1%) | 26.2 (13.0%) | 26.0 (13.0%) | 25.9 (13.0%) |
| OH + CO | 97.8 (39%) | 90.3 (45.1%) | 89.7 (44.9%) | 90.0 (44.6%) | 89.5 (44.6%) | 89.1 (44.6%) |
| $OH + C_1$ VOCs [c] | 37.0 (15%) | 24.8 (12.4%) | 24.0 (12.0%) | 22.5 (11.2%) | 22.7 (11.3%) | 22.8 (11.4%) |
| $OH + C_{2,3}$ VOCs [d] | 34.7 (14%) | 3.5 (1.7%) | 3.4 (1.7%) | 3.5 (1.7%) | 3.5 (1.7%) | 3.5 (1.7%) |
| OH + isoprene and ox. prod. [e] | | 17.0 (8.5%) | 16.5 (8.3%) | 17.1 (8.5%) | 17.0 (8.5%) | 17.0 (8.5%) |
| OH + monoterpenes | | 0.4 (0.2%) | 0.3 (0.2%) | 0.4 (0.2%) | 0.4 (0.2%) | 0.4 (0.2%) |
| OH + halogenated [f] | 1.6 (0.5%) | 0.0 (0.0%) | 0.0 (0.0%) | 0.0 (0.0%) | 0.0 (0.0%) | 0.0 (0.0%) |
| OH + sulphur species [g] | | 1.3 (0.6%) | 1.2 (0.6%) | 1.3 (0.6%) | 1.3 (0.6%) | 1.3 (0.6%) |
| OH + X | - | - | 2.9 (1.5%) | - | - | - |
| $OH + CH_3O_2 \rightarrow HO_2 + CH_3O$ | - | - | - | 4.4 (2.2%) | 3.5 (1.7%) | 2.6 (1.3%) |
| $OH + CH_3O_2 \rightarrow CH_3OH + O_2$ | - | - | - | - | 0.9 (0.4%) | 1.7 (0.9%) |
| **Total OH loss** | **251.2** | **200.1** | **199.9** | **201.9** | **200.9** | **199.9** |

**Notes:**

[a] $HO_y$ = $H_2$, $O_3$, $H_2O_2$, OH, $HO_2$, $O(^3P)$

[b] $NO_z$ = PAN, MPAN, PPAN, HONO, $HNO_3$, $HNO_4$, $NO_3$, NALD, $CH_3ONO_2$, $NO_3$, isoprene nitrate

[c] $C_1$ VOCs = $CH_3OH$, formaldehyde, methyl hydroperoxide, formic acid

[d] $C_{2,3}$ VOCs = ethane, propane, acetaldehyde, propionaldehyde, ethyl, *n*-propyl and *i*-propyl hydroperoxides, acetone, acetone hydroperoxide

[e] isoprene oxidation products = isoprene hydroperoxide, MACR, MACROOH, hydroxyacetone, methyl glyoxal, acetic acid, peracetic acid

[f] halogenated species = $CH_3Br$, ClO, BrO, HBr, HCl, $ClONO_2$, OClO, HOCl

[g] sulphur species = $SO_2$, $H_2S$, dimethyl sulphide, COS, $CS_2$

**Table S1: Annual mean tropospheric OH production and loss fluxes in Tmol yr$^{-1}$.**

| OH production | Base run | X + OH run | CH$_3$O$_2$ + OH run 1 | CH$_3$O$_2$ + OH run 2 | CH$_3$O$_2$ + OH run 3 |
|---|---|---|---|---|---|
| O($^1$D) + H$_2$O | 20.2 (38.4 %) | 20.1 (39.4 %) | 19.9 (37.6%) | 19.9 (37.8%) | 19.9 (38.0%) |
| NO + HO$_2$ | 17.0 (32.4%) | 16.4 (32.0%) | 17.5 (33.0%) | 17.4 (33.0%) | 17.3 (33.0%) |
| O$_3$ + HO$_2$ | 4.5 (8.5%) | 4.3 (8.4%) | 4.5 (8.6%) | 4.5 (8.6%) | 4.5 (8.5%) |
| H$_2$O$_2$ + $hv$ | 2.9 (5.5%) | 2.8 (5.5%) | 3.2 (6.0%) | 3.1 (5.9%) | 3.0 (5.8%) |
| OVOCs, ROOH + $hv$ | 8.0 (15.3%) | 7.5 (14.7%) | 7.8 (14.7%) | 7.7 (14.7%) | 7.7 (14.7%) |
| **Total OH production** | **52.5** | **51.1** | **52.8** | **52.6** | **52.5** |
| **OH loss** | | | | | |
| OH + HO$_y$ $^a$ | 6.9 (13.2%) | 6.5 (12.7%) | 7.0 (13.2%) | 6.9 (13.1%) | 6.8 (13.0%) |
| OH + NO$_x$ | 1.2 (2.3%) | 1.0 (2.0%) | 1.2 (2.2%) | 1.2 (2.3%) | 1.2 (2.3%) |
| OH + NO$_z$ $^b$ | 0.6 (1.1%) | 0.6 (1.1%) | 0.6 (1.1%) | 0.6 (1.1%) | 0.6 (1.1%) |
| OH + CH$_4$ | 6.9 (13.1%) | 6.5 (12.7%) | 6.7 (12.7%) | 6.7 (12.7%) | 6.7 (12.7%) |
| OH + CO | 19.1 (36.3%) | 18.0 (35.2%) | 18.9 (35.8%) | 18.9 (35.9%) | 18.8 (35.9%) |
| OH + C$_1$ VOCs $^c$ | 6.5 (12.4%) | 6.0 (11.7%) | 6.0 (11.4%) | 6.0 (11.5%) | 6.0 (11.5%) |
| OH + C$_{2,3}$ VOCs $^d$ | 0.9 (1.8%) | 0.9 (1.7%) | 0.9 (1.8%) | 0.9 (1.8%) | 0.9 (1.8%) |
| OH + isoprene and ox. prod. $^e$ | 9.4 (18.0%) | 8.7 (17.1%) | 9.4 (17.8%) | 9.4 (17.9%) | 9.4 (17.9%) |
| OH + monoterpenes | 0.3 (0.6%) | 0.3 (0.5%) | 0.3 (0.6%) | 0.3 (0.6%) | 0.3 (0.6%) |
| OH + halogenated $^f$ | 0.0 (0.0%) | 0.0 (0.0%) | 0.0 (0.0%) | 0.0 (0.0%) | 0.0 (0.0%) |
| OH + sulphur species $^g$ | 0.7 (1.3%) | 0.6 (1.2%) | 0.7 (1.2%) | 0.7 (1.2%) | 0.7 (1.2%) |
| OH + X | - | 2.0 (4.0%) | - | - | - |
| OH + CH$_3$O$_2$ → HO$_2$ + CH$_3$O | - | - | 1.0 (2%) | 0.8 (1.6%) | 0.6 (1.2%) |
| OH + CH$_3$O$_2$ → CH$_3$OH + O$_2$ | - | - | - | 0.2 (0.4%) | 0.4 (0.8%) |
| **Total OH loss** | **52.5** | **51.1** | **52.8** | **52.6** | **52.5** |

**Notes:**

$^a$ HO$_y$ = H$_2$, O$_3$, H$_2$O$_2$, OH, HO$_2$, O($^3$P)

$^b$ NO$_z$ = PAN, MPAN, PPAN, HONO, HNO$_3$, HNO$_4$,NO$_3$, NALD, CH$_3$ONO$_2$, NO$_3$, isoprene nitrate

$^c$ C$_1$ VOCs = CH$_3$OH, formaldehyde, methyl hydroperoxide, formic acid

$^d$ C$_{2,3}$ VOCs = ethane, propane, acetaldehyde, propionaldehyde, ethyl, $n$-propyl and $i$-propyl hydroperoxides, acetone, acetone hydroperoxide

$^e$ isoprene oxidation products = isoprene hydroperoxide, MACR, MACROOH, hydroxyacetone, methyl glyoxal, acetic acid, peracetic acid

$^f$ halogenated species = CH$_3$Br, ClO, BrO, HBr, HCl, ClONO$_2$, OClO, HOCl

$^g$ sulphur species = SO$_2$, H$_2$S, dimethyl sulphide, COS, CS$_2$

**Table S2: Annual mean OH production and loss fluxes in the boundary layer in Tmol yr$^{-1}$.**

| OH production | Base run | X + OH run | $CH_3O_2$ + OH run 1 | $CH_3O_2$ + OH run 2 | $CH_3O_2$ + OH run 3 |
|---|---|---|---|---|---|
| $O(^1D) + H_2O$ | 0.78 (30.6%) | 0.78 (32.8 %) | 0.77 (30.1%) | 0.77 (30.2%) | 0.78 (30.4%) |
| $NO + HO_2$ | 1.00 (39.3%) | 0.91 (38.3%) | 1.02 (39.9%) | 1.02 (39.8%) | 1.02 (39.8%) |
| $O_3 + HO_2$ | 0.18 (7.0%) | 0.17 (6.9%) | 0.18 (7.0%) | 0.18 (7.0%) | 0.18 (7.0%) |
| $H_2O_2 + hv$ | 0.10 (3.8%) | 0.09 (3.9%) | 0.11 (4.1%) | 0.10 (4.1%) | 0.10 (4.0%) |
| OVOCs, ROOH $+ hv$ | 0.50 (19.4%) | 0.43 (18.0%) | 0.48 (18.9%) | 0.48 (18.9%) | 0.48 (18.9%) |
| **Total OH production** | **2.56** | **2.38** | **2.57** | **2.56** | **2.55** |
| **OH loss** | | | | | |
| $OH + HO_y$ [a] | 0.27 (10.7%) | 0.25 (10.3%) | 0.27 (10.7%) | 0.27 (10.6%) | 0.27 (10.5%) |
| $OH + NO_x$ | 0.08 (3.2%) | 0.07 (2.7%) | 0.08 (3.2%) | 0.08 (3.2%) | 0.08 (3.2%) |
| $OH + NO_z$ [b] | 0.03 (1.2%) | 0.03 (1.1%) | 0.03 (1.2%) | 0.03 (1.2%) | 0.03 (1.2%) |
| $OH + CH_4$ | 0.29 (11.5%) | 0.27 (11.3%) | 0.29 (11.2%) | 0.29 (11.2%) | 0.29 (11.2%) |
| OH + CO | 0.79 (30.9%) | 0.71 (29.3%) | 0.78 (30.5%) | 0.78 (30.5%) | 0.78 (30.6%) |
| $OH + C_1$ VOCs [c] | 0.27 (10.7%) | 0.24 (10.0%) | 0.26 (10.0%) | 0.26 (10.0%) | 0.26 (10.0%) |
| $OH + C_{2,3}$ VOCs [d] | 0.05 (1.8%) | 0.04 (1.7%) | 0.05 (1.8%) | 0.05 (1.8%) | 0.05 (1.8%) |
| OH + isoprene and ox. prod. [e] | 0.69 (27.1%) | 0.59 (24.8%) | 0.69 (26.9%) | 0.69 (27.0%) | 0.69 (27.0%) |
| OH + monoterpenes | 0.04 (1.6%) | 0.03 (1.1%) | 0.04 (1.6%) | 0.04 (1.6%) | 0.04 (1.6%) |
| OH + halogenated [f] | 0.00 (0.0%) | 0.00 (0.0%) | 0.00 (0.0%) | 0.00 (0.0%) | 0.00 (0.0%) |
| OH + sulphur species [g] | 0.04 (1.4%) | 0.03 (1.4%) | 0.04 (1.4%) | 0.04 (1.4%) | 0.04 (1.4%) |
| OH + X | - | 0.14 (6.0%) | - | - | - |
| $OH + CH_3O_2 \rightarrow HO_2 + CH_3O$ | - | - | 0.04 (1.6%) | 0.03 (1.3%) | 0.02 (1.0%) |
| $OH + CH_3O_2 \rightarrow CH_3OH + O_2$ | - | - | - | 0.01 (0.3%) | 0.02 (0.6%) |
| **Total OH loss** | **2.56** | **2.38** | **2.57** | **2.56** | **2.55** |

**Notes:**

[a] $HO_y = H_2, O_3, H_2O_2, OH, HO_2, O(^3P)$

[b] $NO_z$ = PAN, MPAN, PPAN, HONO, $HNO_3$, $HNO_4$, $NO_3$, NALD, $CH_3ONO_2$, $NO_3$, isoprene nitrate

[c] $C_1$ VOCs = $CH_3OH$, formaldehyde, methyl hydroperoxide, formic acid

[d] $C_{2,3}$ VOCs = ethane, propane, acetaldehyde, propionaldehyde, ethyl, $n$-propyl and $i$-propyl hydroperoxides, acetone, acetone hydroperoxide

[e] isoprene oxidation products = isoprene hydroperoxide, MACR, MACROOH, hydroxyacetone, methyl glyoxal, acetic acid, peracetic acid

[f] halogenated species = $CH_3Br$, ClO, BrO, HBr, HCl, $ClONO_2$, OClO, HOCl

[g] sulphur species = $SO_2$, $H_2S$, dimethyl sulphide, COS, $CS_2$

**Table S3: Annual mean OH production and loss fluxes at the surface in Tmol yr$^{-1}$.**
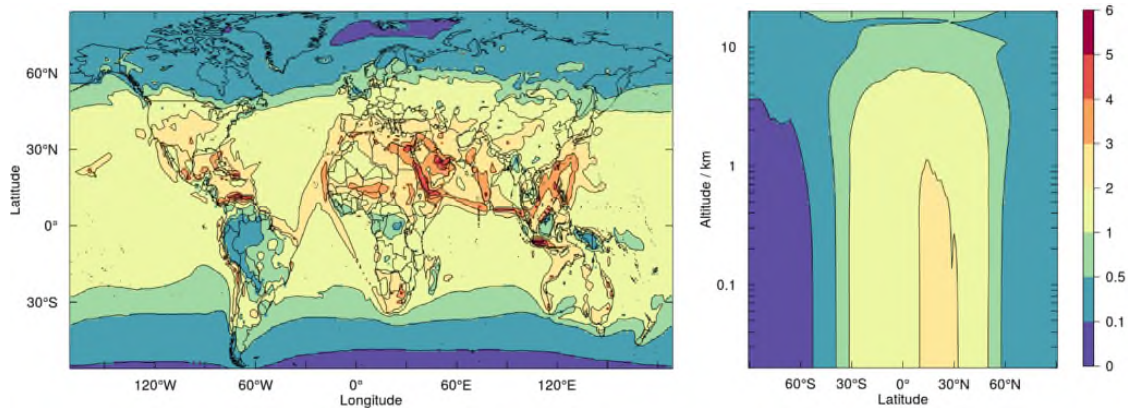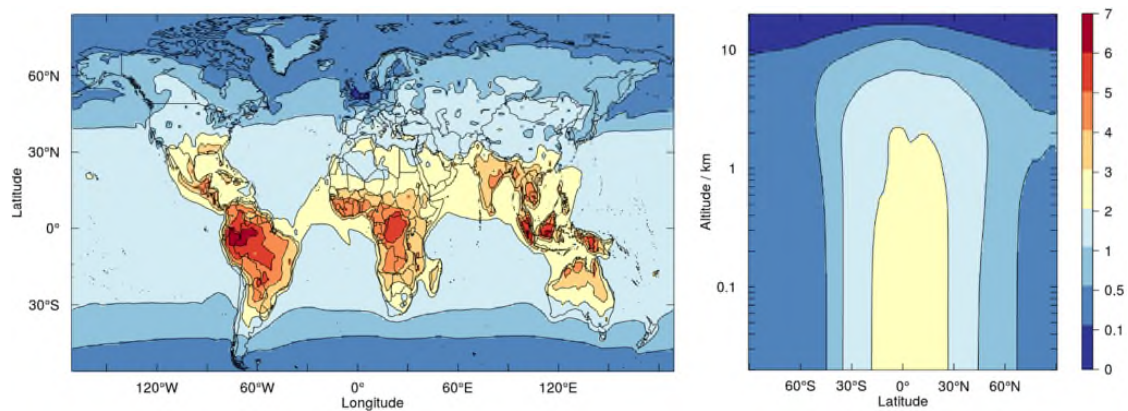
**Figure S1: Annual mean OH number density in $10^6$ molecules $cm^{-3}$ at the surface (left) and as a zonal mean (right).**



**Figure S2: Annual mean HO$_2$ number density in $10^8$ molecules $cm^{-3}$ at the surface (left) and as a zonal mean (right).**
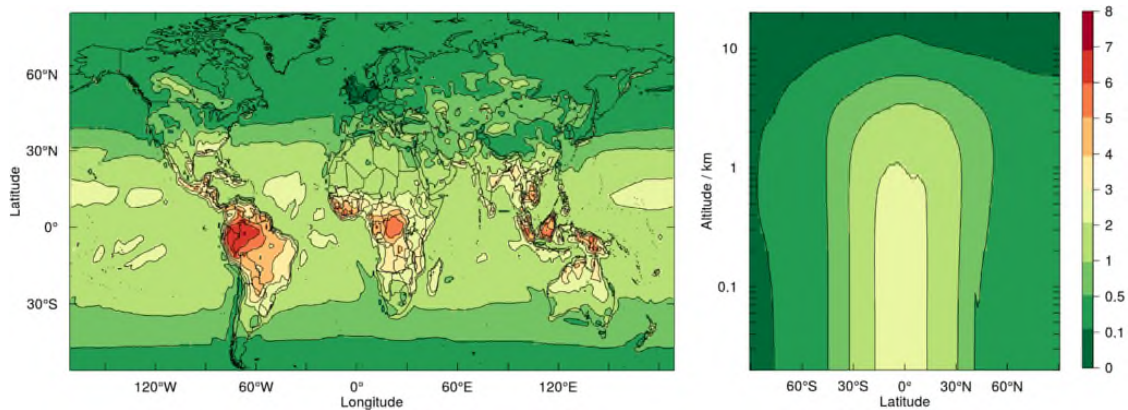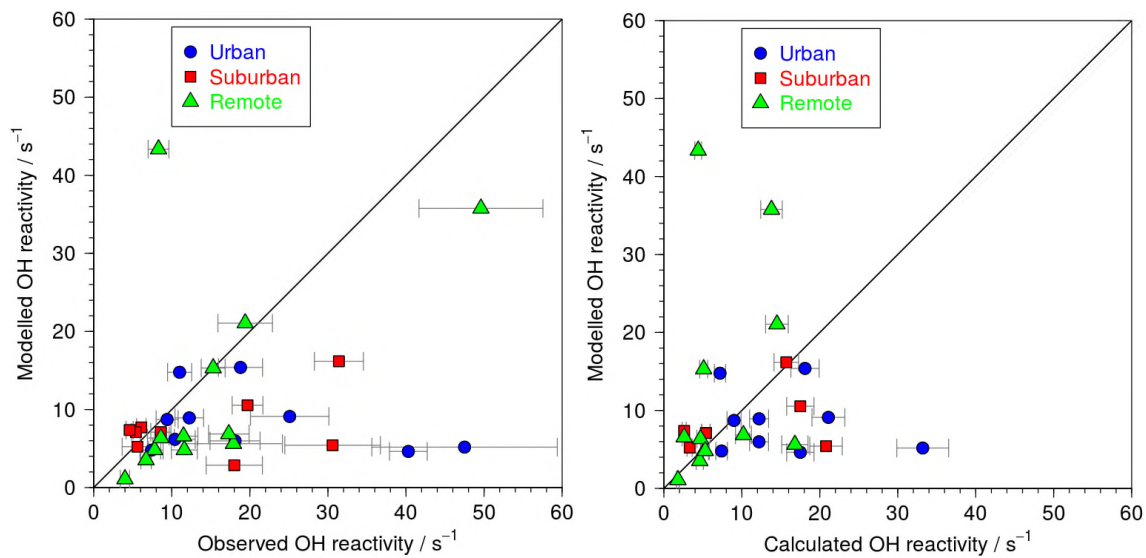


5

**Figure S4: Scatter plots of OH reactivity calculated from modelled sinks against observed total OH reactivity (left) and OH reactivity calculated from individual measured species (right).**
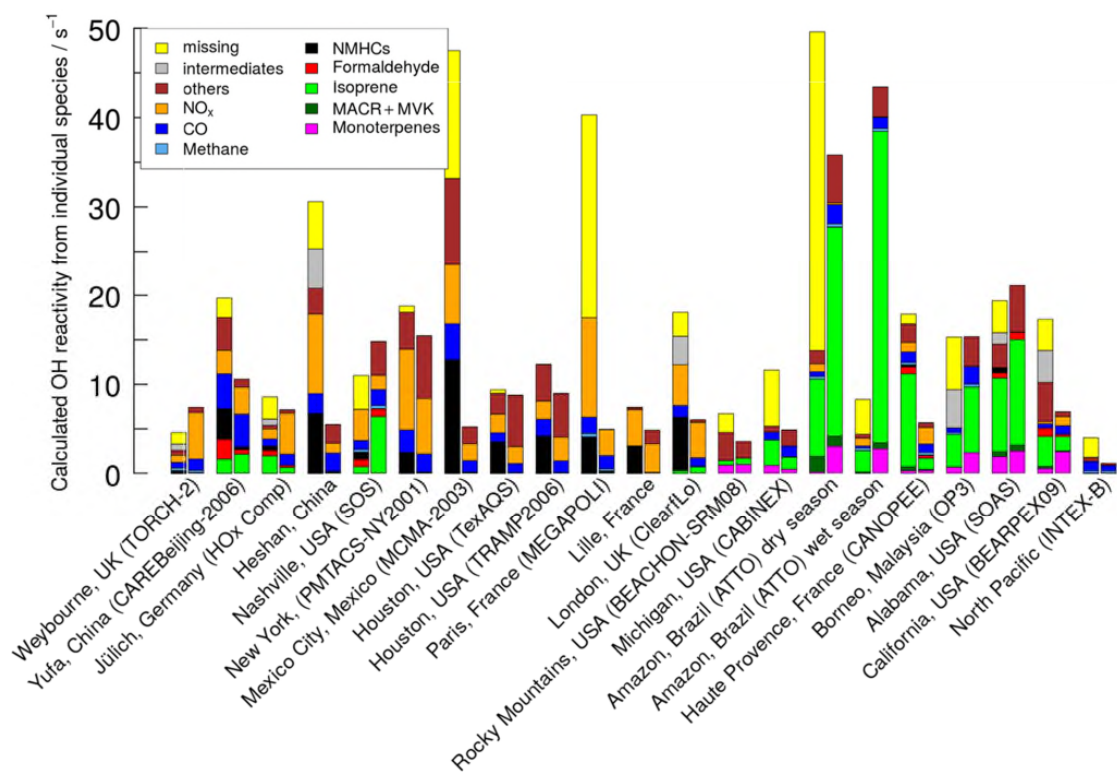
**Figure S5: Bar plot comparing the speciated OH reactivity from individual field campaigns. For each pair of bars, the bar on the left represents the reactivities calculated from measured species and the one on the right the reactivities from modelled species.**
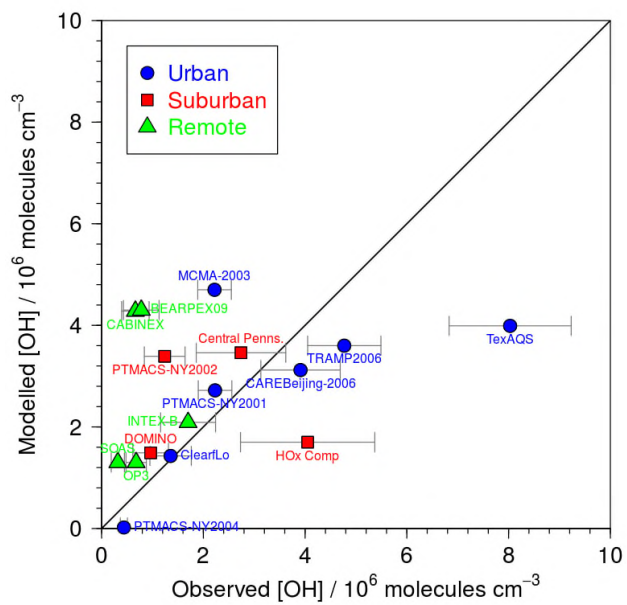
**Figure S6: Scatter plot of modelled against observed [OH]. Error bars represent the $2\sigma$ uncertainty from each individual measurement.**
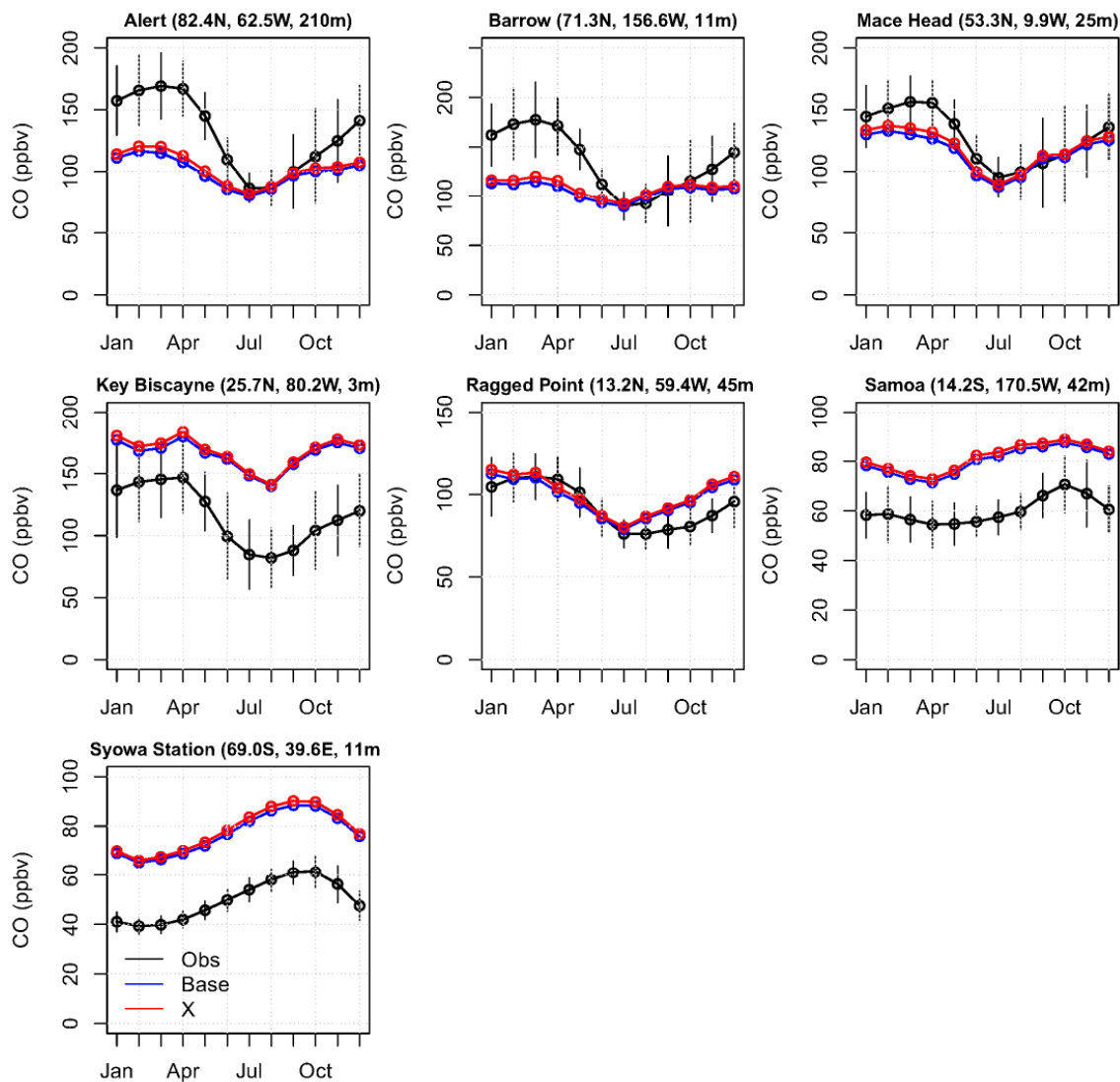
**Figure S17: Comparison of CO observations (black data points and lines) with the base run model (blue points and lines) and the model including OH sink X (red points and lines).**

5
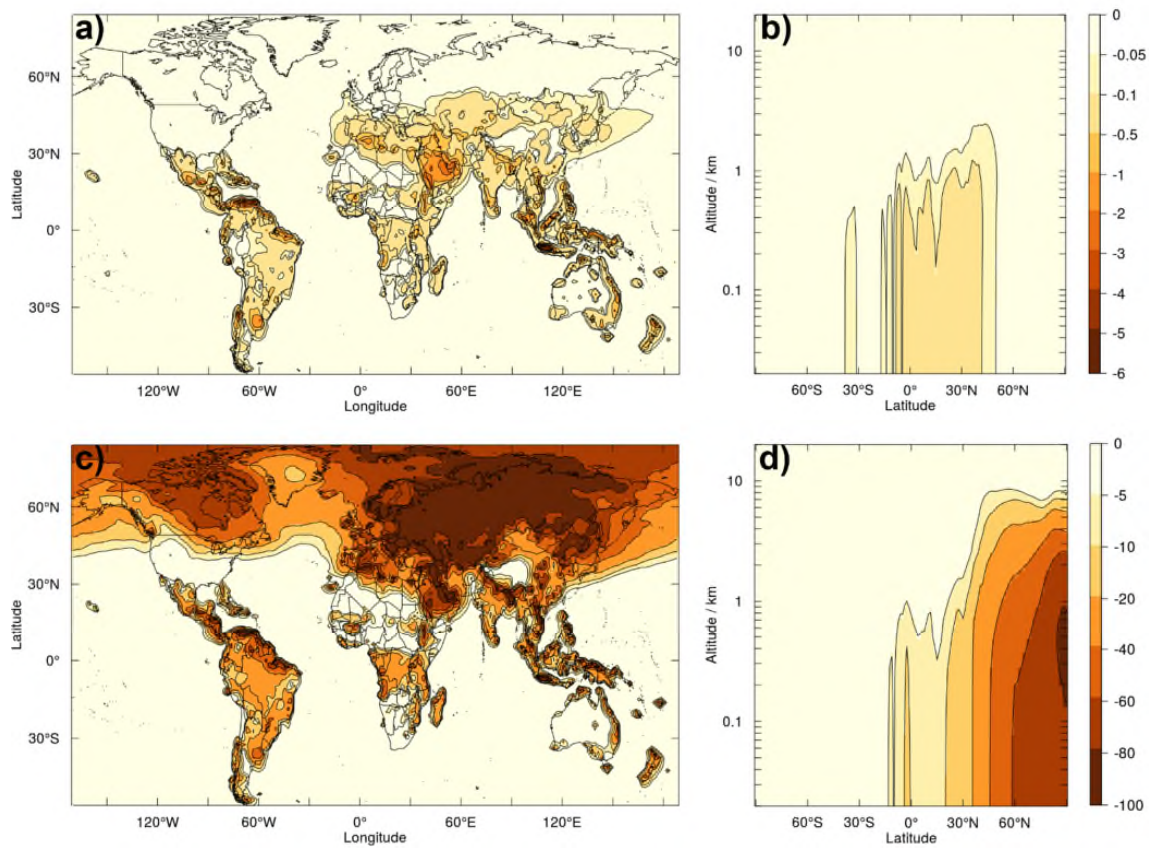
**Figure S2S8: Mean change in OH concentration in the boreal winter (DJF) following inclusion of R3: absolute change in $10^6$ molecules cm$^{-3}$ a) at the surface and b) as a zonal mean, and relative percentage change c) at the surface and d) as a zonal mean.**
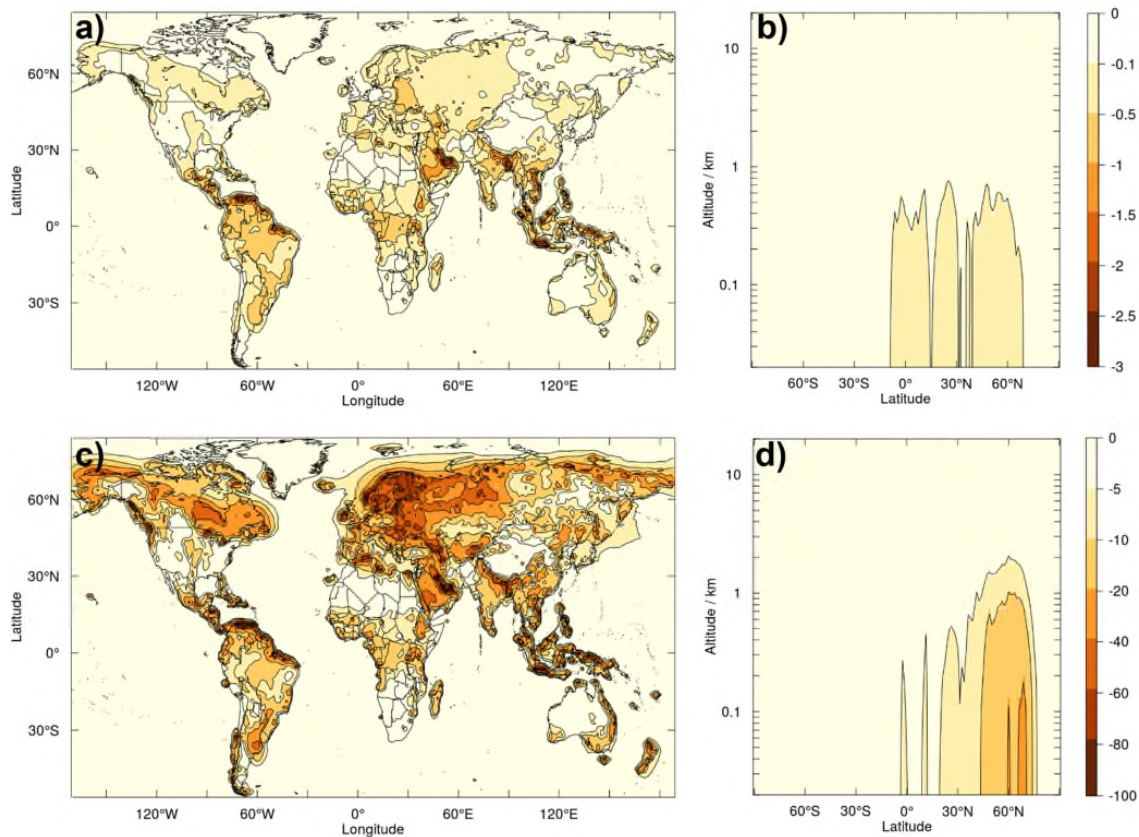
5

10
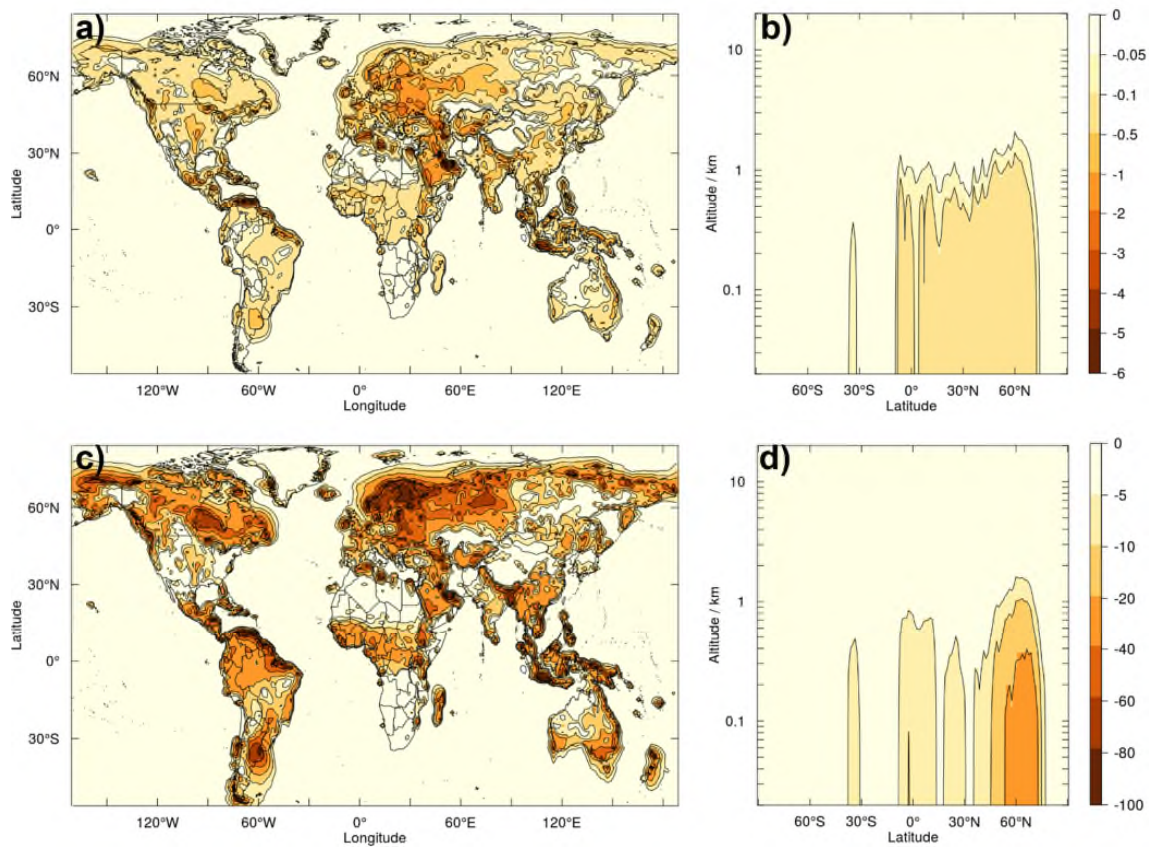
**Figure S39: Mean change in OH concentration in the boreal summer (JJA) following inclusion of R3: absolute change in $10^6$ molecules $cm^{-3}$ a) at the surface and b) as a zonal mean, and relative percentage change c) at the surface and d) as a zonal mean.**

5

10

**Figure S10: Annual mean change in HO$_2$ concentration following inclusion of R3: absolute change in 10$^8$ molecules cm$^{-3}$ a) at the surface and b) as a zonal mean, and relative percentage change c) at the surface and d) as a zonal mean.**

5

10
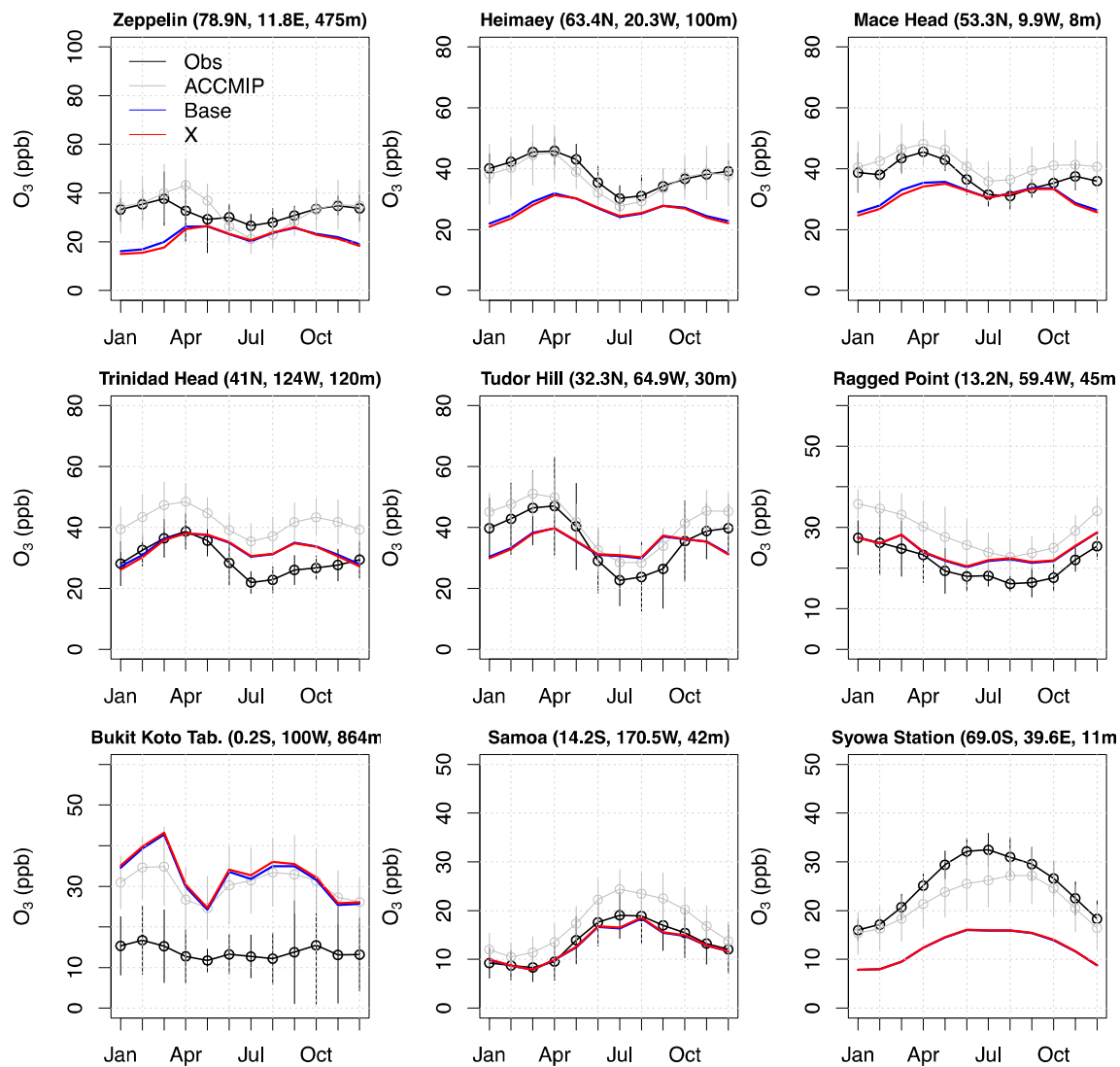
**Figure S114**: Comparison of ozone observations (black data points and lines) with the base run model (red points and lines) and the model including OH sink X (blue points and lines). The multi model mean results from the ACCMIP year 2000 simulations are shown in grey with the grey bars indicating one standard deviation of the ACCMIP multi model ensemble (Young et al., 2013).
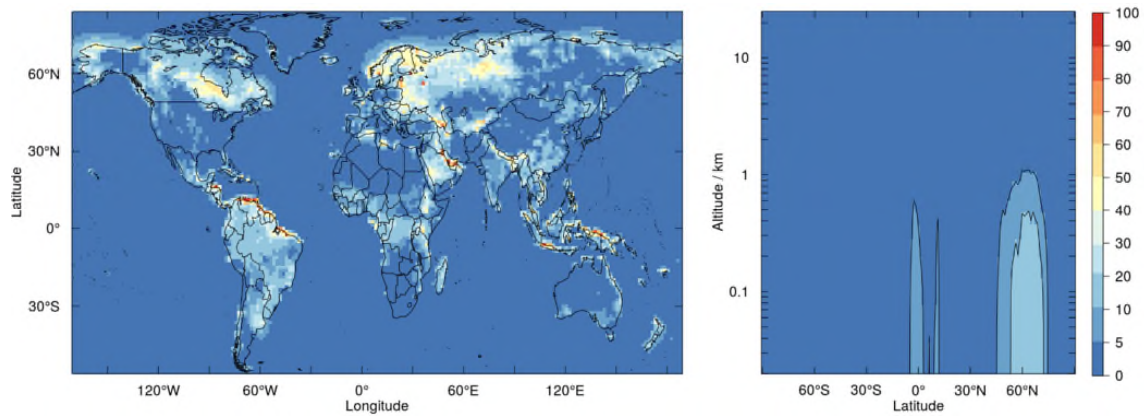
**Figure S125: Percentage contribution of the flux through R3 (X + OH) to the total OH loss flux at the surface (left) and as zonal mean (right).**
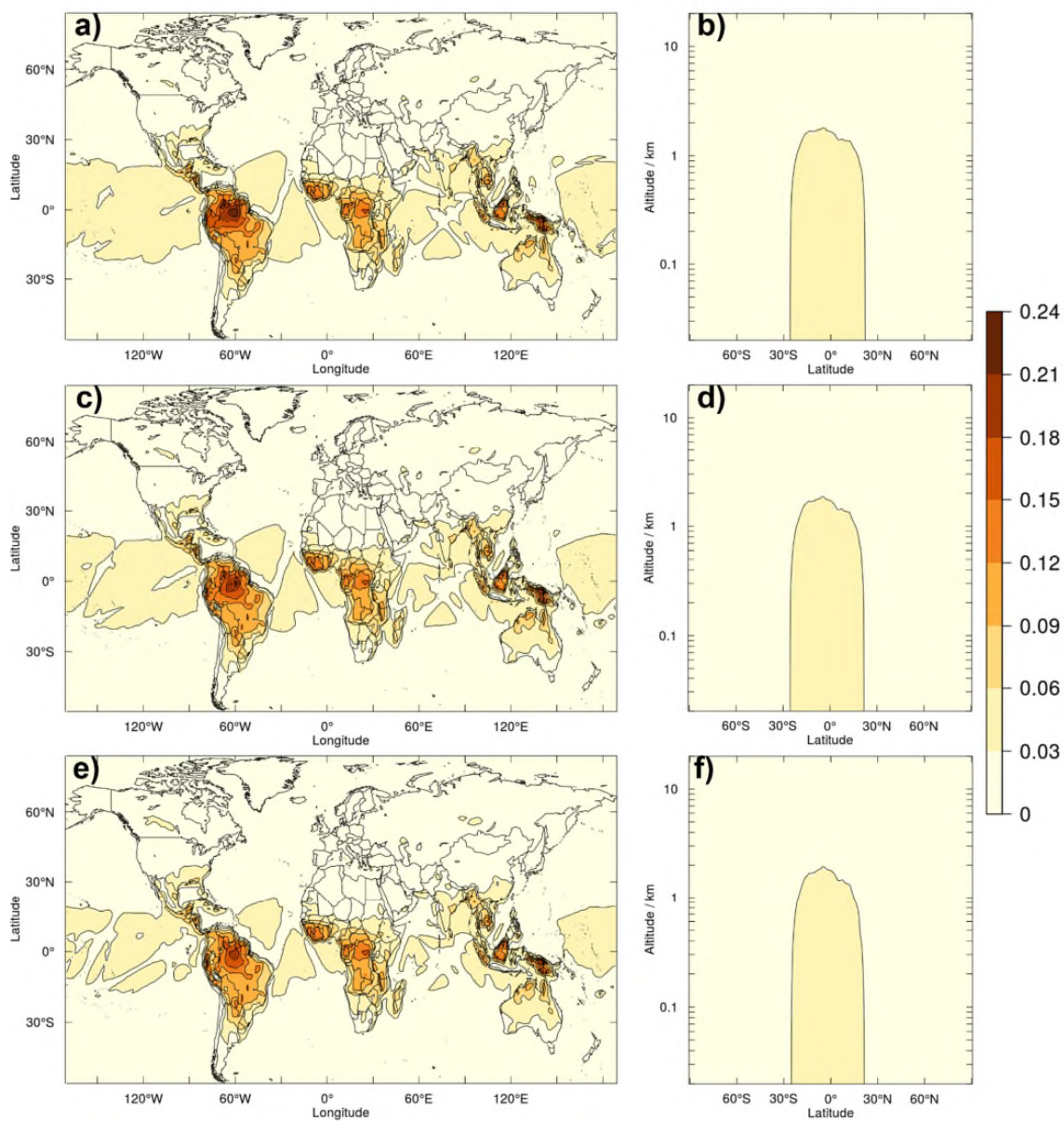
**Figure S13: Mean changes in $k_{OH}$ (in s$^{-1}$) from run 1 (a and b, top row), run 2 (c and d, middle row), and run 3 (e and f, bottom row), relative to the base run. Changes are shown for the surface (left column) and as a zonal mean (right column).**
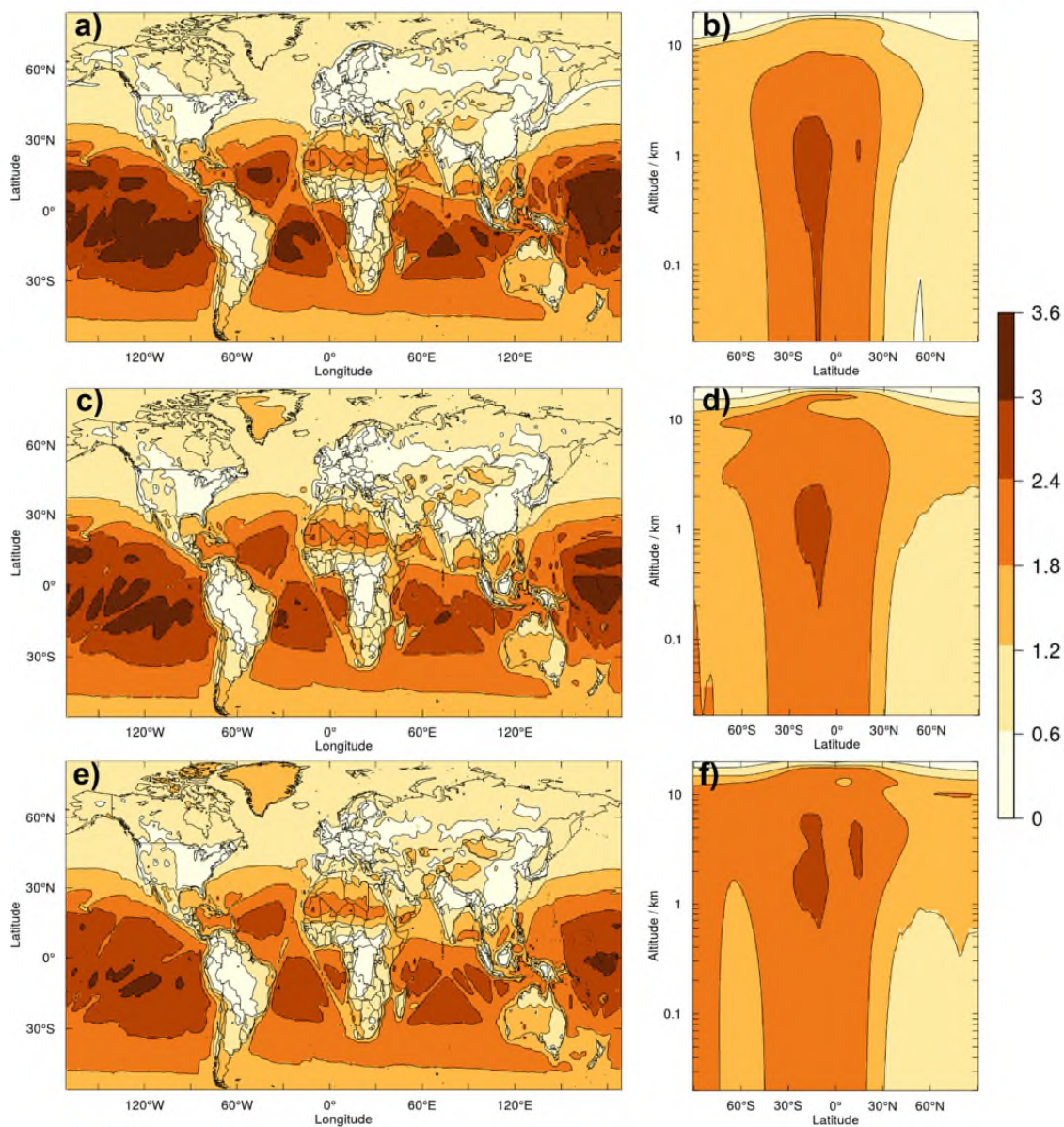
**Figure S14: Mean percentage changes in $k_{OH}$ (in %) from run 1 (a and b, top row), run 2 (c and d, middle row), and run 3 (e and f, bottom row), relative to the base run. Changes are shown for the surface (left column) and as a zonal mean (right column).**